MATERIALS FOR ADAPTIVE STRUCTURAL ACOUSTIC CONTROL

Period February 1, 1996 to January 31, 1997

Final Report

VOLUME III

OFFICE OF NAVAL RESEARCH
Contract No.: N00014-92-J-1510

APPROVED FOR PUBLIC RELEASE — DISTRIBUTION UNLIMITED

L. Eric Cross

PENNSTATE

1855

THE MATERIALS RESEARCH LABORATORY
UNIVERSITY PARK, PA

REPORT DOCUMENTATION PAGE

Form Approved
OMB No. 0704-0188

1. AGENCY USE ONLY (Leave blank)	2. REPORT DATE	3. REPORT TYPE AND DATES COVERED
	4/14/97	FINAL REPORT 2/1/96-1/31/97

4. TITLE AND SUBTITLE

MATERIALS FOR ADAPTIVE STRUCTURAL ACOUSTIC CONTROL

5. FUNDING NUMBERS

ONR CONTRACT NO:
N00014-92-J-1510

6. AUTHOR(S)

L. ERIC CROSS

7. PERFORMING ORGANIZATION NAME(S) AND ADDRESS(ES)

MATERIALS RESEARCH LABORATORY
THE PENNSYLVANIA STATE UNIVERSITY
UNIVERSITY PARK, PA 16802-4800

8. PERFORMING ORGANIZATION REPORT NUMBER

9. SPONSORING/MONITORING AGENCY NAME(S) AND ADDRESS(ES)

OFFICE OF NAVAL RESEARCH
CODE 1513:NRJ
800 NORTH QUINCY STREET
ARLINGTON, VA 22217-5660

GERALD T. SMITH
OFFICE OF NAVAL RESEARCH RES. REP.
536 SOUTH CLARK STREET, RM 286
CHICAGO, ILLINOIS 60606-1588

10. SPONSORING/MONITORING AGENCY REPORT NUMBER

11. SUPPLEMENTARY NOTES

12a. DISTRIBUTION/AVAILABILITY STATEMENT

12b. DISTRIBUTION CODE

13. ABSTRACT *(Maximum 200 words)*

SEE FOLLOWING TWO PAGES.

14. SUBJECT TERMS

15. NUMBER OF PAGES

16. PRICE CODE

17. SECURITY CLASSIFICATION OF REPORT	18. SECURITY CLASSIFICATION OF THIS PAGE	19. SECURITY CLASSIFICATION OF ABSTRACT	20. LIMITATION OF ABSTRACT

GENERAL INSTRUCTIONS FOR COMPLETING SF 298

The Report Documentation Page (RDP) is used in announcing and cataloging reports. It is important that this information be consistent with the rest of the report, particularly the cover and title page. Instructions for filling in each block of the form follow. It is important to ***stay within the lines*** to meet ***optical scanning requirements.***

Block 1. Agency Use Only *(Leave blank)*.

Block 2. Report Date. Full publication date including day, month, and year, if available (e.g. 1 Jan 88). Must cite at least the year.

Block 3. Type of Report and Dates Covered. State whether report is interim, final, etc. If applicable, enter inclusive report dates (e.g. 10 Jun 87 - 30 Jun 88).

Block 4. Title and Subtitle. A title is taken from the part of the report that provides the most meaningful and complete information. When a report is prepared in more than one volume, repeat the primary title, add volume number, and include subtitle for the specific volume. On classified documents enter the title classification in parentheses.

Block 5. Funding Numbers. To include contract and grant numbers; may include program element number(s), project number(s), task number(s), and work unit number(s). Use the following labels:

C	- Contract	PR	- Project
G	- Grant	TA	- Task
PE	- Program Element	WU	- Work Unit Accession No.

Block 6. Author(s). Name(s) of person(s) responsible for writing the report, performing the research, or credited with the content of the report. If editor or compiler, this should follow the name(s).

Block 7. Performing Organization Name(s) and Address(es). Self-explanatory.

Block 8. Performing Organization Report Number. Enter the unique alphanumeric report number(s) assigned by the organization performing the report.

Block 9. Sponsoring/Monitoring Agency Name(s) and Address(es). Self-explanatory.

Block 10. Sponsoring/Monitoring Agency Report Number. *(If known)*

Block 11. Supplementary Notes. Enter information not included elsewhere such as: Prepared in cooperation with...; Trans. of...; To be published in.... When a report is revised, include a statement whether the new report supersedes or supplements the older report.

Block 12a. Distribution/Availability Statement. Denotes public availability or limitations. Cite any availability to the public. Enter additional limitations or special markings in all capitals (e.g. NOFORN, REL, ITAR).

- **DOD** - See DoDD 5230.24, "Distribution Statements on Technical Documents."
- **DOE** - See authorities.
- **NASA** - See Handbook NHB 2200.2.
- **NTIS** - Leave blank.

Block 12b. Distribution Code.

- **DOD** - Leave blank.
- **DOE** - Enter DOE distribution categories from the Standard Distribution for Unclassified Scientific and Technical Reports.
- **NASA** - Leave blank.
- **NTIS** - Leave blank.

Block 13. Abstract. Include a brief *(Maximum 200 words)* factual summary of the most significant information contained in the report.

Block 14. Subject Terms. Keywords or phrases identifying major subjects in the report.

Block 15. Number of Pages. Enter the total number of pages.

Block 16. Price Code. Enter appropriate price code *(NTIS only)*.

Blocks 17. - 19. Security Classifications. Self-explanatory. Enter U.S. Security Classification in accordance with U.S. Security Regulations (i.e., UNCLASSIFIED). If form contains classified information, stamp classification on the top and bottom of the page.

Block 20. Limitation of Abstract. This block must be completed to assign a limitation to the abstract. Enter either UL (unlimited) or SAR (same as report). An entry in this block is necessary if the abstract is to be limited. If blank, the abstract is assumed to be unlimited.

ABSTRACT

This report documents work carried out largely over the fifth and final year of the ONR sponsored University Research Initiative (URI) entitled "Materials for Adaptive Structural Acoustic Control." This program has continued to foster the successful development of new electroceramic single crystal and composite material combinations for both sensing and actuation functions in adaptive structural systems.

For the classical perovskite relaxor, dielectrics typified by lead magnesium niobate, continuing studies of properties in the temperature region above the dielectric maximum T_m have added strong additional support to the superparaelectric/spin glass model for the behavior developed earlier in the IMRL. The most exciting and important discovery of the year has been the ultra high strain capability of relaxor ferroelectric single crystal actuators. For crystal in the lead zinc niobate:lead titanate (PZN;PT) solid solution system, at compositions in the rhombohedral phase close to the morphotropic phase boundary to the tetragonal ferroelectric phase at 9 mole % PT in PZN, crystals cut and poled along the 001 cube axis exhibit massive field induced quasi linear anhysterestic strains up to 0.6%. For this poling d_{33} values up to 2,300 pC/N and coupling coefficients k_{33} of 94% have been achieved and it was the original hypothesis that these extreme numbers must be largely due to extrinsic domain wall motion. Now however it is very clear that the exact equivalence of the effect of an 001 oriented E field on the $111, \bar{1}11, 1\bar{1}1,$ and $\bar{1}\bar{1}1$ rhombohedral domains precludes this field from driving domain wall motion so that quite contrary to our earlier expectation the polarization and associated strain phenomena are purely intrinsic. At higher field levels there is an obvious step in both polarization and strain into an induced tetragonal phase which gives total reproducible induced strains up to 1.7%. Clearly the PZN:PT crystals represent a major breakthrough into a completely new regimen for piezoelectric actuation and sensing.

For antiferroelectric:ferroelectric switching compositions in the lead lanthanum zirconated titanate stannate family, new experimental studies have proven that the induced polarization P_3 and the strain x_{33} onset at different field levels. A new domain re-orientation model has been invoked to explain this startlingly unusual behavior. Both barium and strontium additives have also been explored to control hysteresis between forward and backward switching with good success. As well as being interesting for transduction we believe these compositions are sure to be important for energy storage dielectrics.

In composite sensing it is pleasing to report that the moonie flextensional patent has now been licensed to the Input:Output Corporation who have successfully fabricated and sold more than 80,000 moonie sensors. Work is continuing on the cymbal type modification of the moonie with focus now on array structures for large area panels. This topic is transitioning to a joint study between the IMRL and Penn State's ARL, on a new MURI initiative. For the very small hollow PZT spheres produced by blowing, the emphasis has been upon both poling and driving from outer surface electrodes, and exploring both by experiment and by finite element theoretical methods, the resonant mode structures which can be induced. Studies of the 2:2 composite structures confirm the very high effective hydrostatic sensitivity and are permitting closer consonance between measurement and theoretical analysis.

Actuation studies have been dominated by the initial exploration of the fantastic strain capability of the relaxor ferroelectric MPB single crystals. Obviously the induced strains are on order of magnitude larger than for conventional PZT ceramics, but the blocking force has

not yet been determined. It is expected that d_{31} will also be large and anhysteritic in these crystals, as spontaneous strain depends on Q_{44} which is a pure shear constant. The d_{15} however may be significantly more complex as an E_1 field will certainly drive domain walls in these E_3 poled crystals.

Reliability studies of conventional actuators are continuing with emphasis on using acoustic emission to explore and separate domain wall motion and crack propagation. Most earlier studies were indeterminate and difficult to interpret, recently for these strongly piezoelectric samples we have shown that electrical noise in the power supply induces very strong mechanical noise in the sample giving high spurious emission counts. New studies using a long time constant filter in the supply have permitted clear and effective separation. Over the last few years there has been a strong re-awakening of interest in bimorph type transducer amplifiers with new concepts like rainbow, cerambow and thunder appearing. Under our ONR program with Virginia Polytechnic it has been necessary to sort out the conflicting claims for these 'morph' types and these data are included for completeness. We have also begun serious study of the large electrostriction in the soft polyurethane elastomers where it has been necessary to derive new techniques to measure strain with ultra low constraint on the films.

Processing studies now involved both single crystal flux growth and a wide range of powder and ceramic processing. Current needs for integrity and better mechanical properties are driving new needs for fine grained PZT piezoceramics and new processing is permitting retention of excellent properties down to submicron grain sizes.

From the wide range of thin ferroelectric film activities in the laboratory, only those which refer to the thicker films being produced on silicon for MEMS devices are included.

MATERIALS FOR ADAPTIVE STRUCTURAL ACOUSTIC CONTROL

Period February 1, 1996 to January 31, 1997

Final Report

VOLUME III

OFFICE OF NAVAL RESEARCH
Contract No.: N00014-92-J-1510

L. Eric Cross

TABLE OF CONTENTS

APPENDICES

VOLUME I

General Summary Papers

1. Cross, L.E., "Ferroelectric Materials for Electromechanical Transducer Applications." *Mat. Chem. Phys* **43**, 108-115 (1996).

2. Cross, L.E., "Ferroelectric Ceramics: Materials and Application Issues." *Ceramic Transactions* **68**, 15-55 (1996).

3. Li. S., J.A. Eastman, Z. Li, C.M. Foster, R.E. Newnham, and L.E. Cross, " Size Effects in Ferroelectrics." *Phys. Lett. A* **212**, 341 (1996).

4. Li, Shaoping, J.A. Eastman, R.E. Newnham, and L.E. Cross, "Susceptibility of Nanostructured Ferroelectrics." *Japanese J. Appl. Physics* **35** (Part 2) [No. 4B], L502-L504 (1996).

5. Newnham, R.E., Chapter: Crystal Chemistry and Crystal Physics, in Innovative Ideas in Ceramics and Materials Curricula, edited by T. Stoebe and W. Huebner. Published by the *American Ceramic Society*, pp. 65-72 (1996).

6. Uchino, K., "New Applications of Photostriction." *Innovations in Mater. Res.* **1** (1), 11-22 (1996).

7. Aburatani, H. and K. Uchino, "Acoustic Emission (AE) Measurement Technique in Piezoelectric Ceramics." *Jpn. J. Appl. Phys.* **35** (2) [4B], L516-L518 (1996).

Materials Studies

8. Choi, S., J.M. Jung, and A.S. Bhalla, "Dielectric, Pyroelectric and Piezoelectric Properties of Calcium-Modified Lead Magnesium Tantalate-Lead Titanate Ceramics." *Ferroelectric Letters* **21**, 27-33 (1996).

9. Alberta, E. and A.S. Bhalla, "Preparation of Phase Pure Perovskite Lead Indium Niobate Ceramic." *Mater. Lett.* **29**, 127-129 (1996).

10. Zhang, Q.M., J. Zhao, T.R. Shrout, and L.E. Cross, "The Effect of Ferroelastic Coupling in Controlling the Abnormal Aging Behavior in Lead Magnesium Niobate-Lead Titanate Relaxor Ferroelectrics." *J. Mater. Res.* **12** (7), (1997).

11. Alberta, E., A.S. Bhalla, and T. Takenaka, "Piezoelectric, elastic and Dielectric Constants for Ceramics in the Solids Solution: $xPbZrO_3$ - $(1-x-z)Pb(Zn_{1/3}Nb_{2/3})\ O_3$ - $zPbTiO_3$." *Ferroelectrics* **188**, 109-124 (1996).

Materials Studies–continued

12. Zhang, Q.M. and J. Zhao, "Polarization Responses in Lead Magnesium Niobate Based Relaxor Ferroelectrics." *Applied Physics Letters* (submitted).

13. Müeller, V. and Q.M. Zhang, "Nonlinearity and Scaling Behavior in Donor Doped Lead Zirconate Titanate Piezoceramic." *Physics Review Letters* (submitted).

14. Zhang, Q.M., J. Zhao, K. Uchino, and J. Zheng, "Change of the Weak-Field Properties of $Pb(ZrTi)O_3$ Piezoceramics with Compressive Uniaxial Stresses and Its Links to the Effect of Dopants on the Stability of the Polarizations in the Materials." *J. Mat. Res.* **12**, 226 (1997).

15. Markowski, K., S.-E. Park, S. Yoshikawa, and L.E. Cross, "The Effect of Compositional Variations in the Lead Lanthanum Zirconate Stannate Titanate System on Electrical Properties." *J. Amer. Ceram.* **79** (12), 3297-3304 (1996).

16. Park, S.-E., K. Markowski, S. Yoshikawa, and L.E. Cross, "The Effect of Barium and Strontium Additions in the Lead Lanthanum Zirconate Stannate Titanate System on Electrical Properties." *J. Amer. Ceram.* **80** (2), 407-412 (1997).

VOLUME II

17. Yoshikawa, S., K. Markowski, S.-E. Park, M.-J. Pan, and L.E. Cross, "Antiferroelectric-to-Ferroelectric Phase Switching Lead Lanthanum Zirconate Stannate Titanate (PLZST) Ceramics." *SPIE Proceedings* **IV** (1997).

18. Blue, C.T., J.C. Hicks, S.-E. Park, S. Yoshikawa, and L.E. Cross, "In-situ X-ray Diffraction Study of the Antiferroelectric-Ferroelectric Phase Transition in PLSnZT." *Applied Physics Letter* **68** (21), 2942-2944 (1996).

19. Pan, M.-J., S.-E. Park, K. Markowski, and S. Yoshikawa, "Antiferroelectric-to-Ferroelectric PLZST Ceramics-II: The Effect of Pre-Stress Conditions on the Strain Behavior." Submitted *Proceedings of IEEE International Symposium on the Applications of Ferroelectrics*, Rutgers University, East Brunswick, New Jersey (August 1996).

20. M.-J. Pan, Markowski, K., S.-E. Park, S. Yoshikawa, and L.E. Cross. "Antiferroelectric-to Ferroelectric PLZSnT Ceramics-I: Structure, Compositional Modification and Electric Properties." Submitted *Proceedings of IEEE International Symposium on the Applications of Ferroelectrics*, Rutgers University, East Brunswick, New Jersey (August 1996).

Materials Studies–continued

21. Lopath, P.D., K.K. Shung, S.-E. Park, and T.R. Shrout, "Ultrasonic Transducers Using Piezoelectric Single Crystals Perovskites." Submitted *Proceedings of IEEE International Symposium on the Applications of Ferroelectrics*, Rutgers University, East Brunswick, New Jersey (August 1996).

22. Park, S.-E. and T.R. Shrout, "Characteristics of Relaxor-Based Piezoelectric Single Crystals for Ultrasonic Transducers." Proceedings of 1996 IEEE Ultrasonics Symposium, San Antonio, Texas (November 1996).

23. Park, S.-E., P.D. Lopath, K.K. Shung, and T.R. Shrout, "Relaxor-Based Single Crystal Materials for Ultrasonic Transducer Applications." Proceedings on SPIE's International Symposium on Medical Imaging, Newport Beach, California (February 1997).

24. Lopath, P.D., S.-E. Park, K.K. Shung, and T.R. Shrout, "$Pb(Zn_{1/3}Nb_{2/3})O_3/PbTiO_3$ Single Crystal Piezoelectrics for Ultrasonic Transducers." Proceedings on SPIE's International Symposium on Medical Imaging, Newport Beach, California (February 1997).

25. Park, S.-E. and T.R. Shrout, "Relaxor Based Ferroelectric Single Crystals for Electro-Mechanical Actuators." *Innovations in Materials Research* (accepted).

26. Park, S.-E. and T.R. Shrout, "Characteristics of Relaxor-Based Piezoelectric Single Crystals for Ultrasonic Transducers," *IEEE Trans. on Ultrasonics, Ferroelectric and Frequency Control Special Issue on Ultrasonic Transducers* (to be published).

27. Jin, B., R. Guo, and A.S. Bhalla, "Piezoelectric Properties and Equivalent Circuits of Ferroelectric Relaxor Single Crystals."

28. Mulvihill, M.L., K. Uchino, Z. Li, and W. Cao, "In-situ Observation of the Domain Configurations during the Phase Transitions in Barium Titanate." *Phil. Mag. B.* **74** (1), 25-36 (1996).

29. Mulvihill, M.L., L.E. Cross, and K. Uchino, "Dynamic Motion of the Domain Configuration in Relaxor Ferroelectric Single Crystals as a Function of Temperature and Electric Field." *Ferroelectrics* **186**, 325-328 (1996).

30. Sundar, V. and R.E. Newnham, "Conversion Method Measurements of Electrostriction Coefficients in Low-K Dielectrics." *Mat. Res. Bull.* **31** (5), 545-554 (1996).

31. Sundar, V., J.-F., Li, D. Viehland, and R.E. Newnham, "Interferometric Evaluation of Electrostriction Coefficients." *Mat. Res. Bull.* **31** (5), 555-563 91996).

Materials Studies–continued

32. Sundar, V., N. Kim, C. Randall, R. Yimnirun, and R.E. Newnham, "The Effect of Doping and Grain Size on Electrostriction in $PbZr_{0.52}Ti_{0.48}O_3$." Submitted *Proceedings of IEEE International Symposium on the Applications of Ferroelectrics*, Rutgers University, East Brunswick, New Jersey (August 1996).

33. Erdei, S., L. Galambos, I. Tanaka, L. Hesselik, F.W. Ainger, L.E. Cross, and R.S. Feigelson, "Segregation and Inhomogenities in Photorefractive SBN Fibers." *SPIE Proceedings V–Photorefractive Fiber and Crystal Devices: Materials, Optical Properties, and Applications II*, **2849**, 168-173 (1996).

34. Li, Shaoping, J.A. Eastman, J.M. Vertrone, R.E. Newnham, and L.E. Cross, "Coherent Coupling in Ferroelectric Superlattices." (1996).

35. Su, J., Q.M. Zhang, and R.Y. Ting, "Space Charge Enhanced Electromechanical Response in Thin Film Polyurethane Elastomers." *Applied Physics Letters* (submitted).

36. Zhang, Q.M., J. Su, and C.-H. Kim, "An Experimental Investigation of Electromechanical Responses in a Polyurethane Elastomer." *J. Appl. Phys.* **81** (6), 2770 (1997).

VOLUME III

37. Su, J., Q.M. Zhang, C.H. Kim, R.Y. Ting, and R. Capps, "Effects of Transitional Phenomena on the Electric Field Induced Strain-Electrostrictive Response of a Segmented Polyurethane Elastomer." *J. Appl. Polymer Sci.* (accepted).

Composite Sensors

38. Fernandez, J.F., A. Dogan, Q.M. Zhang, J.F. Tressler, and R.E. Newnham, "Hollow Piezoelectric Composites, Sensors and Actuators." *A: Physical* **51** (2,3), 183-192 (1996).

39. Fernandez, J.F., A. Dogan, Q.M. Zhang, and R.E. Newnham, "Piezoelectric Composites with Enclosed Hollow Spaces." Proceedings 4th Euroceramics Conference, *Electroceramics* **5**, 39-46 (1996).

40. Fernandez, J.F., A. Dogan, J.T. Fielding, K. Uchino, and R.E. Newnham, "Temperature Dependence of New Design Ceramic-Metal Piezocomposites Actuators." Proceeding 4th Euroceramics Conference, *Electroceramics* **5**, 133-138 (1996).

Composite Sensors–continued

41. Newnham, R.E., "Composite Sensors and Actuators," Disordered Materials, edited by G. Milton, K. Godlen, G. Grimmett, and P. Sen, Springer-Verlag, NY (accepted January 1997).

42. Tressler, J.F. and R.E. Newnham, "Doubly Resonant Cymbal Transducers, *IEEE Transactions of UFFC*, Special Issue on Transducers (accepted 1996).

43. Tressler, J.F., W. Cao, K. Uchino, and R.E. Newnham, "Ceramic Metal Composite Transducers for Underwater Acoustic Applications." Submitted *Proceedings of IEEE International Symposium on the Applications of Ferroelectrics*, Rutgers University, East Brunswick, New Jersey (August 1996).

44. Alkoy, S., A. Dogan, A.C. Hladky, J.K. Cochran, and R.E. Newnham, "Vibration Modes of PZT Hollow Sphere Transducers." Submitted *Proceedings of IEEE International Symposium on the Applications of Ferroelectrics*, Rutgers University, East Brunswick, New Jersey (August 1996).

45. Alkoy, S., A. Dogan, A.C. Hladky, and R.E. Newnham, "Miniature Piezoelectric Hollow Sphere Transducers (BBs)." 1996 Proceeding of IEEE International Frequency Control Symposium, pp. 586-594, Honolulu, Hawaii (1996).

46. Alkoy, S., A. Dogan, A.C. Hladky, and R.E. Newnham, "Piezoelectric Hollow Spheres." 1996 Proceeding 3rd Turkish Ceramic Society Meeting., Eds. V. Günay, H. Mandel, S. Ozgen. Istanbul, Turkey (October 1996).

47. Koc, B., A. Dogan, J.F. Fernandez, R.E. Newnham, and K. Uchino, "Accelerometer Application of the Modified Moonie (Cymbal) Transducer." *J. App. Phys.* **35**, 65-67 (1996).

VOLUME IV

48. Kumar, S., A. Bhalla, and L.E. Cross, "Underwater Acoustic Absorption by Collocated Smart Materials." *Ferroelectric Letters* **21**, 11-16 (1996).

49. Geng, X. and Q.M. Zhang, "Evaluation of Piezocomposites for Ultrasonic Transducer Applications–Influence of the Unit Cell Dimensions and the Properties of Constituents the Performance of 2-2 Piezocomposites." *IEEE Transactions of UFFC* (accepted).

50. Zhang, Q.M. and X. Geng, "Acoustic Properties of the Interface of a Uniform Medium-2-2 Piezocomposite and the Field Distributions in the Composite." *J. Appl. Phys.* (accepted).

Actuator Studies

51. Park, S.-E., and T.R. Shrout, "Ultrahigh Strain and Piezoelectric Behavior in Relaxor Based Ferroelectric Single Crystals."

52. Uchino, K. and S. Takahashi, "Multilayer Ceramic Actuators." *Current Opinion, Ceramic, Composites and Intergrowths*, p. 98-705 (1996).

53. Zheng, J., S. Takahashi, S. Yoshikawa, and K. Uchino, "Heat Generation in Multilayer Piezoelectric Actuators." *J. Amer. Ceram.* **79** (12), 3193-3198 (1996).

54. Dogan, A., J.F. Fernandez, K. Uchino, and R.E. Newnham, "New Piezoelectric Composite Actuator Designs for Displacement Amplification." *Proceeding Euroceramic Conference, Electroceramics* (5), 127-132 (1995) (in press).

VOLUME V

55. Poosanaas, P., A. Dogan., A.V. Prasadarao, S. Komarneni, and K. Uchino, "Photostriction of Sol-Gel Processed PLZT Ceramics." *J. Electroceramics* (1996) (in press).

56. Uchino, K., "Reliability of Ceramic Actuators." Submitted *Proceedings of IEEE International Symposium on the Applications of Ferroelectrics*, Rutgers University, East Brunswick, New Jersey (August 1996).

57. Uchino, K., "High Electromechanical Coupling Piezoelectrics-How High Energy Conversion Rate is Possible?-." *Proceeding MRS 1996* (1996) (in press).

58. Uchino, K., "Recent Developments in Ceramic Actuators-Comparison Among USA, Japan and Europe."

59. Xu, B., Q.M. Zhang, V.D. Kugel, Q. M. Wang, and L.E. Cross, "Optimization of Bimorph Based Double Amplifier Actuator under Quasistatic Situation." Submitted *Proceedings of IEEE International Symposium on the Applications of Ferroelectrics*, Rutgers University, East Brunswick, New Jersey (August 1996).

60. Kugel, V.D., S. Chandran, and L.E. Cross, "Caterpillar-Type Piezoelectric d_{33} Bimorph Transducer." *Appl. Phys. Lett.* **69** (14), 2021-2023 (1996).

61. Kugel, V.D., Q.M. Zhang, B. Xu, Q.-M. Wang, S. Chandran, and L.E. Cross, "Behavior of Piezoelectric Actuators under High Electric Field." Submitted *Proceedings of IEEE International Symposium on the Applications of Ferroelectrics*, Rutgers University, East Brunswick, New Jersey (August 1996).

62. Kugel, V.D., B. Xu, Q.M. Zhang, and L.E. Cross, "Bimorph-Based Piezoelectric Air Acoustic Transducer Model." *Sensors and Actuators A* (submitted 1996).

Actuator Studies–continued

63. Chandran, S., V.D. Kugel, and L.E. Cross, "CRESCENT: A Novel Piezoelectric Bending Actuator." *Proceeding SPIE's 4th Annual Symposium on Smart Structures* accepted 1997).

64. Kugel, V.D., S. Chandran, and L.E. Cross, "A Comparative Analysis of Piezoelectric Bending-Mode Actuators." Submitted *SPIE Proceedings*, Smart Structures and Materials: Smart Materials Technologies, 3040, 70-80 (1997).

65. Wang, Q.M., B. Xu, V.D. Kugel, and L.E. Cross, "Characteristics of Shear Mode Piezoelectric Actuators," Submitted *Proceedings of IEEE International Symposium on the Applications of Ferroelectrics*, Rutgers University, East Brunswick, New Jersey (August 1996).

Integration Studies

66. Elissalde, C., L.E. Cross, and C.A. Randall, "Structural-Property Relations in a Reduced and Internally Biased Oxide Wafer (RAINBOW) Actuator Material." *J. Amer. Ceram.* **79** (8), 2041-2048 (1996).

67. Xu. B., Q.M. Zhang, V.D. Kugel, Q. Wang, and L.E. Cross, "Optimization of Bimorph Based Double Amplifier Transducer under Quasistatic Conditions." Submitted *Proceedings of IEEE International Symposium on the Applications of Ferroelectrics*, Rutgers University, East Brunswick, New Jersey (August 1996).

68. Xu, B., Q. M. Zhang, V.D. Kugel, and L.E. Cross, "Piezoelectric Air Transducer for Active Noise Control." *Proceeding SPIE, Smart Structures and Integrated Systems* **271** (7), 388 (1996).

VOLUME VI

69. Chandran, S., V.D. Kugel, and L.E. Cross, "Characterization of the Linear and Non-Linear Dynamic Performance of RAINBOW Actuator." Submitted *Proceedings of IEEE International Symposium on the Applications of Ferroelectrics*, Rutgers University, East Brunswick, New Jersey (August 1996).

70. Wang, H., Q.M. Zhang, L.E. Cross, and C.M. Trottier, "Tailoring Material Properties by Structure Design–Radially Poled Piezoelectric Cylindrical Tube." *Ferroelectrics* **173**, 181-189 (1995).

Processing Studies

71. Park, S.-E., M. Mulvihill, P.D. Lopath, M. Zipparo, and T.R. Shrout, "Crystal Growth and Ferroelectric Related Properties of (1-x) Pb $(A_{1/3}Nb_{1/3})O_3$ - $xPbTiO_3$(A=Zn^{2+}, Mg^{2+})." Submitted *Proceedings of IEEE International Symposium on the Applications of Ferroelectrics*, Rutgers University, East Brunswick, New Jersey (August 1996).

72. Mulvihill, M., S.-E. Park, G. Risch, Z. Li, K. Uchino, and T.R. Shrout, "The Role of Processing Variables in the Flux Growth of PZN-PT Relaxor Ferroelectric Single Crystals." *Jpn. J. Appl. Phys.* **35** (Pt. 1; No. 7), 3984-3990 (1996).

73. Pan, M.-J., S.-E. Park, C.W. Park, K.A. Markowski, S. Yoshikawa, and C. Randall, "Superoxidation and Electrochemical Reactions during Switching in $Pb(Zr,Ti)O_3$ Ceramics." *J. Amer. Ceram.* **79** (11), 2971-2974 (1996).

74. Park, S.-E., M.L. Mulvihill, G. Risch, and T.R. Shrout, "The Effect of Growth Condition on Dielectric Properties of $Pb(Zn_{1/3}Nb_{2/3})O_3$ Crystal." *Jpn. J. Appl. Phys.* **36** (1) (1997).

75. Yoshikawa, Y. and K. Uchino, "Chemical Preparation of Lead-Containing Niobate Powders." *J. Amer. Ceram.* **79** (9), 2417-2421 (1996).

76. Ravindrathan, P., V. Srikanth, S. Komarneni, and A.S. Bhalla, "Processing of $Pb(Zn_{1/3}Nb_{2/3})O_3$: Ceramics at High Pressure." *Ferroelectrics* **188**, 135-141 (1996).

77. Ravindrathan, P., S. Komarneni, A.S. Bhalla, and R. Roy, "Low Temperature Chemical Routes to Smart Materials." *Ferroelectrics* **188**, 125-133 (1996).

78. Alberta, E.F. and A.S. Bhalla, "A Processing and Electrical Property Investigation of the Solid Solution: (x) $Pb(In_{1/2}Nb_{1/2})O_3$ - (1-x)$Pb(Sc_{1/2}Ta_{1/2})O_3$." *Ferroelectrics* **188**, 95-107 (1996).

Thin Film Ferroelectrics

79. Chen, H.D., K.R. Udayakumar, C.J. Gaskey, and L.E. Cross, "Fabrication and Electrical Properties of Lead Zirconate Titanate Thick Films." *J. Amer. Ceram.* **79** (8), 2189-2192 (1996).

80. Chen, H.D., K.K. Li, C.J. Gaskey, and L.E. Cross, "Thickness-Dependent Electrical Properties in Lanthanum-Doped PZT Thick Films." *Mat. Res. Soc. Symp. Proc.* **433**, 325-332 (1996).

81. Ravichandran, D., R. Meyer, Jr., R. Roy, R. Guo, A.S. Bhalla, and L.E. Cross, "Sol-Gel Synthesis of $Ba(Mg_{1/3}Ta_{2/3})O_3$: Phase Pure Powder and Thin Films." *Mat. Res. Bull.* **31** (7), 817-825 (1996).

82. Ravichandran, D., K. Yamakawa, R. Roy, A.S. Bhalla, S. Trolier-McKinstry, R. Guo, and L.E. Cross, "The Effect of Annealing Temperature on the Formation of $SrBi_2Ta_2O_9$ (SBT) Thin Films." Submitted *Proceedings of IEEE International Symposium on the Applications of Ferroelectrics*, Rutgers University, East Brunswick, New Jersey (August 1996).

Instrumentation

83. Su, J., P. Moses, and Q.M. Zhang, "A Bimorph Based Dilatometer for Field Induced Strain Measurement in Soft and Tin Free Standing Polymer Films." *Reviews of Scientific Instruments* (submitted).

MATERIALS STUDIES

(continued)

APPENDIX 37

Accepted.
J. Appl. Polym. Sci.

Effects of Transitional Phenomena on the Electric Field Induced Strain-Electrostrictive Response of a Segmented Polyurethane Elastomer

J. Su[1], Q. M. Zhang[1], C. H. Kim[1†], R. Y. Ting[2] and R. Capps[2]

[1] Intercollege Materials Research Laboratory,
The Pennsylvania State University, University Park, PA 16802, USA
[2] Naval Undersea Warfare Center, USRD,
Materials Research Division, Orlando, FL, 32856 USA

†Permanent address: Department of Chemistry, Chongju University,
Chongju City, 360-764, Korea

Effects of Transitional Phenomena on the Electric Field Induced Strain-Electrostrictive Response of A Segmented Polyurethane Elastomer

SYNOPSIS

The electromechanical properties of a segmented polyurethane elastomer were investigated as functions of temperature and frequency. Two transitional phenomena were observed in the temperature range from -50 °C to 85 °C. In these transition regions, the electric field induced strain coefficient exhibits large increases, which indicates that the effect of the transition processes is significant. The experimental analysis suggests that the transitional processes in the polyurethane are related to the chain segment motions. From the elastic compliance and the dielectric constant data, the contribution of the uniform Maxwell stress was determined. It was found that the contribution of the Maxwell stress effect to the measured strain coefficient increased from about 10 % below the glass transition temperature, T_g, (~-25 °C) to about 50 % and 35 % for the frequencies of 10 Hz and 100 Hz, respectively, at -40 °C, which is above T_g. The large difference between the measured strain response and the calculated Maxwell stress effect indicates a significant contribution to the field induced strain from other mechanisms such as electrostriction.

Keywords: Polyurethane elastomer, electric field induced strain, Maxwell stress, electrostriction and transitional phenomena.

I. INTRODUCTION

Electromechanical coupling effects such as piezoelectricity and electrostriction have been widely utilized in transducer, sensor and actuator technologies.[1,2] During the last three decades, electromechanical polymers, especially piezoelectric poly(vinylidene fluoride) (PVDF) and its copolymers with trifluoroethylene (TrFE), have drawn much attention because of their low acoustic impedance, mechanical flexibility and good processing properties as well as low manufacturing cost.[3,4] However, their applications have been limited due to the lower electromechanical activity when compared with those of piezoceramic Lead Zirconate Titanate (PZT).[5,6] The recent development in electromechanical properties of polymers showed that some thermoplastic polymer elastomers, especially segmented polyurethane elastomers, can exhibit very high electric field induced strain response. These electromechanically active polyurethane elastomers have drawn more and more attention and many experimental investigations have been conducted[7-9] since the large electric field induced strain of this class of polyurethane elastomers was reported.[10]

The objective of this study is to provide understanding of the possible mechanisms for the observed large electric field induced strain in this class of polyurethane elastomers through investigations on the temperature-frequency dependence of the field induced strain, the dielectric and the elastic properties. In addition, the temperature dependence of the molecular motions in the material were also examined using Differential Scanning Calorimetry (DSC), Fourier Transform Infrared (FTIR) spectroscopy and Thermal Expansion (TE) techniques to elucidate the property-molecular motion relationship.

II. EXPERIMENTAL

A. Sample Preparation

The material used in this investigation was produced by Deerfield Urethane, Inc. using a Dow polyurethane (Dow 2103-80AE). The polyurethane is a segmented elastomer consisting of poly(tetramethylene glycol) (PTMEG) as the soft segment and methylenedi-p-phenyl diisocyanate (MDI) as the hard segment with 1,4-butanediol (Bdiol) acting as the extender. The molar ratio of the components in the polyurethane is 1.8 mol. MDI/0.8 mol. Bdiol/1.0 mol. PTMEG. The samples for experimental measurements were prepared by solution casting. The thickness of the sample in this investigation was 2 mm. The gold electrodes were vacuum evaporated onto the opposing surfaces of the cast samples.

The result of x-ray diffraction, shown in figure 1, indicates that there is no detectable crystalline phase, in the samples investigated within the experimental resolution, or it can be said that the sample is amorphous.

B. Electric-Field-Induced Strain Measurement

A double-beam laser interferometer was employed to measure the strain induced by the applied electrical field at frequencies of 10 Hz and 100 Hz in the temperatures range from -30 ^{o}C to 80 ^{o}C. A detailed description of the technique, including the basic principle, the set-up and the sample-mounting for the strain measurements was reported with schematic representation in a previous publication.[8]

C. Dielectric and Elastic Measurements

The temperature-frequency dependence of the dielectric constant of the polyurethane was measured in a temperature controlled chamber by a lock-in amplifier. The temperature range for the measurement was from -40 ^{o}C to 80 ^{o}C and the heating rate was 2 ^{o}C/min.. The measurement frequencies were 10 Hz and 100 Hz.[8]

The temperature-frequency dependence of the elastic compliance of the polyurethane was investigated using a Dynamic Mechanical Analyzer (DMA) from -40 ^{o}C to 80 ^{o}C with a heating rate of 2 ^{o}C/min. The measurement frequencies were also 10 Hz and 100 Hz.

D. DSC, FTIR and Thermal Expansion Measurements

To understand how the observed macroscopic properties are related to the molecular structures, molecular motions and transitional phenomena, Differential Scanning Calorimetry (DSC), Fourier Transform Infrared (FTIR) spectroscopy and Thermal Expansion (TE) measurements of the polyurethane were examined as functions of temperature. The temperature range for DSC and FTIR measurement was from 25 °C to 190 °C and from 25 °C to 180 °C, respectively, while for TE, the temperature range was from 40 °C to 100 °C. The heating rate was 10 °C/min. for the DSC and TE measurements.

III. Results and Discussion

A. Temperature and Frequency Dependence and Transitions

The experimental results of the electric-field-induced strain are presented in figure 2a. The strain coefficient, R_{33}, ($S_3 = R_{33} E_3^2$, where S is the strain, E is the applied electric field, and the subscript 3 represents the direction perpendicular to the sample surface) increases with temperature and decreases with frequency. In the temperature range from -30 °C to 60 °C, two relatively sharp increments are observed: one starts at the temperature about -20 °C and the other starts at about 50 °C. Similar trends are also observed in the dielectric and elastic data shown in figures 2b and 2c, respectively. The dielectric constant, K, shows a rapid increase at about -20 °C but a relatively small change at about 60 °C while the temperature dependence of the elastic compliance shows two rapid increases starting at about -25 °C and 60 °C, respectively. The sharp change in the material properties at the lower temperature, observed in these measurements, is related to the glass transition of the polyurethane due to large scale molecular motions of the soft segments, PTMEG.[11] In order to understand the change at higher temperature transition, DSC, FTIR and TE investigations, which are employed extensively in studies of structures and molecular motions of segmented polyurethane elastomers,[11-13] were carried out. The DSC

curve, shown in figure 3, exhibits an endothermic peak at about 75 °C, starting at about 50 °C and ending at about 90 °C, which is much higher than the glass transition temperature, (about -20 °C) and much lower than the melting temperature, (about 170 °C), which is reflected by another endothermic peak starting at about 100 °C and ending at about 185 °C. From the DSC results, the enthalpy change associated with the transition between 50 °C and 100 °C was calculated by assuming the change is associated with the dissociation of the hydrogen bonding in hard segments since some previous publication suggested the endothermic peak might be associated with hydrogen bonding dissociation. However, the value obtained, which is 3.71 kcal/mol., is obviously lower than the previously reported enthalpy change due to hydrogen-bond dissociation in segmented polyurethanes having similar chemical structure.[12] The thermal expansion measurement of the segmented polyurethane elastomer also exhibits a characteristic transitional change in the temperature range between 50 °C and 100 °C. As can be seen in figure 4, the material exhibits a rapid thermal expansion in the temperature range from about 50 °C to about 90 °C.

The temperature dependence of the absorbency spectroscopy of the FTIR study on the polyurethane is shown in figures 5a-5d. The change in the infrared absorption related to the -NH and -C=O related hydrogen bonding was investigated at 60 °C, 100 °C, 140 °C and 180 °C. As the temperature is increased from 60 °C to 100 °C, the absorption of bonded -NH (3327 cm^{-1}) associated with the absorption of bonded -C=O (1714 cm^{-1}) show only a minor decrease. The absorption of unbonded, or free, -NH (3448 cm^{-1}) and the unbonded -C=O (1730 cm^{-1}) shows very little increase in the same temperature range, which indicates that the transitional change observed in the DSC and TE measurements is not mainly associated with the dissociation of the hydrogen bonding in the MDI segments. However, when the temperature is increased from 100 °C to 140 °C, a relatively large change, i.e. a large drop, in the absorption of the H-bonded groups and increase in the absorption of the unbonded groups, can be observed. Further increase of the temperature to 180 °C results in a significant dissociation of the hydrogen bonding, which is reflected by the disappearance of the bonded -NH (3327 cm^{-1}) and -C=O (1714 cm^{-1})

absorption peaks, and the large increase of the absorption peak due to the unbonded -NH (3448 cm^{-1}) and -C=O (1730 cm^{-1}). This observation corresponds to the endothermic peak observed in the temperature region from 100 °C to 180 °C in the DSC measurement, which is associated with the hard segment dissolution (melting) as a consequence of the dissociation of the hydrogen bonding in MDI.

The experimental results obtained from the DSC, TE and FTIR investigations show that the transition between 50 °C and 100 °C, which might be the key factor resulting in the increased field induced strain response of the segmented polyurethane in the temperature region, is neither the glass transition nor the melting if the glass transition reflects the molecular motion of the soft segments and the melting reflects the molecular flow of whole polymer chains when the hydrogen bond dissociation occurs. The molecular origin of the transition might be related to the molecular motion of the extenders within the hard segments, which might occur without destroying the hydrogen bonding sheet structure,[12] and result in expanding in the direction perpendicular to the hydrogen bonding sheets and increasing free volume. When this happens, it should lead to transitional changes in elastic and thermal expansion properties, as observed in figures 2c and 4, respectively. The asymmetric endothermic peak, i.e. slow increase before the peak position (about 75 °C) and rapid decrease after the peak observed in the DSC curve, could be a result of the restraining of the hydrogen bonding in MDI segments to the extender (Bdiol) related molecular motion. This restraint can limit the molecular motion of extenders between MDI segments, which results in the slow increase. When temperature is high enough to cause the motion of or dissociation of the hydrogen bonds in the hard segments to a significant level, the limited molecular motion of the extenders can be accelerated, which results in the rapid decrease.

B. Contributions from the Maxwell Stress Effect and Non- Maxwell Stress Effects

In general, the electric field induced strain in a non-piezoelectric material can be from the electrostrictive effect and also from the Maxwell stress effects. The electrostrictive effect is a

direct coupling between the polarization and mechanical response in the material. It can be expressed as the strain change induced by a change in the polarization level in the material

$$S_E = QP^2 \qquad (1)$$

where S is the strain, P is the polarization level and Q is the electrostrictive coefficient of the material. For a linear dielectric, $P = \varepsilon_0 (K-1) E$. So that the equation (1) can also be rewritten as

$$S_E = Q \varepsilon_0^2 (K-1)^2 E^2 \qquad (2)$$

where K is the dielectric constant of the material, ε_0 is the vacuum dielectric permittivity and E is the applied electric field. On the other hand, Maxwell stress, T, which is due to the interaction between the free charges on the electrode (Coulomb interaction) , can also contribute to the electric field induced strain response. For the situation considered here, it is also proportional to the square of the applied electric field and can be expressed as

$$T = -\varepsilon_0 K E^2 / 2 \qquad (3)$$

Therefore, the dimensional change due to the Maxwell stress is obtained as

$$S_M = -s \varepsilon_0 K E^2 / 2 \qquad (4)$$

where s is the compliance of the material. As can be seen, the strain induced by the Maxwell stress can be quite substantial for a soft, or high compliance, material such as the polyurethane elastomer investigated.

From the temperature dependence of the dielectric constant and elastic compliance measurements, the electric field induced strain due to the Maxwell stress effect and percentage of this contribution to the total strain response were determined, which are shown in figures 6a and 6b, respectively. When the temperature is lower than the glass transition temperature, T_g, the contribution of the Maxwell stress is relatively small, which is only about 10%, since the elastic compliance is low. During the glass transition period, which is approximately from -20 ^oC to 30^oC, the Maxwell stress contribution increases from about 10 % to about 35 % and 50 % for 100 Hz and 10 Hz, respectively, while the elastic compliance, s, increases about one order of magnitude and the dielectric constant, K, increases from 4 to 6.5. From 50 ^oC to 80 ^oC, the

temperature region for the observed second transition from DSC analysis, the increase of the strain is also observed. Associated with this increase, the elastic compliance shows a corresponding increase while the dielectric constant does not show a significant change.

From the discussion above, it can be seen that the Maxwell stress contribution is important for the electric field induced strain, especially when the temperature is higher than the glass transition temperature of the polyurethane. On the other hand, the non-Maxwell contribution, which is assumed to be electrostrictive strain, is also very significant. As can be seen in figures 7a and 7b, the non-Maxwell stress part of the field-induced strain coefficient, which is represented as Re-Rm, where Re is the total measured strain coefficient and Rm is the Maxwell stress contribution, shows significant values in the whole temperature region where the measurement was conducted, and when the temperature is lower than the glass transition temperature, the electrostrictive contribution dominates (at about 90 %). Even though the Maxwell stress contribution is significantly increased when the temperature is raised to above 60 ^{o}C, which is higher than Tg, the electrostrictive strain is still contributing to the total field induced strain of about 40 % at 10 Hz and about 60 % at 100 Hz, respectively.

C. Temperature and Frequency Dependence of the Electrostrictive Coefficient

The experimental results show that the glass transition plays an important role in the observed large electric field induced strain of the polyurethane investigated. During the transition, both the dielectric and elastic properties show transitional change, therefore the contribution of Maxwell stress effect shows similar characteristics, as discussed. Based on the equation (2), the electrostrictive coefficient Q can be evaluated. The temperature dependence of the coefficient Q at 10 Hz and 100 Hz is presented in figures 8. As can be seen, when the electrostrictive coefficient, Q, is examined over the temperature range of the glass transition, it does not show the temperature dependence as that observed in the Maxwell stress effect which depends directly on the elastic compliance. However, when the temperature is raised to the second transitional region, the coefficient Q exhibits increase with temperature. Considering the

fact that the electromechanical response of a polymer material is contributed by the molecular motions which participate in both the polarization and elastic processes,[8] the increase in the electrostrictive coefficient Q is a result of the increased elasticity per unit polarization change, which can be caused by lowering the energy barrier for the mechanically related segment motion as reflected by the increase in the elastic compliance in this temperature range, where the dielectric constant does not show much change. On the other hand, when the electrostrictive coefficient Q is examined as a function of the frequency, it is observed that Q measured at 100 Hz is about 25% lower that measured at 10 Hz. The decrease of the Q with frequency indicates that the component of the polarization motions of high frequency (short relaxation time) does not generate as much strain in the material and therefore it is more like pure dielectric. It should be mentioned that the relatively large data scatter in figures 8 is due to the fact that the calculated results are obtained from three sets of experimental data (the dielectric constant, the elastic compliance and the electric field-induced strain measurements).

IV. CONCLUSIONS

The temperature and frequency dependence of the electric field induced strain, dielectric and elastic properties show that both the Maxwell stress effect and electrostriction are important to the electric field induced strain of the polyurethane elastomer investigated. The Maxwell stress contribution increases markedly during the glass transition, along with the sharp increase in the elastic compliance and dielectric constant. In spite of these large changes, the non-Maxwell contribution such as the electrostrictive coefficient Q seems to be independent of temperature in the glass transition region. In addition to the glass transition, another transitional change at about 75 ^{o}C was also observed in the experimental temperature range. The thermal and chemical structural analysis such as the DSC, thermal expansion and FTIR studies indicates that the transition might be related to the molecular motion of the extenders in the hard segments. Interestingly, the electrostrictive coefficient Q exhibits an increase with temperature along with

the elastic compliance, while there is only a small change in the dielectric constant in the same temperature range. The experimental results show that the two transitional phenomena, which are reflections of the molecular motions of the soft segment and the extender in hard segment, are important for the observed electric field induced strain of the polyurethane elastomer. Even though these transitional phenomena can significantly increase the Maxwell stress contribution, the non-Maxwell stress contribution such as the electrostrictive coefficient, which seems not changing with temperature in the glass transition region, is also important for the field induced strain of the segmented polyurethane elastomer. The different behaviors, observed in the two transitional regions, of the electrostrictive coefficient, the elastic constant, and the dielectric constant suggest that in this class of the material, the chain segment motions can be grouped into those related to polarization, those related to the elastic process, and those related to both. The change in the relative activation energies related to these motions with temperature results in the different behaviors in the dielectric, elastic, and electrostrictive coefficient.

ACKNOWLEDGMENT

The authors are grateful for stimulating discussions with Professor L. E. Cross. The technical assistance of Drs. M. M. Coleman, M. Sobkowiak and V. Kugel is greatly appreciated.

This work was supported by the Office of Naval Research through grants No. N00014-95-1-1225 and N 00014-96-1-0418.

REFERENCES:

1. W. G. Cady, "*Piezoelectricity*", Dover Publications, Inc., New York, 1964.
2. J. M. Herbert, "*Ferroelectric Transducers and Sensors*", Gordon and Breach Science Publishers, New York, 1982.
3. A. J. Lovinger, *Science*, **220**, 1115 (1983).
4. H. R. Gallantree, *IEE Proceedings*, **130**, 219 (1983).
5. H. Wang, Ph. D. Thesis, The Pennsylvania State University, 1994.
6. B. Jaffe, W. R. Cook, Jr., and H. Jaffe, "*Piezoelectric Ceramics*", Academic Press, London and New York, 1971.
7. H. Wang, Q. M. Zhang, L. E. Cross, R. Ting, C. Coughlin, and K. Rittenmyer, *Proc. Int. Symp. Appl. Ferro.*, **9**, 182 (1994).
8. Q. M. Zhang, J. Su, C. H. Kim, R. Ting, and R. Capps, Accepted for publication in *J. Appl. Phys.* (1997).
9. S. Tasaka, T. Shouko, K. Asami and N. Inagaki, *Jpn. J. Appl. Phys.*, 33, L1376 (1994).
10. M. Zhenyi, J. I. Scheinbeim, J. W. Lee, and B. A. Newman, *J. Polym. Sci. Part B: Polym. Phys.*, **32**, 2721 (1994).
11. V. W. Srichatrapimuk and S. L. Cooper, *J. Macromol. Sci.-Phys.*, **B15(2)**, 267 (1978).
12. N. R. Legge, G. Holden, and H. E. Schreoder, *"Thermoplastic Elastomers: A Comprehensive Review"*, Hanser Publishers, Munich, Vienna and New York, 1993.
13. W. J. Macknight and M. Yang, *J. Polym. Sci.: Symposium*, **42**, 817 (1973).
14. R. W. Seymour and S. L. Cooper, *Macromolecules*, **6**, 48 (1973).

FIGURE CAPTION:

Figure 1. X-ray diffraction data of the polyurethane elastomer at room temperature where the broad hola near 20 degree (2θ) is the reflection of the amorphous phase. No crystalline phase was observed within the data resolution.

Figure 2. Temperature dependence of (a) the electric field induced strain coefficient, R, (b) the dielectric constant, K, and (c) the elastic compliance, s, of the polyurethane elastomer (Dow 2105-80AE), at 10 Hz and 100 Hz. The solid line are drawn to guide the eye.

Figure 3. Differential Scanning Calorimetry (DSC) trace of the segmented polyurethane (Dow 2105-80AE) elastomer, from 25 °C to 190 °C.

Figure 4. The thermal expansion measurement of the segmented polyurethane elastomer exhibits a transitional characteristic change in the temperature region from 50 °C to 100 °C.

Figure 5. FTIR spectroscopy of the polyurethane elastomer (Dow 2105-80AE) at (a) 60 °C, (b) 100 °C, (c) 140 °C and (d) 180 °C. (Absorbency wavenumber: 1: 3448 cm^{-1}, 2: 3327 cm^{-1}, 3: 1730 cm^{-1}, and 4: 1714 cm^{-1}).

Figure 6. Comparison of the temperature dependence of (a) the total electric field induced strain coefficient, R_e, (filled circle for 10 Hz and filled square for 100 Hz) and the Maxwell Stress contributed strain coefficient, R_m, (open circle for 10 Hz and open square for 100 Hz), and (b) the percentage of Maxwell Stress contribution to the

total strain coefficient, at 10 Hz and 100 Hz. The solid lines are drawn to guide the eye.

Figure 7. (a) The temperature dependence of non-Maxwell contribution to the electric field induced strain response, -(Re-Rm), and (b) of the percentage of the non-Maxwell contribution. The solid lines and the dashed lines are drawn to guide the eye.

Figure 8. The electrostrictive coefficient, Q, as a function of temperature at the measurement frequencies of 10 Hz and 100 Hz. The open circles and open diamonds are data points and the solid line are drawn to guide the eye.

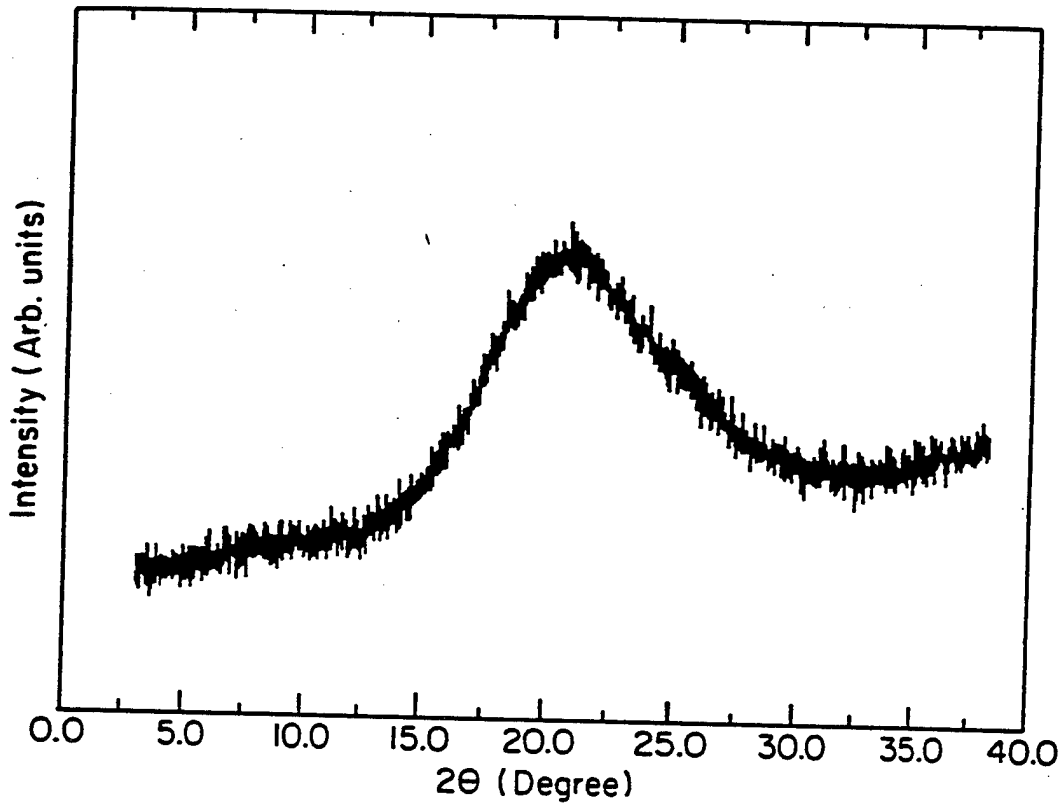
Intensity (Arb. units)
0.0
5.0
10.0
15.0
20.0
25.0
30.0
35.0
40.0
2θ (Degree)

Fig. 1

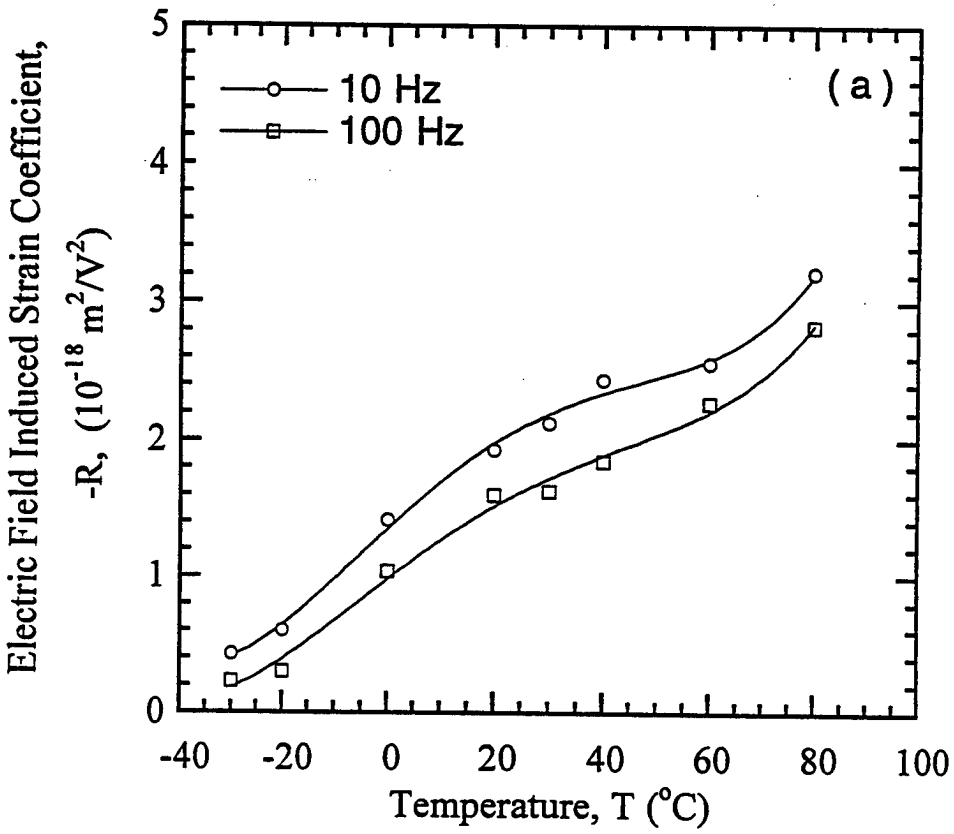
10 Hz
100 Hz
(a)
Electric Field Induced Strain Coefficient,
-R, (10^{-18} m^2/V^2)
Temperature, T (°C)
0
1
2
3
4
5
-40
-20
0
20
40
60
80
100

Fig. 2a

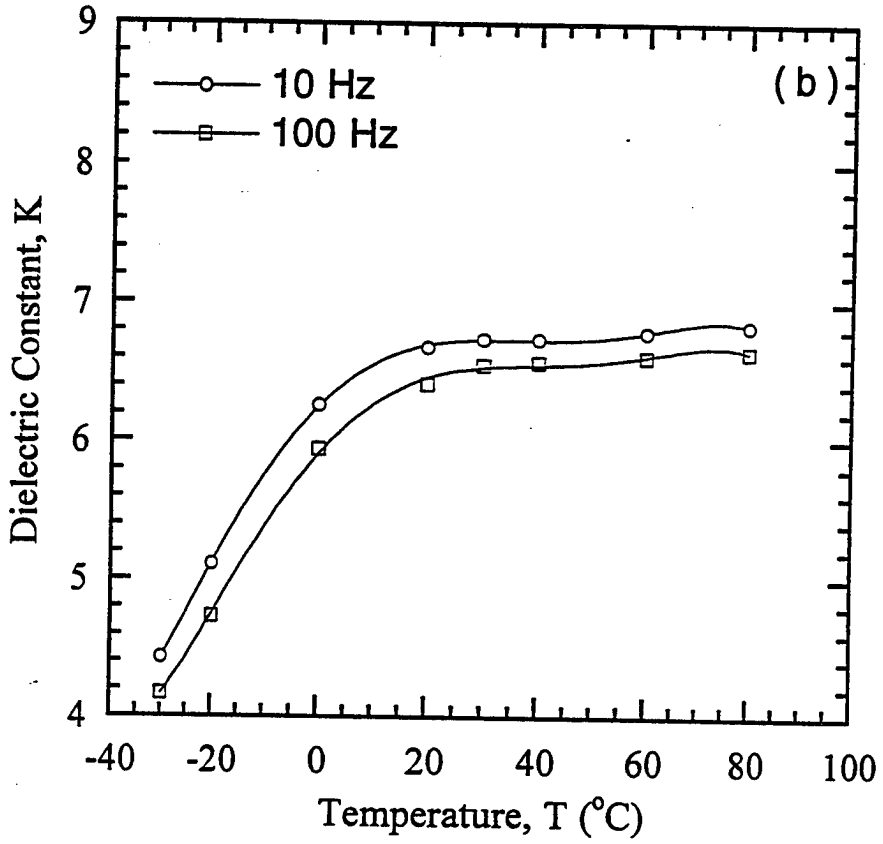
10 Hz
100 Hz
(b)
Dielectric Constant, K
9
8
7
6
5
4
-40
-20
0
20
40
60
80
100
Temperature, T (°C)

Fig. 2b

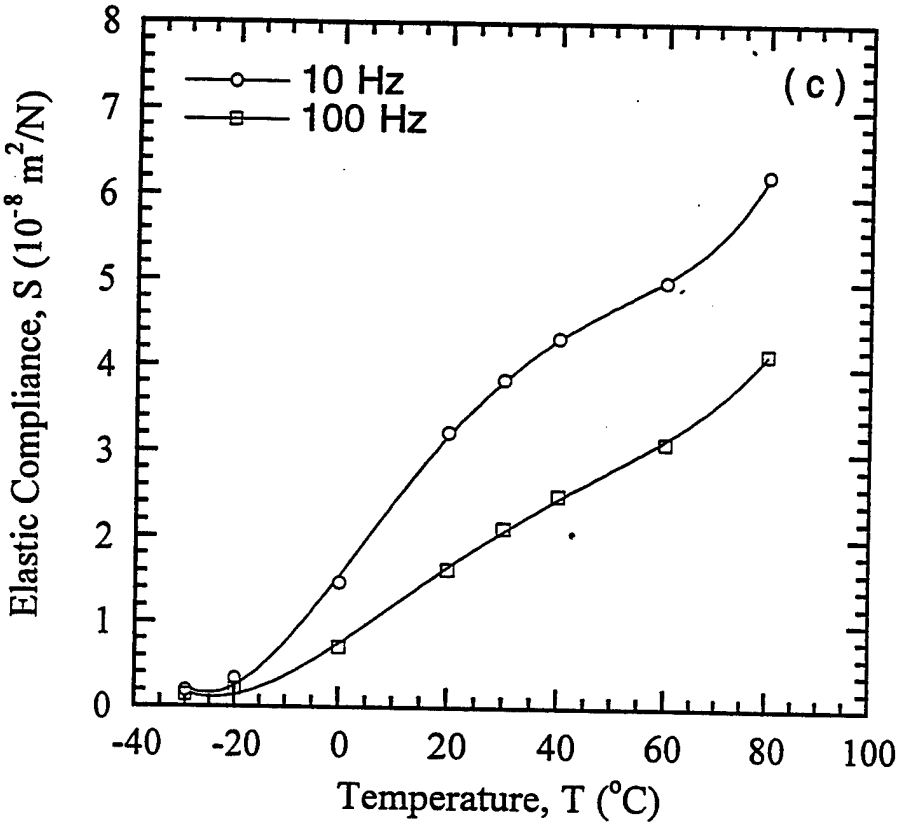
10 Hz
100 Hz
(c)
Elastic Compliance, S (10^{-8} m^2/N)
Temperature, T (°C)
0
1
2
3
4
5
6
7
8
-40
-20
0
20
40
60
80
100

Fig. 2C

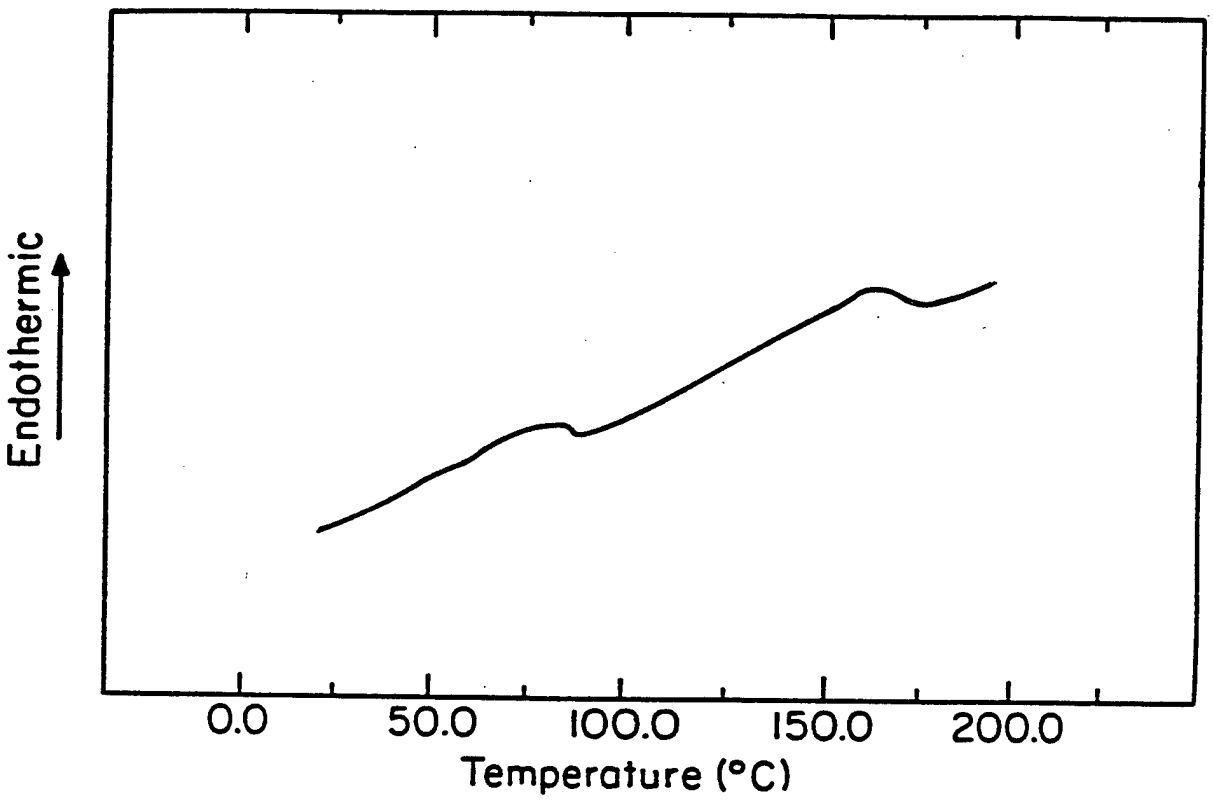

Fig. 3

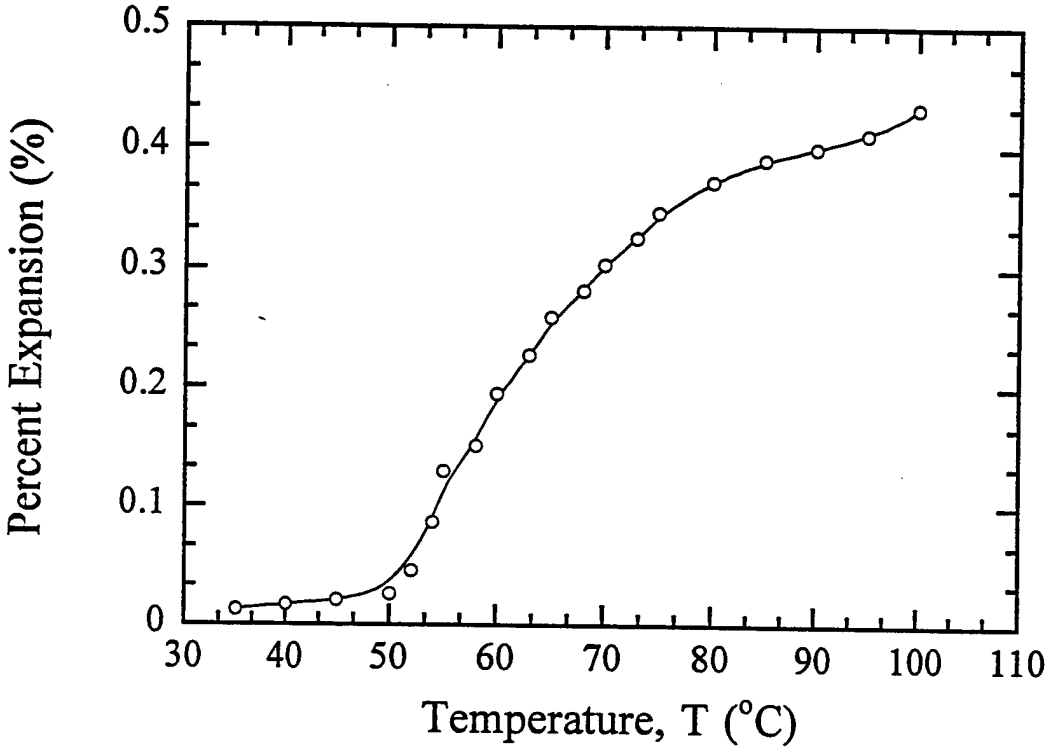
Percent Expansion (%)
0.5
0.4
0.3
0.2
0.1
0
30
40
50
60
70
80
90
100
110
Temperature, T (°C)

Fig. 4

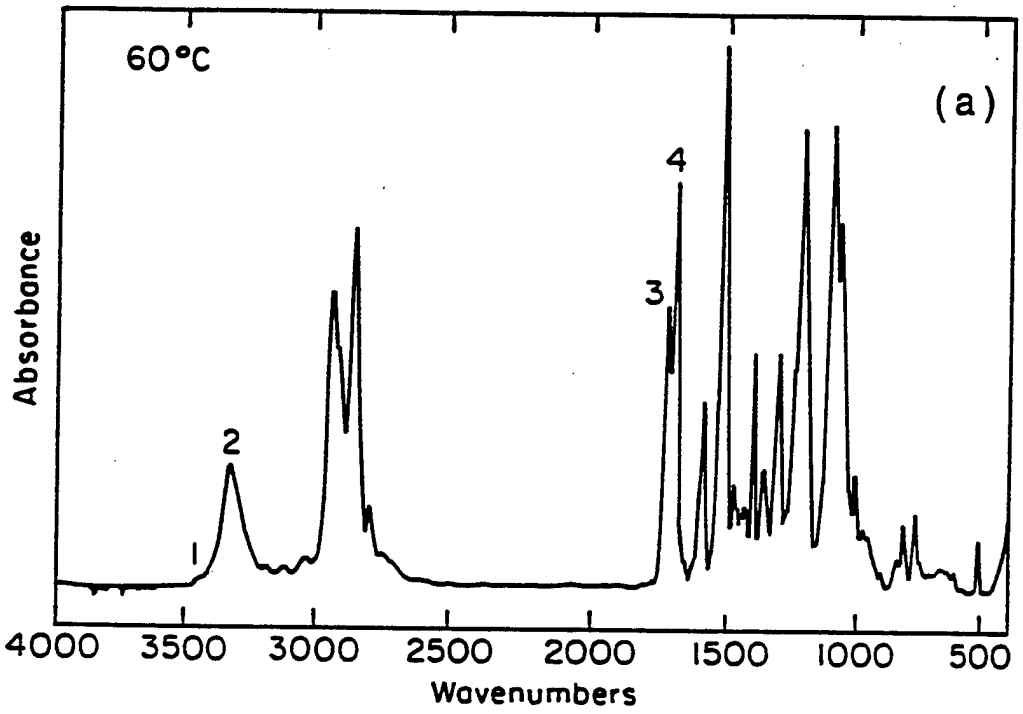
60°C
(a)
Absorbance
1
2
3
4
4000
3500
3000
2500
2000
1500
1000
500
Wavenumbers

Fig. 5a

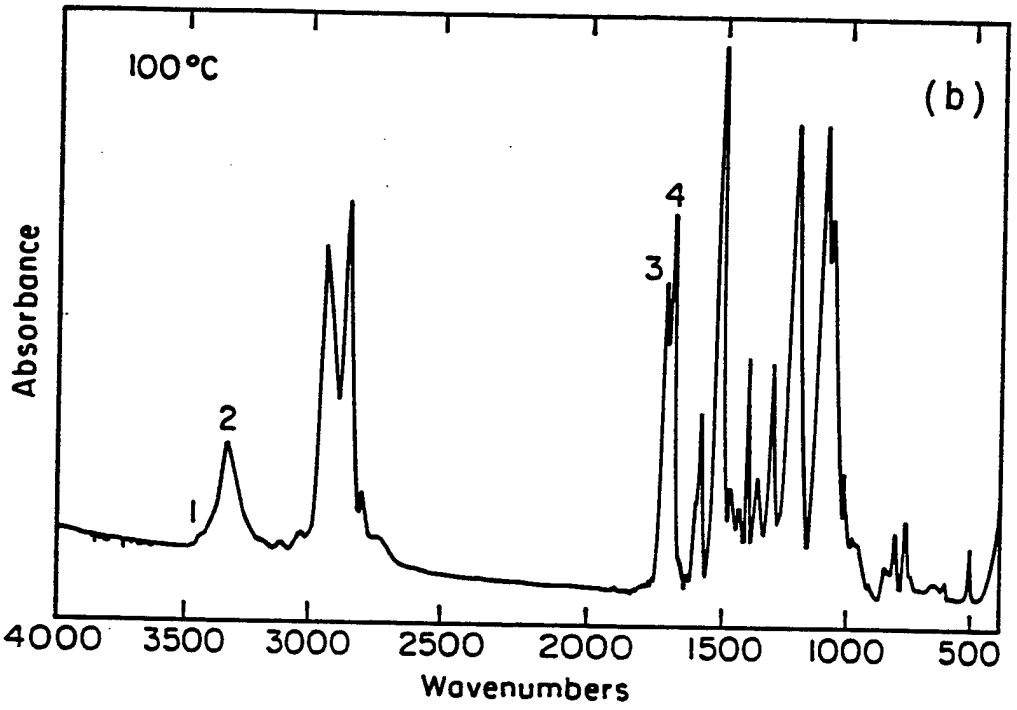
100°C
(b)
Absorbance
1
2
3
4
4000
3500
3000
2500
2000
1500
1000
500
Wavenumbers

Fig. 5 b

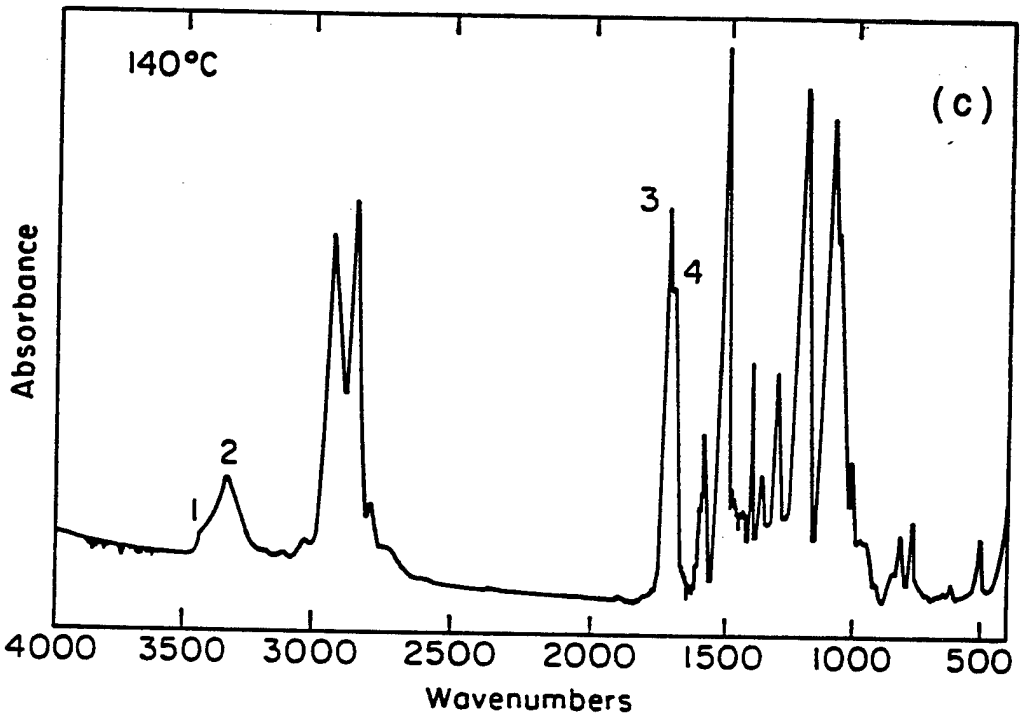
140°C
(c)
Absorbance
1
2
3
4
4000
3500
3000
2500
2000
1500
1000
500
Wavenumbers

Fig. 5c

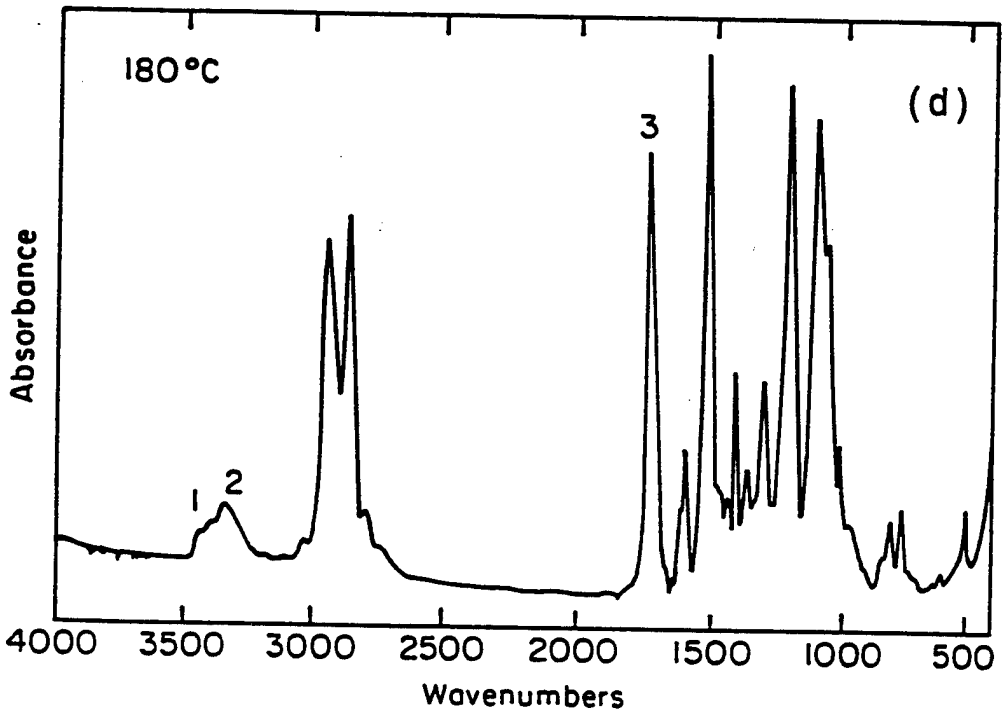
180°C
(d)
3
1
2
Absorbance
4000
3500
3000
2500
2000
1500
1000
500
Wavenumbers

Fig. 5 d

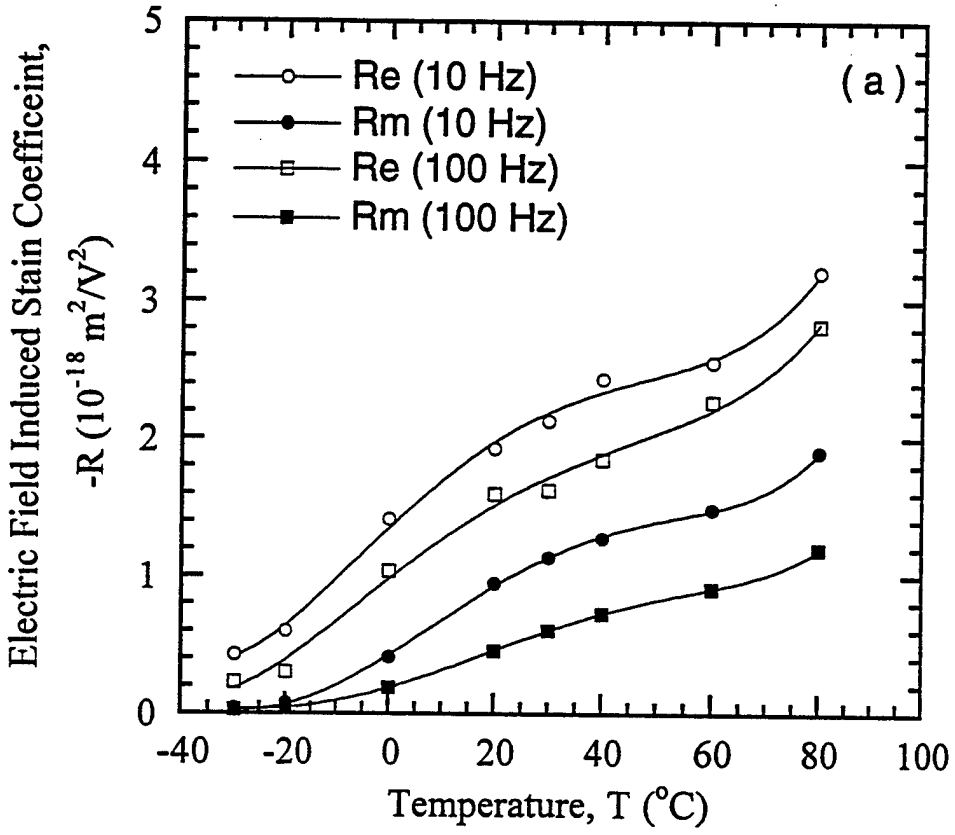
Re (10 Hz)
Rm (10 Hz)
Re (100 Hz)
Rm (100 Hz)
(a)
Electric Field Induced Stain Coefficeint,
-R (10^{-18} m^2/V^2)
Temperature, T (°C)
0
1
2
3
4
5
-40
-20
0
20
40
60
80
100

Fig. 6a

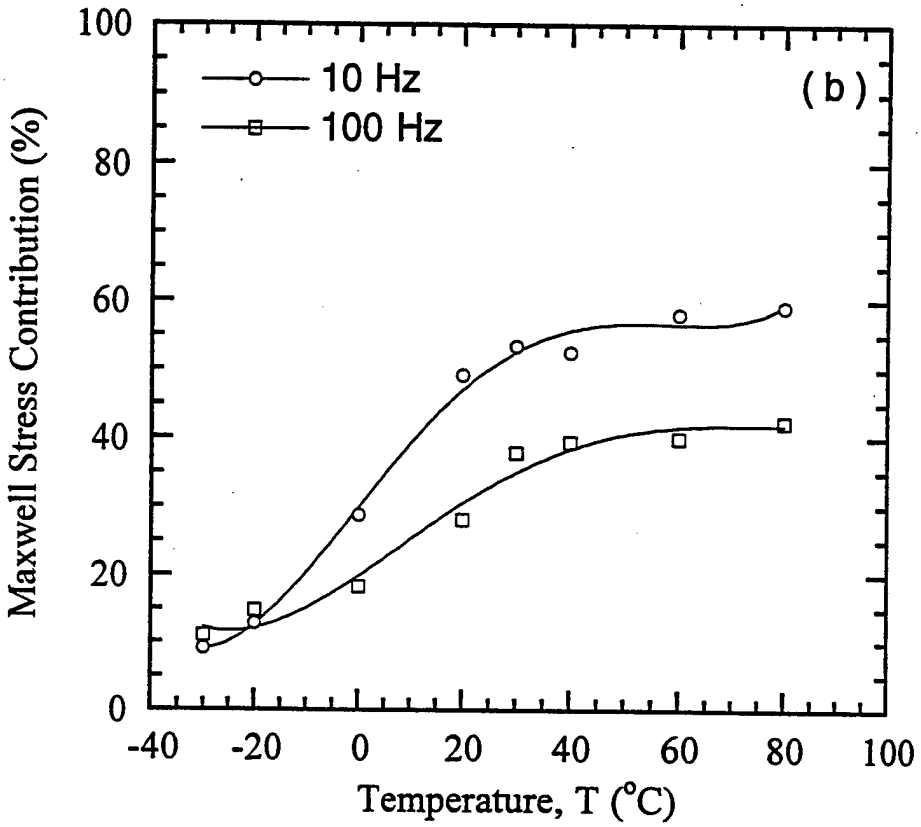
10 Hz
100 Hz
(b)
Maxwell Stress Contribution (%)
Temperature, T (°C)
0
20
40
60
80
100
-40
-20
0
20
40
60
80
100

Fig. 6b

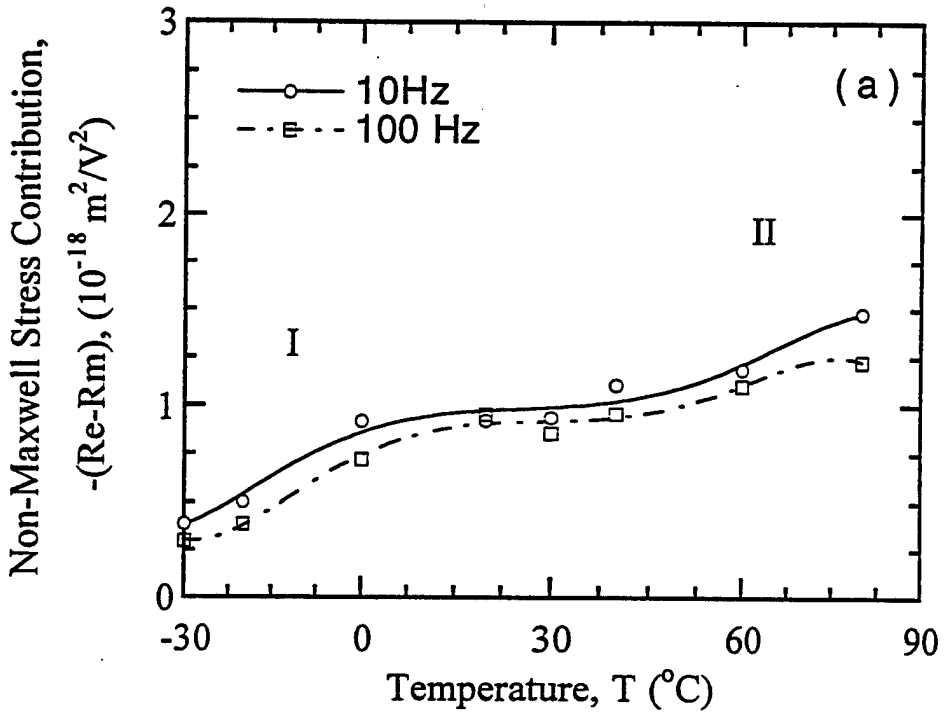
Non-Maxwell Stress Contribution,
-(Re-Rm), (10^{-18} m^2/V^2)
10Hz
100 Hz
(a)
I
II
3
2
1
0
-30
0
30
60
90
Temperature, T (°C)

Fig. 7a

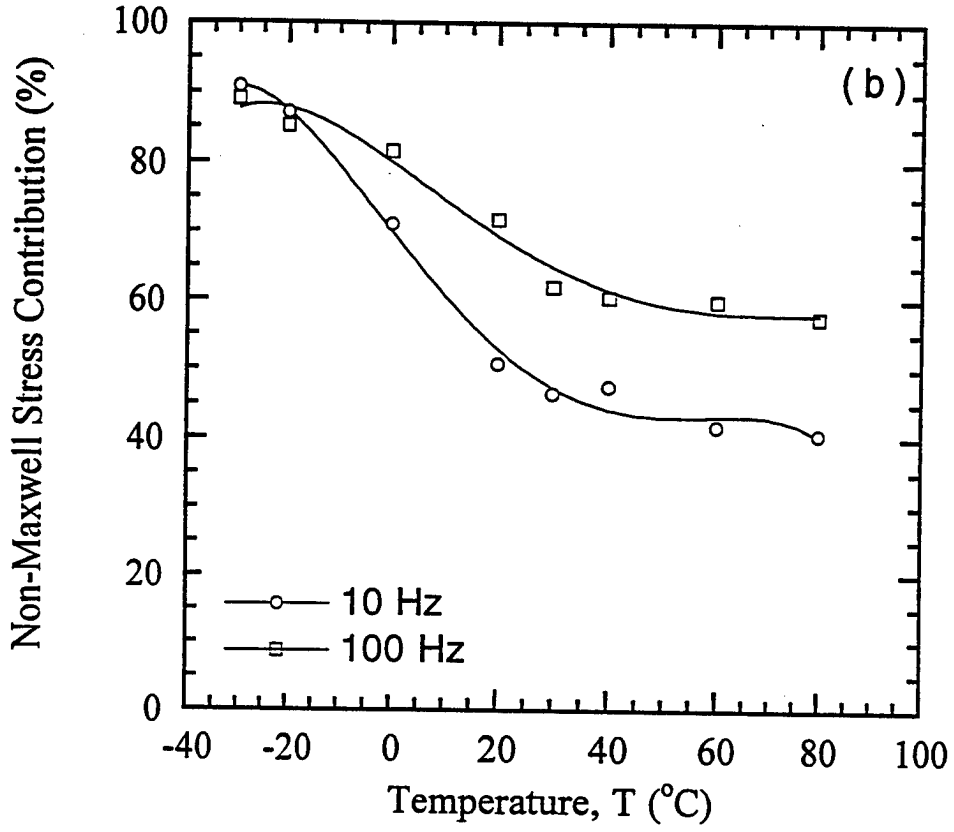
(b)
Non-Maxwell Stress Contribution (%)
100
80
60
40
20
0
-40
-20
0
20
40
60
80
100
Temperature, T (°C)
10 Hz
100 Hz

Fig. 7b

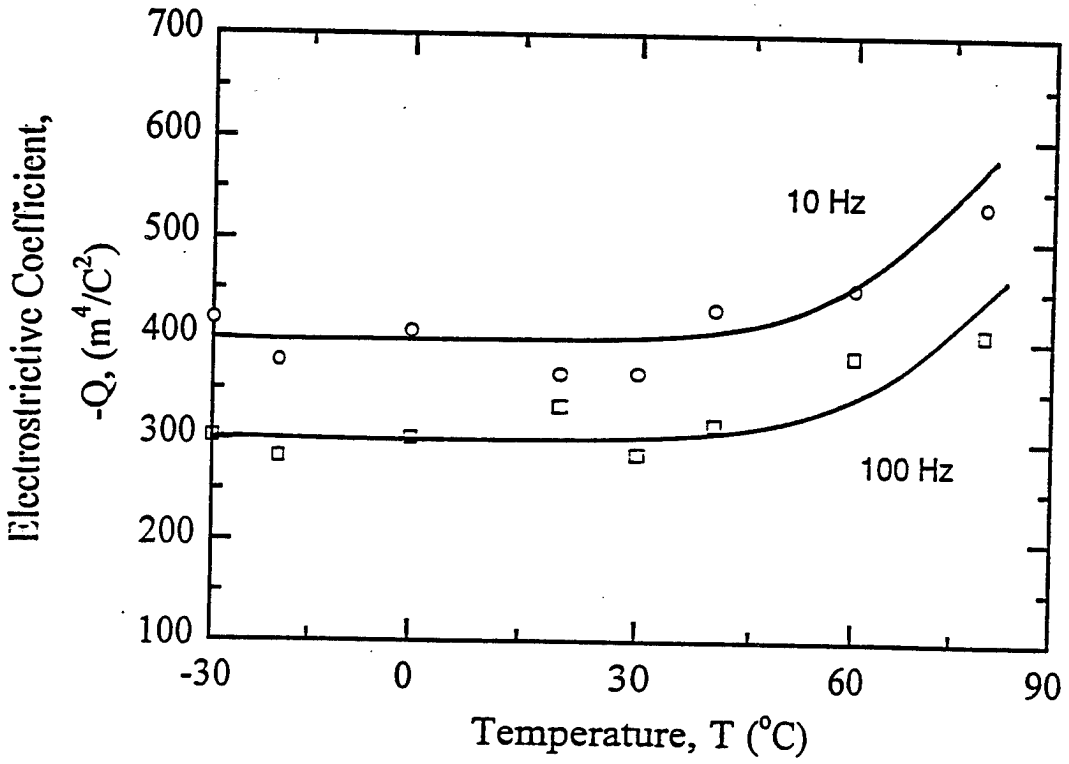
Electrostrictive Coefficient,
-Q, (m⁴/C²)
700
600
500
400
300
200
100
-30
0
30
60
90
Temperature, T (°C)
10 Hz
100 Hz

Fig. 8

COMPOSITE SENSORS

APPENDIX 38

HOLLOW PIEZOELECTRIC COMPOSITES

J. F. Fernandez*, A. Dogan, Q. M. Zhang, J. F. Tressler and R. E. Newnham.

Intercollege Materials Research Laboratory, The Pennsylvania State University, University Park, PA 16802.

* (Current adress: Electroceramic Department, Instituto de Ceramica y Vidrio, CSIC, 28500 Arganda del rey, Madrid, SPAIN)

Abstract

Current research activity in piezoelectric sensors and actuators is moving toward better resolution and higher power densities. Higher resolution and smaller sizes are needed in applications such as biomedical ultrasound, probes for invasive procedures, flow noise control, non-destructive testing, and automotive instrumentation. Piezoelectric transducers with enclosed hollow space offer several special advantages including low acoustic impedance, reduced mass, sensitivity to weak hydrostatic waves, and enlarged displacements through flextensional and rotational motions.

This paper describes recent advances in the processing and properties of five types of hollow piezoelectric composites with connectivity patterns of 0(0)-3, 1(0)-3, 2-0-2, 3-1(0) and 2(0)-2-2(0). Piezocomposites with hollow space included within the structure clearly demonstrate the advantages of functional composites in the field of smart systems.

Keywords: piezoelectrics, piezocomposites, actuators, hydrophones.

1. INTRODUCTION

An electromechanical transducer is a device that converts mechanical energy into electrical energy and vice versa. In a passive mode, operating at a low frequency, it can function as a hydrophone, detecting sound underwater. Typical operating frequencies lie in the low kilohertz range; since the acoustic wavelengths in that range are much larger than the transducer, it must respond to an isotropic stress. Sonar transducers are quite large. For ultrasonic imaging applications, piezolectric composites must transmit a strong acoustic pulse, and then detect the weak echoes reflected from the internal organ of the human body. Typical medical ultrasonic probes are a few centimeters in size and operate in the low megahertz range. Closely allied to medical ultrasonics are the pulse-echo acoustic imaging system used in non-destructive testing. These applications range from inspecting casting for internal flaws to the processing of integrated circuits. The operating frequencies extend to much higher values, nearing gigahertz in some cases. Another interesting class of pulse-echo devices that requires frequencies down to the mid kilohertz range involves imaging through air. Typical examples are autonomous vehicle guidance and manufacturing assembly. When designing a transducer for a particular application, the choice of transducer material is critical. Ideally the properties include high piezoelectric response in both transmission and receiving modes, while maintaining low density and high flexibility.

Lead Zirconate Titanate ceramic, PZT, is widely used as a transducer material because of its high piezoelectric coefficients. However, for hydrophones applications, PZT is a poor material for several reasons. The hydrostatic piezoelectric coefficient, d_h ($=d_{33}+2d_{31}$), is very low. The piezoelectric voltage coefficients, g_{33} and g_h, are also low because of the high dielectric constant of PZT (1800). Moreover, the acoustic matching of PZT with water is poor because of its high density (7.9 g/cm^3), ans the mechanical properties leave much to be desired because it is a brittle, inflexible ceramic.

In the last decade, a number of investigators have fabricated composites of PZT and polymers to overcome the aforementioned problems of PZT. The manufacure of piezoelectric composites requires careful replacement of a portion of the ceramic with polymer. This

replacement reduces the acoustic impedance of the piezoelectric ceramic, bringing it closer to that of water and the human body. It has been shown that it is possible to improve upon the piezoelectric properties of homogeneous PZT by the composite approach [1]. The concept that the connectivity of the individual phases controls the resulting properties has been demonstrated in a number of composites with different geometry and different connectivity patterns of the individual phases. The hydrostatic piezoelectric properties of these composites are far superior to those of single-phase PZT. However, some of the earlier composites are difficult to prepare and suffer a reduction in hydrostatic sensitivity with increasing pressure.

Early investigators concentrated on polymer-ceramic composites for use as hydrophones [2]. Several interesting connectivity patterns [3] were developed including 3-3 structures made by the replamine process [4] and by the fugitive phase technique [5,6]. Then came the more widely used 1-3 composites consisting of parallel PZT fibers embedded in a polymer matrix. These structures were made by extrusion [7], by dicing [8], and more recently by injection molding and lithographic lost-wax techniques [9]. The coupling between the ceramic fibers and the polymer matrix is important [10]. In optimizing hydrophone performance, the $d_h g_h$ product was chosen as a figure of merit. The 1-3 composite increases effective values of d_h and g_h by reducing the d_{31} piezoelectric coefficient and the dielectric constant while maintaining the large d_{33} coefficient.

The usefulness of the 1-3 composite in high frequency applications for non-destructive testing and medical diagnostics was recognized later [1-14]. Biomedical transducers require resonant frequencies in the 1-10 MHz range, high electromechanical coupling coefficients, low acoustic impedance, and broad bandwidth. The 1-3 transducers manufactured by Siemens [9] have thickness resonances of 5-10 MHz, coupling coefficient k_t=0.67, K=600, tan $\delta <$ 0.025, and a mechanical Q of about 10. Other variants on the basic 1-3 structure include the 1-2-3 composite with transverse load bearing fibers [14], and the 1-3-0 composite with a foamed polymer matrix [15], and the interesting woven fiber composites devised by Safari and co-workers [16-18].

Perhaps the simplest piezoelectric composite is the 0-3 transducer made by dispersing ceramic particles in a polymer matrix [19]. The NTK Piezo-Rubber films and cables are used as flexible hydrophones, keyboards, blood pressure cuffs, and musical instruments. They are made by hot-rolling $PbTiO_3$/PZT ceramic powder mixtures into a chloroprene rubber matrix [19-20]. New piezoelectric mechanical dampers have been produced using composites of piezoelectric-polymer-carbon black [21]. Damping characteristics are controllable by changing the conductivity through the carbon black concentration.

It was demonstrated by Safari [22] that based on the theory of connectivity, new composites with different connectivity patterns could be fabricated with enhanced performance. Most of the work involved composites with 3-1 and 3-2 connectivity. These composites were prepared by drilling either circular or square holes in prepoled PZT blocks, in a direction perpendicular to the poled axis, and by filling the drilled holes with epoxy. On the samples optimized for hydrophone performance, the g_h and $d_h g_h$ coefficients were about 4 and 40 times greater, respectively, for the 3-1 composites; and 25 and 150 times greater for the 3-2 composites compared to those of solid PZT. For 3-1 composites, there was practically no variation of g_h with pressure up to 8.4 MPa. In the case of 3-2 composites, there was a slight variation of g_h with pressure.

A new type of 2-2 piezoelectric ceramic polymer composite operated at the transverse piezoelectric mode has exceptionally high hydrostatic response, high reliability, and can made at low cost [23]. This type of composite made of PZT plates in a soft polymer matrix with elastically unidirectional face plates yield effective hydrostatic piezoelectric coefficient d_h of 6,000 pC/N and hydrostatic figure of merit $d_h g_h$ higher than 30,000 10^{-15} m^2/N.

There still exists a need to further improve the piezoelectric properties of these composites. A primary goal is to reproducibly fabricate composite transducers with high figures of merit and minimal pressure sensitivity, under hydrostatic loading, for hydrophone applications. On the other hand, there is also a need of new systems that can afford more complex functions combining sensing and actuating capabilities. This paper rewievs recent advances in the

processing and properties of different connectivity pattern composites based on the idea of hollow space within the structure.

2. HOLLOW PIEZOCOMPOSITES

Current research on piezoelectric sensors and actuators is moving toward miniaturized devices to achieve better resolution and higher power densities. High resolution and small sizes are needed in applications such as biomedical ultrasound, ultrasonics, probes for invasive procedures, flow noise control, nondestructive testing of composites, and automotive instrumentation. Higher frequencies and better impedance matching are specially advantageous in underwater transducers and biomedical ultrasonics. The introduction of open space in piezocomposites meets both of these criteria. In most of the cases, careful design of piezocomposites with open spaces leads to the development of reliable, robust, low cost transducers with improved piezoelectric properties. Table I summarizes recent trends in the design of piezocomposites with open spaces.

Perhaps, the first hollow piezoelectric composite were piezoelectric rings, ring stacks and tubes, thin wall or stripe elecroded. In that cases the hollow space allows reduction of the piezoelectric radial mode. At the same time, these structures permit the introduction of a stress bolt. This basic configuration is common to tunable transducers [24], active vibration control devices [25] and ultrasonic motors [26]. Another hollow piezoelectric family are the etched PZTs[27], in which hollow spiral patterns eliminate radial modes. Etched piezoelectric are utilized at higher frequencies for biomedical ultrasound diagnosis. Hollow piezoelectric composites possess many of the advantages of other composites and make possible the reduction of undesirable modes of vibration and most important, act as an amplifiers of the sensing and actuating characteristics of ceramics. Metals and epoxies contribute to the amplification factor by different mechanisms depending on the design.

3. BB TRANSDUCERS

BBs are hollow spherical transducers a few millimeters in diameter, about the same size as the metallic pellets used in air rifles (BB guns). PZT BBs are mass produced, by a patented forming process in which air is blown through a PZT slurry of carefully controlled viscosity [28]. The hollow spheres are 1-6 mm in diameter with wall thickness of 0.1 mm. Densities are about 1.3 g/cm^3 giving the BB a low acoustic impedance close to that of water and human tissue.

Two poling configurations were investigated (figure 1): radial poling and external top-to-bottom poling. Electroding the inside of the sphere was necessary to pole in the radial direction. A circular hole was drilled in the wall such that silver electrode could be injected into the sphere. The outside surface was also electroded, leaving a small, uncoated region around the hole. The two principal vibration modes associated with this configuration were a volumetric expansion mode or breathing mode and a wall thickness mode at much higher frequency. Top-to-bottom poling was accomplished using silver caps on opposite sides of the sphere, figure 1B. The principal mode of vibration was the distortion of the sphere to an ellipsoidal shape.

When electroded inside and out, and poled radially the BB becomes an omnidirectional transducer suitable for underwater or biomedical applications. For spheres with a 2.6 mm diameter and 90 μm thick walls, the resonant frequencies are 700 kHz for the breathing mode (d_{31}) and 10 MHz for the wall thickness mode (d_{33}) [29].

When embedded in a polymer matrix to form a 0-3 composite the BB spheres are surprisingly strong, and able to withstand large hydrostatic pressure without collapse. Close-packed transducer arrays are easily assembled [29]. Hydrostatic piezoelectric coefficients well in excess of 1000 pC/N have been measured.

BBs are small enough to be used in catheters for non-invasive surgery to act as beacons, sensors, and actuators [30]. More than a million such procedures are now carried out annually in the United States.

4. PZT MACARONI

Poling is sometimes difficult for the long, slender PZT fibers used in 1-3 composites. Electric breakdown often occurs before poling is complete, and the transducer is ruined. Lower poling and driving fields are obtained when the spaghetti-like PZT fibers are replaced with macaroni-like PZT tubules [31]. When electroded inside and outside, the thin-walled tubes are poled and driven radially at relatively modest voltages (figure 2). The effective piezoelectric constant in the radial direction can be tuned to positive, zero, and negative values by varying the ratio of the outer radius (R) to the inner radius (r) of the tube. For a suitable ratio of R/r, this effective constant can also be adjusted in sign and magnitude with a DC bias field for tubes made of electrostrictive materials [31]. Endcapped thin wall tubes (figure 2) also exhibit exceptionally high hydrostatic response with an effective d_h coefficient of -14,000 pC/N and effective figure of merit $d_h g_h$ higher than 10,000 10^{-15} m^2/N.

For large area applications, these tubes can be readily integrated into a 1-3 composite structure to provide low acoustic impedance and high piezoelectric activity. Acoustic transmitters requiring large uniaxial strains utilize the d_{31} constant of transverse piezoelectric mode composites. The effective d_{33} is proportional to the dimensional amplification factor, L/(R-r) where L is the length of the tube. A d_{33} constant of -10,000 pC/N [32] about 16 times greater than that of a conventional PZT ceramic, has been obtained for 1-3 tubular composites with R=1.27 mm, r=0.76 mm and L=13.5 mm.

A different approach to the 1-3 composites was recently reported [33] and consist of PZT rods covered by compliant soft epoxy sandwiched between stiffnes polycarbonate sheets machined to give grooves. The PZT rods extend beyond the polymer matrix and were capped with flat cover. This structure generates an air cavity. The figure of merit is 22,460 10^{-15} m^2/N, about six times larger than similar configurations without cavities. This composite, however, showed instability under steady state hydrostatic preassure, but the approach suggested new designs for tubular 1-3(0) piezocomposites with improved properties.

5. ZIG- ZAGs.

Zig-zag actuators are split bimorphs in which two ceramic legs are driven independently to generate synchronized horizontal and vertical displacements. The legs are joined in a teepee-like configuration which imparts a rolling motion to the load. Typical motions are in the 1-30 μm range and look to be useful in piezomotor and conveyor belt applications because of the ability to drive a load in two directions [34]. The required motion for a linear motor can be achieved by driving one leg with a sine wave and the other leg with a sine wave tath is 90° out of phase. If the second leg is 90° ahead of the first, the resulting motion will be clockwise, and moves the load from right to left. If the second leg is 90° behind the first, the resulting motion will be counterclockwise and the load will be moved from left to right. A schematic view of the resulting motion when the actuator is driven in this manner is shown in figure 3. The mechanical impedance can be optimized by changing the angle between the legs, and the actuator's working parameter controlled by changing the driving voltage and frequency.

6. HONEYCOMB CERAMIC COMPOSITES

The basic structure of this composite is schematically illustrated in figure 4, where the ceramic is poled perpendicular to the z-direction as indicated [35]. The transducer is operated in the transverse piezoelectric mode (TP). It should be mentioned that two types of honeycomb composite transducers were investigated earlier [36-37]. The earlier honeycomb transducers were operated in the longitudinal piezoelectric mode. Due to the limitations of this mode, the effective hydrostatic piezoelectric response of the earlier honeycomb composite transducers are an order of magnitude smaller than that of the TP honeycomb transducers. An endcapped honeycomb structure was made by placing thin layers of epoxy over the two ends to block the openings. When this endcapped honeycomb is subjected to hydrostatic pressure, the d_{33} response is eliminated and the piezoelectric response comes from the d_{31} component of the piezoelectric. This is due to fact that the stress component perpendicular to the wall is zero because the interior is filled with air. The stress field in the x-, y- and z-directions induces three d_{31} responses in the corresponding ceramic plates. Exceptionally high hydrostatic

piezoelectric d_h values up to -4,700 pC/N were obtained. One of the biggest advantages of such a composite is the extrusion process that permits the development of complex geometries by a cost effective procedure.

7. MOONIES AND CYMBALS.

In recent years, piezoelectric and electrostrictive ceramics have been used in many actuator applications. To meet these needs a new type of composite actuator based on a flextensional transducer has been developed [38-42]. This ceramic-metal composite actuator, or "moonie", consists of either a piezoelectric ceramic disc or a multilayer stack, sandwiched between two specially designed metal end caps. The basic configuration of the moonie is shown in figure 5. The metal endcaps serve as mechanical transformers for converting and amplifying the lateral motion of the ceramic into a large axial displacement normal to the end caps. Both the d_{31} ($=d_{32}$) and d_{33} coefficients of the piezoelectric ceramic contribute to the axial displacement of the composite. Figure 6 shows the enhanced displacement of the moonie actuator compared to that of a PZT ceramic. This design provides a sizable displacement, as well as a large generative force. In other words, it bridges the gap between the two most common types of actuators, the multilayer and the bimorph [43]. The shallow spaces under the end caps produce a substantial increase in strain by combining the d_{33} and d_{31} coefficients of the ceramic. It is attractive for hydrophone, transceiver and actuator applications, and is especially advantageous for use as a non-resonant, low frequency projector in deep water.

Hydrophone sensitivity depends on d_h, the hydrostatic piezoelectric charge coefficient, and g_h, the hydrostatic piezoelectric voltage coefficient. The moonie transducer was introduced as a hydrophone having the highest figure of merit, $d_h\, g_h = 50{,}000 \times 10^{-15}$ m^2/N [44], about 500 times larger than the uncapped PZT ceramic. The moonie also possesses high capacitance and excellent pressure tolerance. The stress distribution within the moonie hydrophone under a hydrostatic pressure was determined using Finite Element Analysis. Extensional stresses along the radial and tangential directions are generated under a hydrostatic pressure, and contribute significantly to the very high figure of merit of the moonie.

In addition to this, the effect on prestresses caused by thermal treatment of the moonie were also estimated. The maximum stress concentration reached several hundred MPa. Compressive stresses of 300 MPa are generated along the radial direction at the inner bonding edge, and 400 MPa extensive stresses occur in the cavity near the top of the endcap.

The combined effect of high hydrostatic pressure (7 MPa corresponding to a 700 m water depth), and thermal processes were also estimated. Even 7 MPa hydrostatic pressure causes little deformation to the moonie hydrophone because the effect of relatively large prestress pressures exceed those of the hydrostatic environment. This is one of the reasons that the moonie hydrophone has high pressure tolerance.

Moonie actuators also have very high effective d_{33} coefficients depending on the geometry. Effective d_{33} coefficients as large as 13,000 pC/N were obtained with brass caps 0.3 mm thick, but the value decreases rapidly toward the edge of the transducer. This is approximately thirty times higher than the d_{33} of a PZT-5A ceramic. The characteristics of the moonie actuator depend markedly on both the geometry and the choice of materials. Among the geometric parameters, cavity diameter, cavity depth, and cap thickness are the main parameters which control the displacement of a moonie actuator. An applied 1 kV/mm electric field produces a displacement of 22 μm at the center of a carefully designed brass-capped moonie actuator. By stacking two identical single moonies with these dimensions, the double stacked moonie actuator produces a 40 μm displacement, (figure 6).

The generative force of the moonie was measured experimentally and calculated by FEA. The calculated maximum force (30 N) at the effective working area of 3 mm^2 agrees with that obtained by the extrapolation of the experimental data.

For actuators, however, the stress concentration on the brass endcap just above the bonding layer reduces the effective force transfer from the PZT to the cap. It is possible to eliminate part of the stress concentration by removing a portion of the endcap just above the bonding region where the maximum stress concentration is observed. An enhancement in properties has been obtained by introducing a ring shaped groove on the exterior of the end caps [44]. The largest displacement was achieved when the groove was positioned above the

bonding layer. The deeper and wider the groove, the higher the displacement. Since the stress concentrates at the groove edges, this becomes a potential source of fatigue and may eventually produce failure under long term usage.

The effect of cavity diameter on the piezoelectric coefficient of moonie transducers with different cavity depths is shown in figure 7 and 8 [45]. The effective piezoelectric coefficient decreases with increasing the cavity diameter and cavity depth. After a certain cavity depth, the cavity does not transfer the applied stress to the ceramic efficiently.

Figure 9 shows the fatigue test of a moonie actuator with different end cap thicknesses under a high cyclic electric field (1kV/mm, 100 Hz) [45]. Experiments were carried out at room temperature with no load. After cycling 10^7 times, a deviation in displacement of only ± 0.8% was observed. The reason for the deviation is probably due to the effect of environmental temperature change on the bonding layer. Before and after the cycling test, the admittance spectra of the actuators were recorded with no significant changes. The resonant and anti-resonant frequencies as well as their peak amplitudes were the same as the original values observed before the fatigue test.

A modified moonie with "cymbal" shaped endcaps has recently been developed [45-46], figure 10. The endcaps are fabricated by punching metal sheets. The cymbal design removed most of the region with stress concentration, and yields higher and more reproducible displacements. Even though this new design looks similar to the earlier moonie design, it has a different displacement mechanism. Displacement is primarily a result of flexural motion of moonie endcaps. For the cymbal, the displacement is created by the combination of flexural and rotational motion of the endcaps. Figure 11 shows the displacement values and the position dependence of the different endcap designs with fixed cavity depth (0.2 mm) and cavity diameter (0.9 mm). The cymbal actuator generated a 40 μm displacement which is about twice the moonie displacement.Because of its flexural nature, the displacement of the moonie actuator is highly dependent on position. Displacement decreases dramatically away from the center of the endcap, where the maximum displacement is observed, at the edgeof the moonie actuator the displacement is equal to that of the PZT. A moonie with grooved endcaps

show significantly less position dependence of displacement. The cymbal actuator exhibits a more uniform displacement over a wide section about 4 mm in diameter at the center of the endcap. The large flat contact surface of the new endcap design makes it more practical to stack the individual actuators together to achieve higher displacement. Additionally, the new multistacked cymbal structure is more stable under uniaxial external loading. This actuator consists of five elements, 12.7 mm in diameter, 10 mm total thickness, and exhibits a displacement of 175 μm.

Properties and performance of ceramic-metal composites such as the moonie and cymbal, can be tailored through geometrical design and material selection [47]. Because of their large displacement and charge, moonie and cymbal composites show great potential for several applications [44-49], including hydrophone sensors with figure of merit higher than 100,000 10^{-15} m^2/N, transceivers for fish finders, positional actuators and highly sensitive accelerometers [49].

8. SMART MATERIALS

Smart materials [50] have the ability to perform both sensing and actuating functions. Passively smart materials respond to external change in a useful manner without assistance, whereas actively smart materials have a feedback loop which allows them to both recognize the change through an actuator circuit. Many smart materials are analogous to biological systems; the piezoelectric hydrophones described earlier are similar to the thin fibers and air bladders by which a fish senses vibrations. Piezoelectrics with electromechanical coupling, shape memory materials that can "remember" their original shape, electrorheological fluids with adjustable viscosities, and chemical sensors which act as synthetic equivalents to the human nose are examples of smart electroceramics. "Very smart" materials, in addition to sensing and actuating, have the ability to "learn" by altering their property coefficients in response to the environment. Integration of these different technologies into compact, multifunction packages is the ultimate goal of research in the area of smart materials. Hollow

piezoelectric composites introduce new tools in the search of smart and very smart materials. Thepossibility of integrating piezoelectric composites with open space intoduces another family of sensors and actuators with complex functions. Substantial progress in this field will occur during the coming decades.

A new vibration control device based on the moonie actuator has been developed by Tressler [51], figure 12. The actuator portion of the device consist of the standard (11 mm diameter, 2 mm thick) moonie, with a small piezoelectric ceramic embedded in the upper end cap to serve as a sensor (0.1 mm thick). This prototype sensor/actuator piezocomposite is capable of detecting and suppressing in real time, small vibration displacements (< 1 μm), with low force (< 100 gf). The dynamic frequency range of the device spans from 100 Hz to at least 2500 Hz. The sensor detects sinusoidal vibrations normal to the actuator surface, via a feedback loop, and sends a signal of appropiate amplitude and phase shift to the actuator so that it effectively cancel is the external vibration. Potential aplications for this device include active optical systems, rotor suspension systems, and other low level vibration suppression devices

ACKNOWLEDGMENTS

The authors would like to express their gratitude for the support to the following agencies and organizations: Office of Naval Research Contract no. N00014-92 J 1510, National Science Foundation Grant no. DMR-9223847, Spanish Science Ministry (CICYT MAT94-807 and DGICYT PR94-028), Turkish Science and technology Council and Middle East Technical University, Ankara.

REFERENCES

[1] R. E. Newnham, Composite Electroceramics, *J. Mat. Education*, 7 (1985) 605-651.

[2] T. R. Gururaja, R. E. Newnham, K. A. Klicker, S. Y. Lynn, W. A. Schulze, T. R. Shrout and L. J. Bowen, Composite Piezoelectric Transducers, in *Proceedings of the IEEE Ultrasonics Symposium*, vol. 2 (1980) 576-581.

[3] R. E. Newnham, D. P. Skinner and L.E. Cross, Connectivity and Piezoelectric-Pyroelectric Composites, *Mat. Res. Bull.* 13 (1978) 525-536.

[4] D. P. Skinner, R. E. Newnham and L. E. Cross, Flexible Composite Transducers, *Mat. Res. Bull.* 13 (1978) 599-607.

[5] T. R. Shrout, W. A. Schulze and J. V. Biggers, Simplified Fabrication of PZT/polymer composites, *Mat. Res. Bull.* 14 (1979) 1553-59.

[6] K. Rittenmyer, T. R. Shrout, W. A. Schulze and R. E. Newnham, Piezoelectric 3-3 Composites, *Ferroelectrics* 41 (1982) 189-195.

[7] K. A. Klicker, J. V. Biggers and R. E. Newnham, Composites of PZT and Epoxy for Hydrostatic Transducer Applications, *J. Am. Ceram. Soc.* 64 (1981) 5-9.

[8] H. P. Savakus, K. A. Klicker and R. E. Newnham, PZT Epoxy Piezoelectric Transducers: A Simplified Fabrication Procedure, *Mat. Res. Bull.* 16 (1981) 677-680.

[9] G. Preu, A. Wolff, D. Crames and U. Bast, Microstructuring of Piezoelectric Ceramics, *Euro-Ceramics II* Vol.3 (1991) 2005-10.

[10] C. Richard, P. Eyraud, L. Eyraud, A. Pelourson and M. Richard, A Pressure Dependence Approach of New 1.3.1 Piezoelectric Polymer Composite for Hydrophone, *Euro-Ceramics II* Vol.3 (1991) 2001-4.

[11] T. R. Gururaja, W. A. Schulze, L. E. Cross, R. E. Newnham, B. A. Auld and Y. J. Wang, Piezoelectric Composite Materials for Ultrasonic Transducer Applications. Part I: Resonant Modes of Vibration of PZT Rod-Polymer Composites, *IEEE Transactions on Sonics and Ultrasonics*, Vol. 32, no. 4 (1985) 481-498.

[12] T. R. Gururaja, W. A. Schulze, L. E. Cross, R. E. Newnham, B. A. Auld and Y. J. Wang, Piezoelectric Composite Materials for Ultrasonic Transducer Applications. Part

II: Evaluation of Ultrasonic Medical Applications, *IEEE Transactions on Sonics and Ultrasonics*, 32, 4 (1985) 499-513.

[13] W. Smith, The Role of Piezocomposites in Ultrasonic Transducers, *Proceedings of the 1988 IEEE Ultrasonics Symposium* (1988) pp. 755-66.

[14] M. J. Haun, R. E. Newnham and W. E. Schulze, 1-2-3 and 1-2-3-0 Piezoelectric Composites for Hydrophone Application, *Adv. Ceram. Mat.* 1, 4 (1986) 361-365.

[15] M. J. Haun and R. E. Newnham, An Experimental and Theoretical Study of 1-3 and 1-3-0 Piezoelectric PZT-Polymer Composites for Hydrophone Applications, *Ferroelectrics* 68 (1986) 123-129.

[16] R. J. Card, M. P. O'Toole and A. Safari, Method of Making Piezoelectric Composites, U.S. pat # 4,726,099 (1988).

[17] J. Giniewicz, R. E. Newnham and A. Safari, (Pb,Bi)(Ti,Fe,Mn)O_3 -Polymer 0-3 Composites for Hydrophone Applications, *Ferroelectrics* 73 (1987) 405-418.

[18] S. S. Livneh, S. M. Ting and A. Safari, Development of Fine Scale and Large Area Piezoelectric Ceramic Fiber Polymer Composites for Transducer Applications, *Ferroelectrics* 157 (1994) 421-426.

[19] H. Banno, Recent Developments of Piezoelectric Ceramic Products and Composite of Synthetic Rubber and Piezoelectric Ceramic Particles, *Ferroelectrics* 50 (1993) 329-338.

[20] H. Banno and K. Ogura, Piezoelectric Properties at Polarization Reversal Process and Coercive Force of 0-3 Composite Polymers and Ceramic Powder Mixture of PZT and $PbTiO_3$, *Jap. J. Applied Physics* 30,93 (1991)2250-52.

[21] Y. Suzuki, K. Uchino, H. Gouda, M. Sumita, R. E. Newnham and A. R. Ramachandran, Mechanical Damper Using Piezoelectric Composites, *J. Ceram. Soc. Jap. (Int. Ed.)* 99 (1991) 1096-98.

[22] A. Safari, Perforated PZT-Polymer Composites with 3-1 and 3-2 Connectivity for Hydrophone Applications, Ph.D. Thesis, The Pennsylvania State University, University Park, PA (1983).

[23] Q. M. Zhang, J. Chen, H. Wang, J. Zhao, L. E. Cross and M. C. Trottier, A Transverse Piezoelectric Mode 2-2 Piezocomposite for Underwater Transducer Applications, *IEEE Transactions on Ultrasonics, Ferroelectric and Frequency Control* (in press).

[24] M. A. Blaskiewicz, Tunable Transducers, Ph.D. Thesis, The Pennsylvania State University, University Park, PA (1994).

[25] A. R. Ramachandran, Complex Electromechanical Coefficients of Piezoelectric Composites: Applications to Pasive Vibration Damping, Ph.D. Thesis, The Pennsylvania State University, University Park, PA (1992).

[26] S. Ueda and U. Tomikawa, Ultrasonic Motor: Theory and Applications, Oxford University Press, (1993) Oxford.

[27] S. Troiler, Q. C. Xu and R. E. Newnham, Preparation of Chemically Etched Piezoelectric Resonator for Density Meter and Viscosimeters, *Mat Res. Bull.* 22,4(1987)1267-1274.

[28] L.B. Torobin, Methods of Making Hollow, Porous Microspheres, U.S. Patent #4,671,909, (1987).

[29] R. Meyer Jr, H. Weitzing, Q. Xu, Q. Zan and R. E. Newnham, Lead Titanate hollow Sphere Transducers, *J. Am. Ceram. Soc.* 77,6 (1994) 1669-72.

[30] D. Kilkomerson, B. Gardineer and H. Hojeibane, Quasi-Omnidirectional Transducers for Ultrasonic Electro-Beacon Guidance of Invasive Devices, *Proceedings of SPIE* 1733 (1992) 154-65.

[31] Q. M. Zhang, H. Wang and L. E. Cross, Piezoelectric Tubes and Tubular Composites for Actuator and Sensor Applications, *J. Mater. Sci.* 28 (1993) 3962-68.

[32] H. Wang, Q. M. Zhang, L. E. Cross and M. C Trottier, Transverse Piezoelectric Mode Composites: A New Design Approach for Smart Material Applications", *Proceedings of SPIE Conference on Smart Structures and Materials.* (1995)

[33] C. Kim, K. M. Rittenmeyr and M. Kahn, 1-1-3 Piezocomposite for Hydrophone Transducer, *Ferroelectrics* 156 (1994) 19-24.

[34] M.G. Matsko, Q. C. Xu and R. E. Newnham, Zig-Zag Piezoelectric Actuators: Geometrical Control of Displacement and Resonance, *J. of Intelligent Mat. Systems and Structures*, (in press).

[35] Q.M. Zhang, H. Wang, J. Zhao, J. T. Fielding, R. E. Newnham and L. E. Cross, A High Sensitivity Piexzoelectric Transducer Based on Transverse Piezoelectric Mode Honeycomb Ceramic Composites, *IEEE Transactions on Ultrasonics, Ferroelectric and Frequency Control* (in press).

[36] T. R. Shrout, L.J. Bowen and W. A. Schulze, Extruded PZT-Polymer Composites for Electromechanical Transducer Applications, *Mater. Res. Bull.* vol 15 (1980) 1371-80.

[37] A. Safari, A. Halliyal, R. E. Newnham and I. M. Lachman, Transverse Honeycomb Composite Transducers, *Mater. Res. Bull.* Vol 17 (1982) 301-9.

[38] R. E. Newnham, Q. C. Xu and S. Yoshikawa, Transformed Stress Direction-Acoustic Transducer, U.S. Patent # 4,999,819, March 12, (1992).

[39] Q. C. Xu, S. Yoshikawa, J. Belsick and R. E. Newnham, Piezoelectric Composites with High Sensitivity and High Capacitance for Use at High Pressures, *IEEE Transactions on Ultrasonics, Ferroelectrics and Frequency Control*, 38, 6 (1991) 634-639.

[40] Y. Sugawara, K. Onitsuka, S. Yoshikawa, Q. Xu, R. E. Newnham and K. Uchino, Metal-Ceramic Composite Actuators, *J. Am. Ceram. Soc.* 75, 4 (1992) 996-998.

[41] A. Dogan, Q. C. Xu, K. Onitsuka, S. Yoshikawa, K. Uchino and R. E. Newnham, High Displacement Ceramic-Metal Composite Actuators (Moonie), *Ferroelectrics* 156 (1994) 1-6.

[42] K. Onitsuka, A. Dogan, Q.C. Xu, J. Tressler, S. Yoshikawa, and R.E. Newnham, Design Optimization for Ceramic-Metal Composite Actuators (Moonie), *Ferroelectrics* 156 (1994) 37-42.

[43] K. Uchino, Piezoelectric and Electrostrictive Actuators, Morikita Publication,Tokyo, Japan (1986).

[44] K. Onitsuka, Effects of Bonding and Geometry on the Flextensional Transducer, "Moonie", Ph.D. Thesis, The Pennsylvania State University, University Park, PA (1993).

[45] A. Dogan, Flextensional Moonie and Cymbal Actuators, Ph.D. Thesis, The Pennsylvania State University, University Park, PA (1994).

[46] A. Dogan and R. E. Newnham, Flextensional Cymbal Transducer, U.S.A. Patent, PSU Invention Diclosure No 94-1395 (1994).

[47] J. F. Fernandez, A. Dogan, J. T. Fielding, K Uchino and R. E. Newnham, "Tailoring High Displacement Performance of Ceramic-Metal Composite Actuators "Cymbals", *IEEE UFFC*, .submitted.

[48] R. E. Newnham, A. Dogan, J. T. Fielding, J. F. Fernandez, D. Smith, J. Tressler, J. Wallis, K. Uchino, W. Zhu, Moonies, Cymbals and BB's, *Office of Naval Research Transducer Materials and Transducers Workshop*, April 1995 State College, PA, USA.

[49] B. Koc, A. Dogan, J. F. Fernandez, K. Uchino and R. E. Newnham, "Accelerometer Application of the Moonie and Cymbal" *in preparation.*

[50] R. E. Newnham and G. Ruschau, Smart Electroceramics, *J. Am. Ceram. Soc.* 74, 3 (1991) 463-480.

[51] J. F. Tressler, Q. C. Xu, S. Yoshikawa, K. Uchino and R. E. Newnham, Composite Flextensional Transducer for Sensing and Actuating, *Ferroelectrics* 156 (1994) 67-72.

Jose F Fernandez was born in Madrid, Spain on September 23, 1961. He received the B. S. degree in applied physics in 1985, M.S. degree in physics in 1987 and Ph.D in physics in 1990, all of them from Autonomous University of Madrid, Spain.
He is a staff member of the Electroceramics Department at the Instituto de Ceramica y Vidrio, CSIC, Arganda del Rey, Madrid, Spain. In 1994-95 he was a Visiting Scientist at the Materials Research Laboratory, Pennsylvania State University. His research interest are in the processing of ceramics, dielectric and piezoelectric ceramics and composite materials for electronic aplications.
He is a member of the American Ceramic Society and Spanish Ceramic and Glass Society.

Aydin Dogan was born in Ankara, Turkey, on February 22, 1966. He received the B.S. degree in materials science & metallurgical engineering in 1988 and the M.S. degree in 1990, both from Middle East Technical University in Ankara-Turkey. He received its Ph.D. in Solid State Science at the Pennsylvania State University, University Park, PA, in 1994. His research interests include electronic ceramics, sensors and actuators, smart materials and systems, and ferroelectrics.
He is a member of the Materials Research Society and is a NATO- TUBITAK science fellowship recipient.

Q. M. Zhang was born in ZeiJian, China in 1957. He received the B.S. degree from Nanjing University, China in 1981 and Ph. D. degree from Pennsylvania State University, University Park, in 1986. From 1986 to 1988, he was a Post-Dr at Materials Research Laboratory at Penn State. From 1988 to 1991, he was a research scientist at Brookhaven National Laboratory, NY, conducting research on interface, surface, and thin film with neutron and synchrotron X-ray scattering techniques.
He is currently an Associated Professor of Materiales and Senior Research Associate at the Intercollege Materials Research Laboratory of the Pennsylvania State University. His research interest invlove piezoceramic and polymer actuator, sensor, and transducer applications: new design and modeling of piezocomposites: smart materials and structures: novel, artificial, and nano-composite materials; effects of defect structure on the dielectric, piezoelectric, and elastic properties of ferroelectric materials; and structure studies on the interfaces and defects in ferroelectrics.
Dr. Zhang is member of American Ceramic Sociaty, American Physical Society, Materials Ressearch Society, and Neutron Scattering Society of America.

James F. Tressler was born in Lock Haven, PA, on May 2, 1968. He received the B.S. degree in ceramic science and engineering in 1991 and the M.S. degree in 1993, both from the Pennsylvania State University, University Park, PA. In 1994, he was a Visiting Scientist at the Sony Corporation Research Center in Yokohama, Japan, where he was involved in the processing of dielectric thin films. His research interests are in the areas of smart materials and systems, composites, and thin films.

Robert E. Newnham was born in Amsterdam, NY, on March 28, 1929. He received the B.S. degree in mathematics in 1950 from Hartwick College, Oneonta, NY, the M.S. degree in physics and mineralogy from the Colorado State University, Fort Collins, CO, and the Ph.D. in crystallography in 1960 from Cambridge University, Cambridge, England.
He is ALCOA Professor of Solid State Science at the Materials Research Laboratory at the Pennsylvania State University, University Park, PA. Previously, he was a staff member of the Laboratory for Insulation Research at the Massachusetts Institute of Technology, Cambridge, MA. His research interests are in structure-property relations, electroceramics, and composite materials for electronic applications.

TABLE I
New trends in piezocomposite design with open spaces

Previous			New design		
Connectivity pattern	Type	Name	Connectivity pattern	Type	Name
0-3	PT/PZT in polymer	Piezorubber	0(0)-3	PZT hollow spheres	BBs
1-3	PZT fiber in polymer	PZT spaghetti	1(0)-3	PZT tubules in polymer	PZT macaroni
3-1	PZT with drilled holes	Perforated PZT	3-1(0)	PZT honeycomb skeleton	Honeycomb
2-2	Cantilever	PZT bimorph	2-0-2	split bimorph	Zig Zag
2-2	Tape cast PZT multilayer	PZT actuator	2(0)-2-2(0)	Capped PZT	PZT moonie and cymbal

FIGURE CAPTIONS

Figure 1 Electrode design for (A) the radial poling configuration showing the small uncoated ring used to separate the inner and the outside electrode, and (B) the electrode configurtion for top-to-bottom poling. Shaded areas represent the air-dry silver coating.

Figure 2 Schematic of capped 1(0)-3 piezocomposite configuration showing a single PZT tube poled radially.

Figure 3 Schematic view of the Zig-Zag Actuator motion being driven by sine and cosine waves.

Figure 4 Schematic drawing of a honeycomb ceramic structure. Poling directions are indicated in the insert of the figure. Notice the difference in the poling directions between neighboring cells.

Figure 5. The geometry of the ceramic-metal composite actuator "Moonie". The arrows describe the displacement directions when the moonie is driven by a field parallel to the poling direction of the ceramic.

Figure 6. The displacement characteristics of the moonie actuator as a function of the applied electric field. Dimensions: d_m=12.7, d_p=12.7, d_c=9.0, h=0.2, t_p=1.0, t_m=0.3 (all in mm).

Figure 7. Effect of cavity diameter and cavity depth on the effective piezoelectric coefficient of the moonie. Dimensions:d_m=12.7, d_p=12.7, t_p=1.0 (all in mm).

Figure 8. Effect of End cap thickness on the effective piezoelectric coefficient of the moonie. Dimensions:d_m=12.7, d_p=12.7, d_c=9.0, t_p=1.0 (all in mm).

Figure 9. Fatigue characteristics of the moonie actuators.

Figure 10. The geometry of the ceramic-metal composite actuator "Cymbal".The arrows describe the displacement directions when the moonie is driven by a field parallel to the poling direction of the ceramic.

Figure 11. The position dependence of displacement for different endcap designs.

Figure 12. Integrated sensor and actuator for active vibration control.

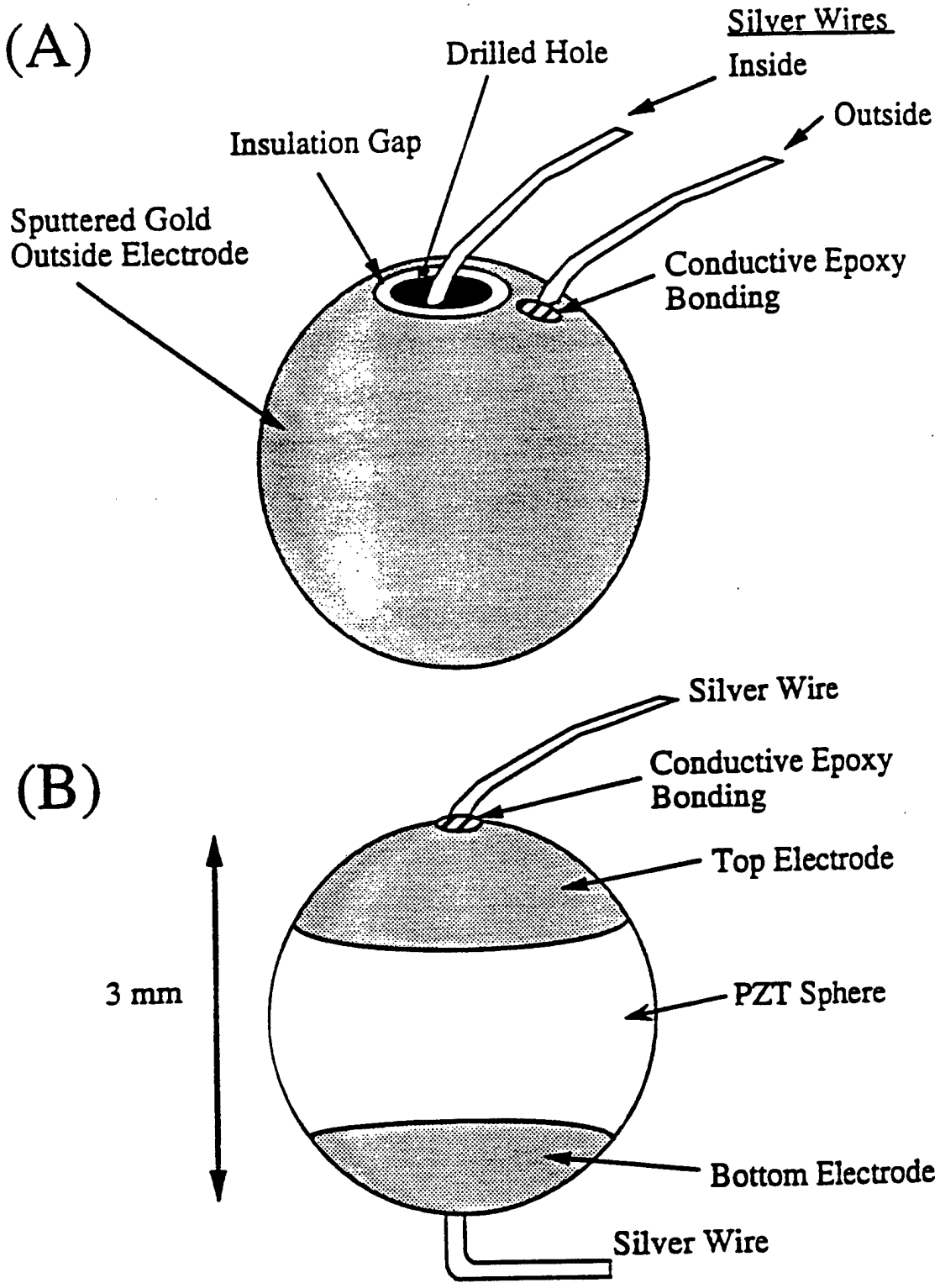
(A)
Silver Wires
Inside
Outside
Drilled Hole
Insulation Gap
Sputtered Gold
Outside Electrode
Conductive Epoxy
Bonding
(B)
Silver Wire
Conductive Epoxy
Bonding
Top Electrode
3 mm
PZT Sphere
Bottom Electrode
Silver Wire

Figure 1

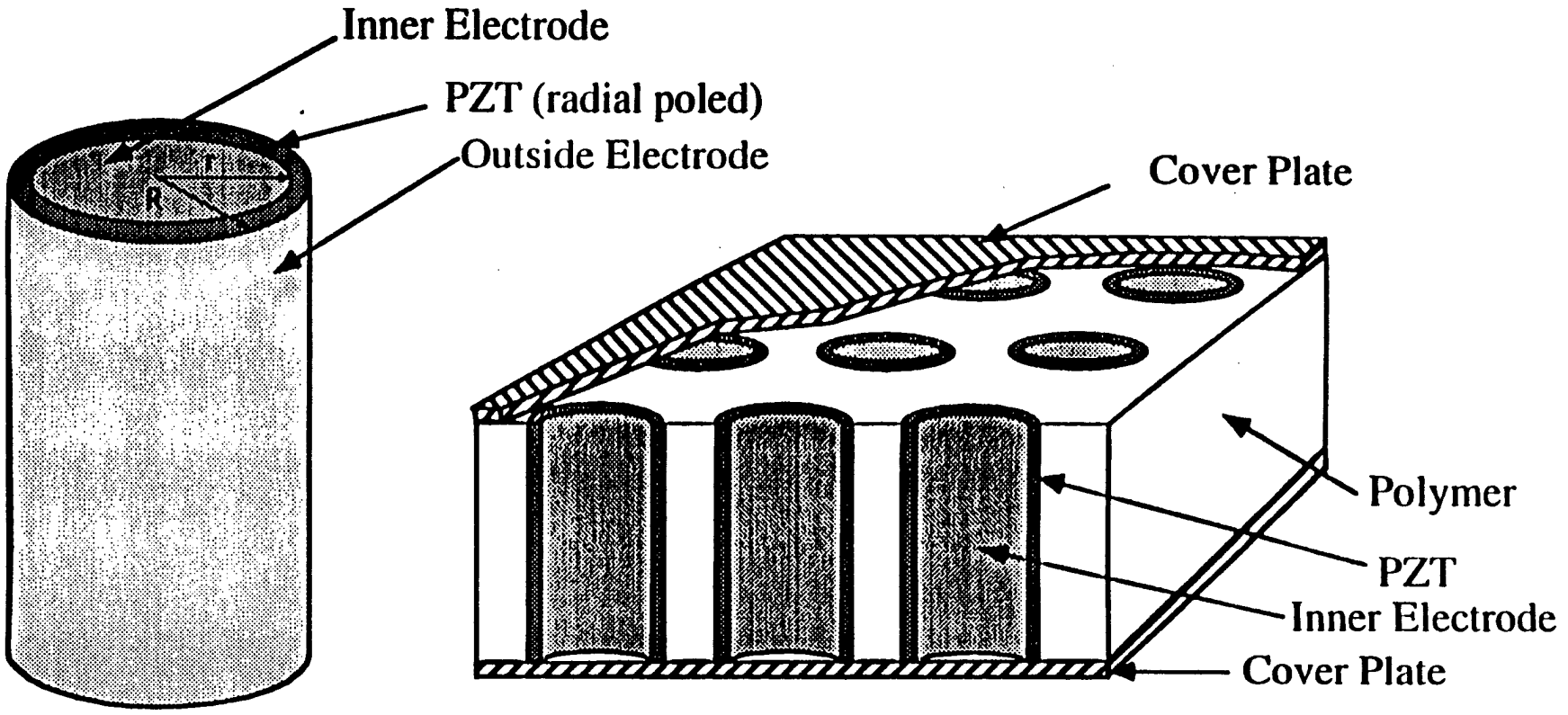

Single Tube

Capped 1(0)-3 Composite

Figure 2

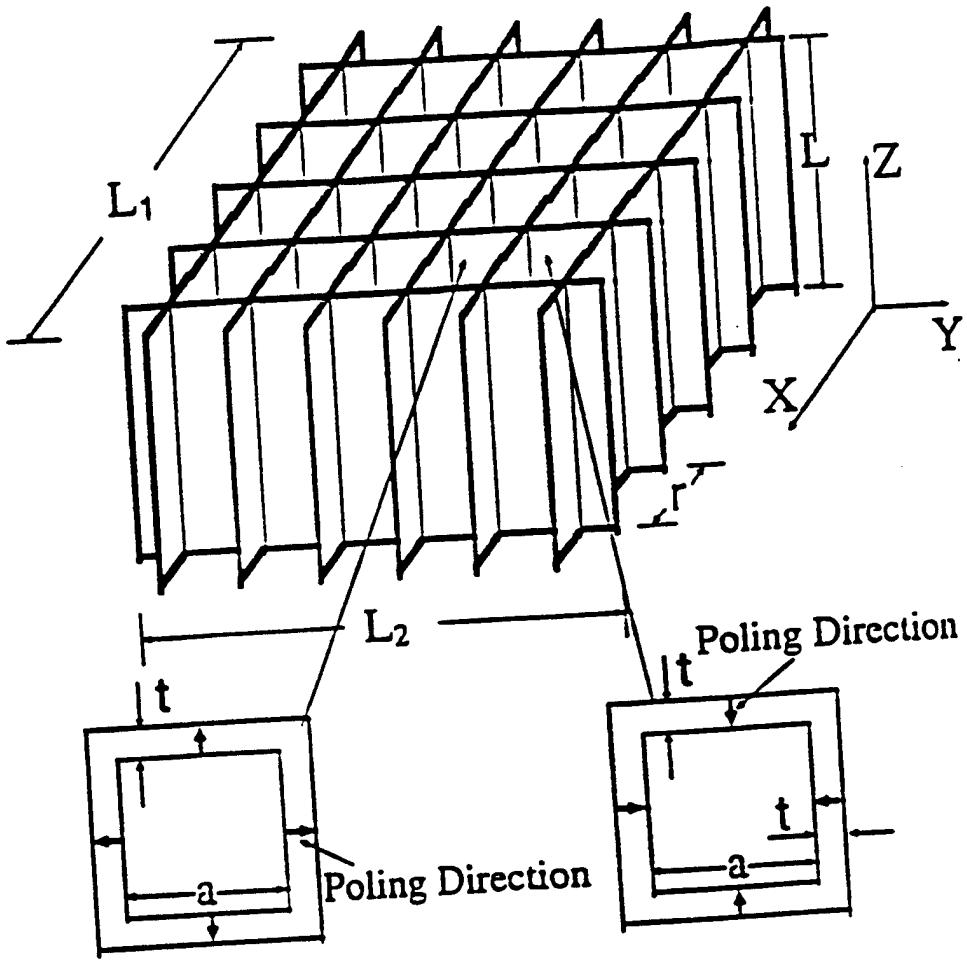

F. 3

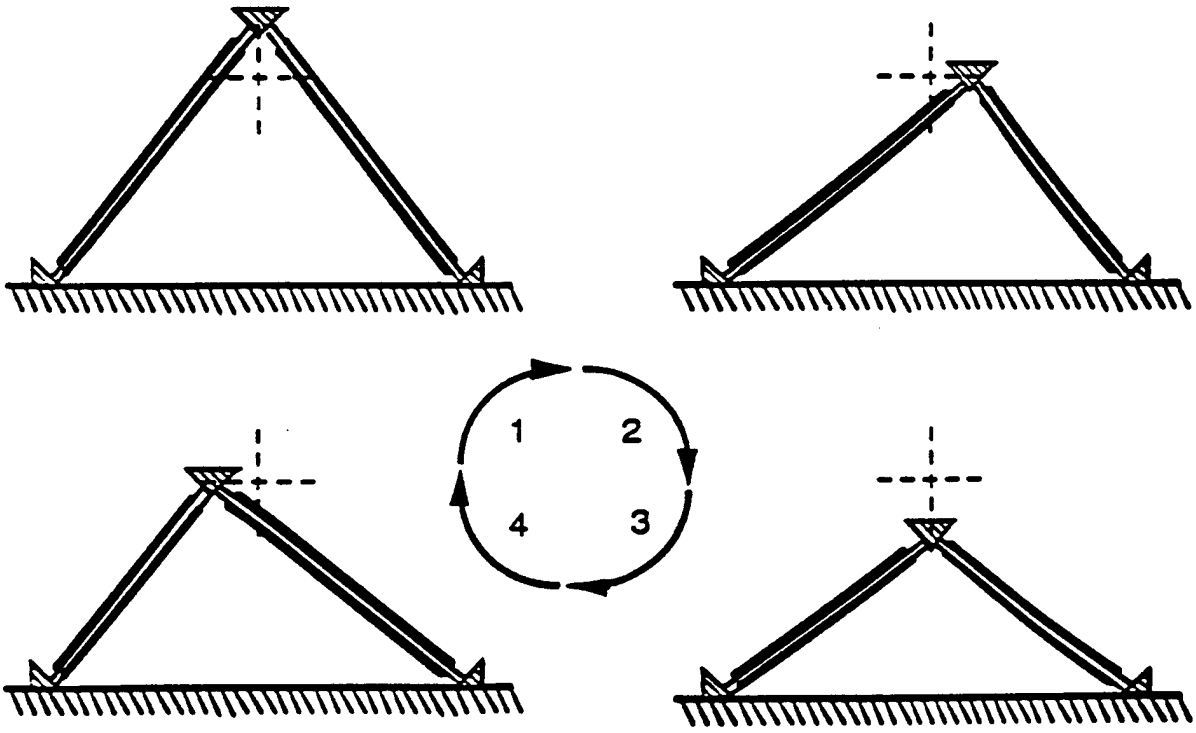

F 4

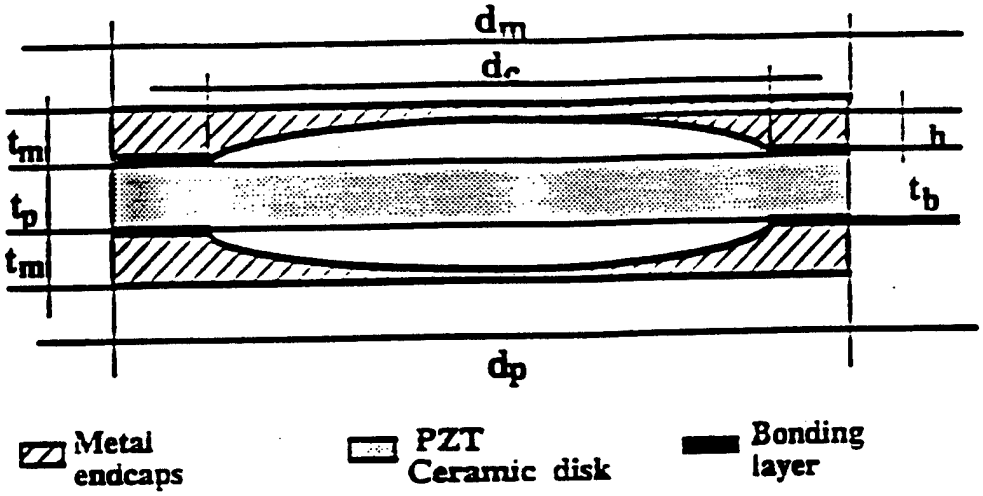

Dimensions: Endcap diameter. d_m= 12.7 mm PZT diameter. d_p= 12.7 mm

Cavity diameter. d_c= variable: 3.0, 5.0, 7.0, 9.0 mm

Cavity depth. h= variable: 0.3, 0.5, 0.7, 0.9 mm

Metal cap thickness. t_m=1.0 mm PZT thickness. tp= 1.0 mm

Bonding layer thickness. t_b= 0.01 mm

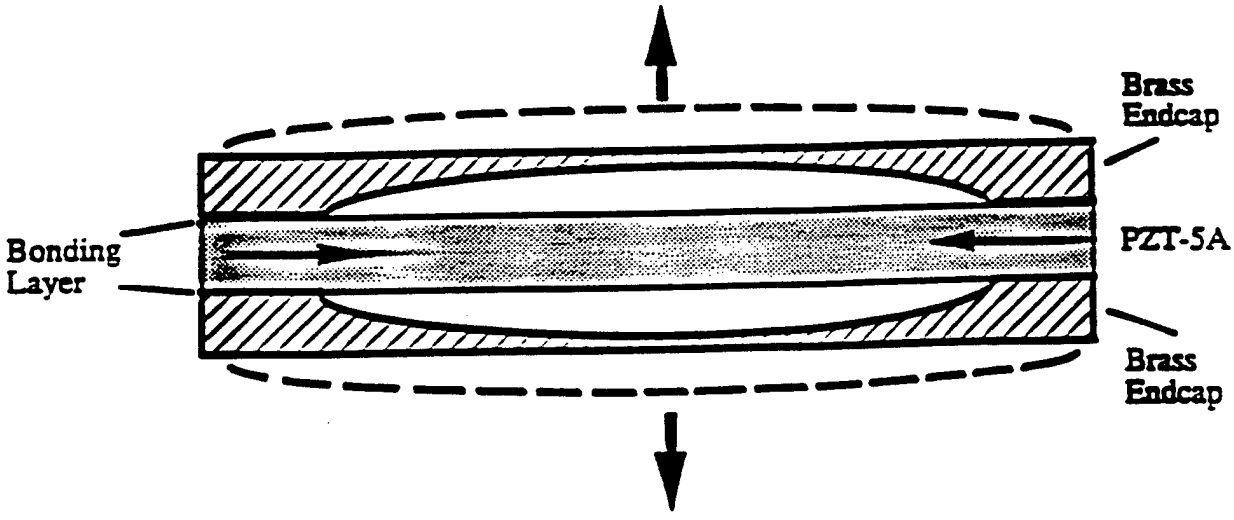

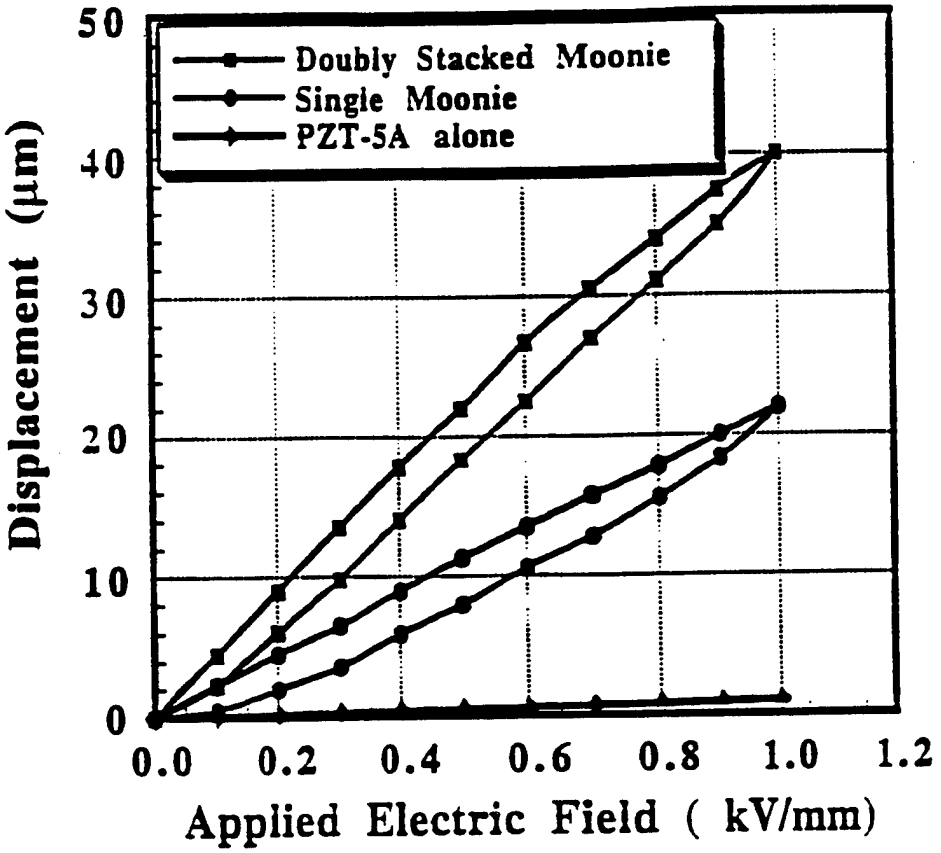

Dimensions: d_m= 12.7, d_p= 12.7, d_c= 9.0, h= 0.2, t_p=1.0, t_m=0.30 (all in mm)

t_b (Ceramic-metal bonding layer)= 0.020, t_{bi} (inter-stack bonding layer) = 0.040

FC

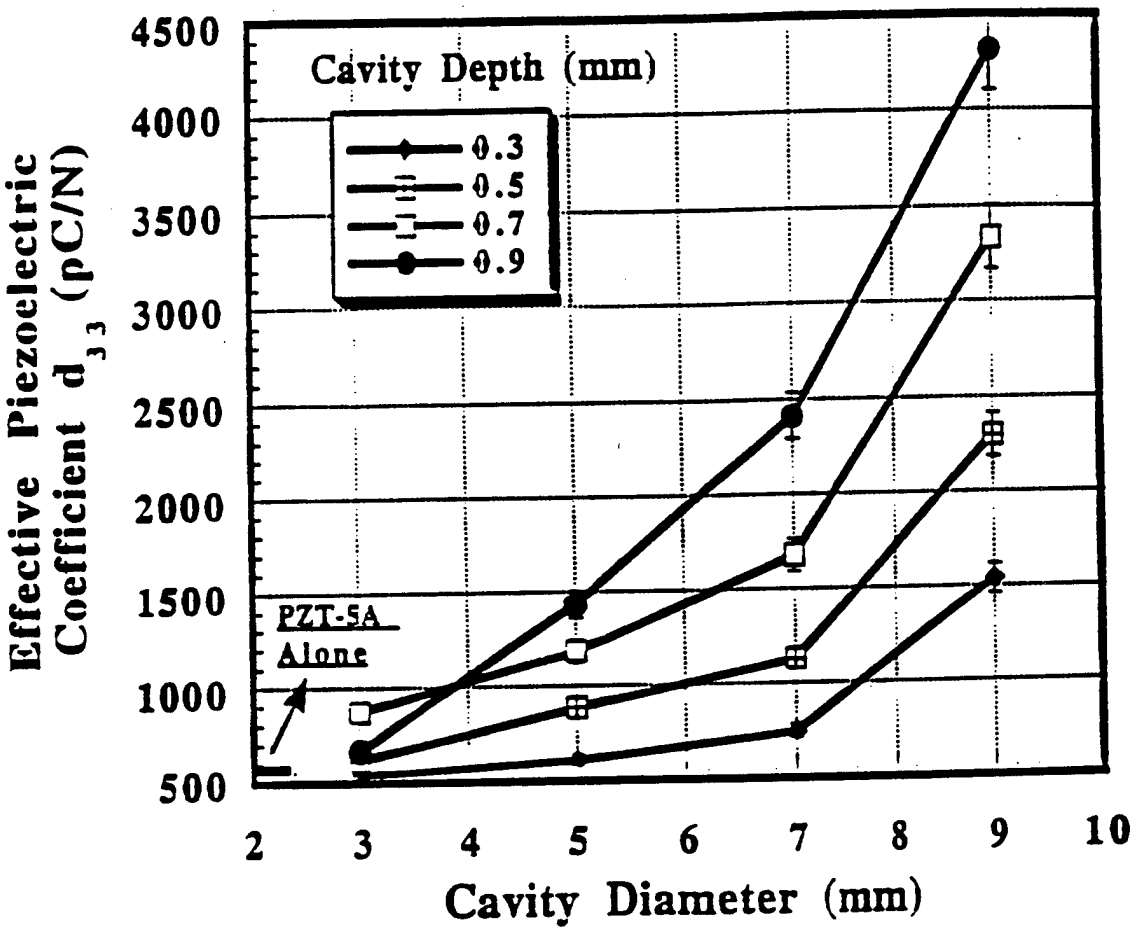

Dimensions: d_m= 12.7, d_p= 12.7, t_p=1.0 (all in mm)

F 7

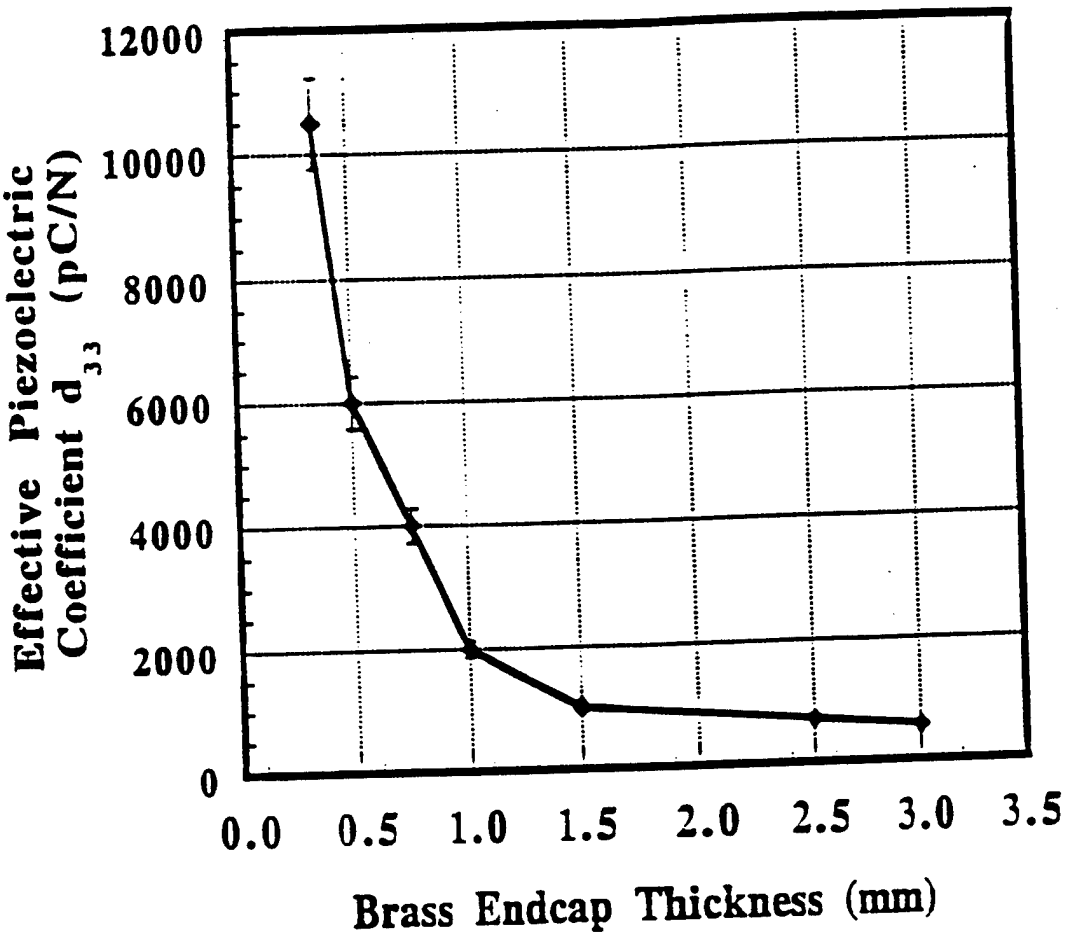

Dimensions: d_m= 12.7, d_p= 12.7, d_c= 9.0, h= 0.2, t_p=1.0, (all in mm)

F 8

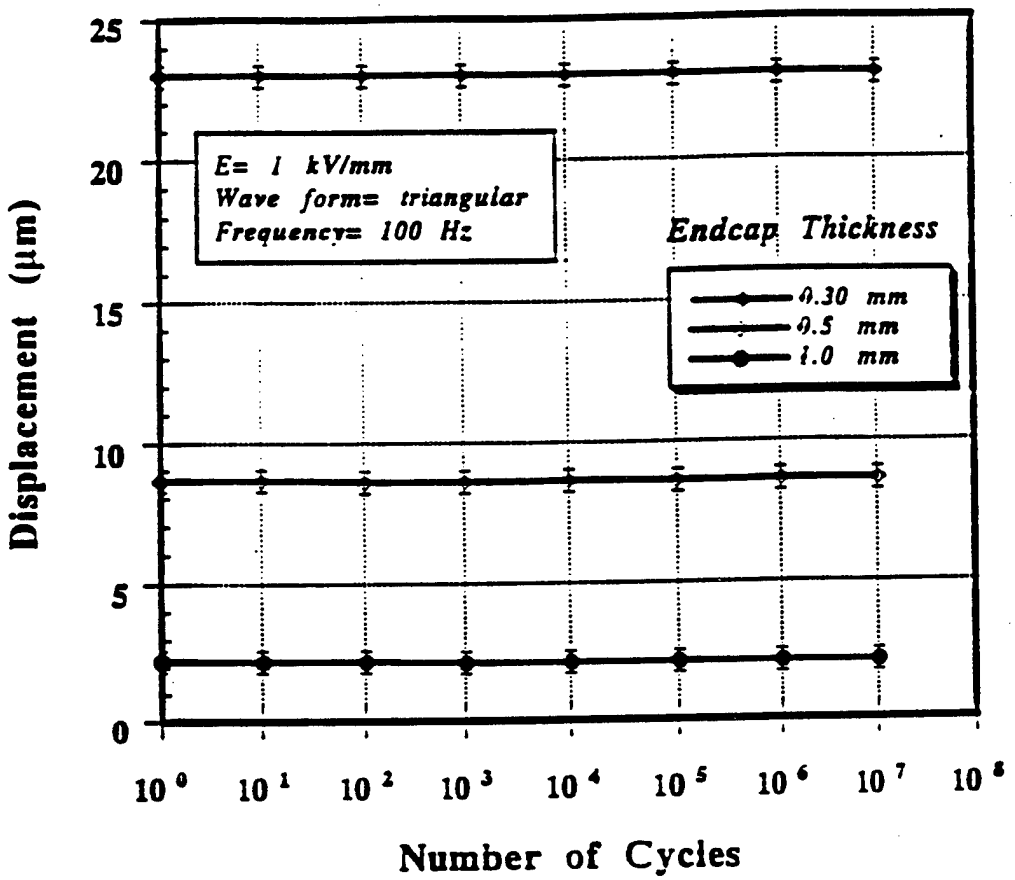
25
20
15
10
5
0
Displacement (µm)
E= 1 kV/mm
Wave form= triangular
Frequency= 100 Hz
Endcap Thickness
0.30 mm
0.5 mm
1.0 mm
10 0
10 1
10 2
10 3
10 4
10 5
10 6
10 7
10 8
Number of Cycles

F9

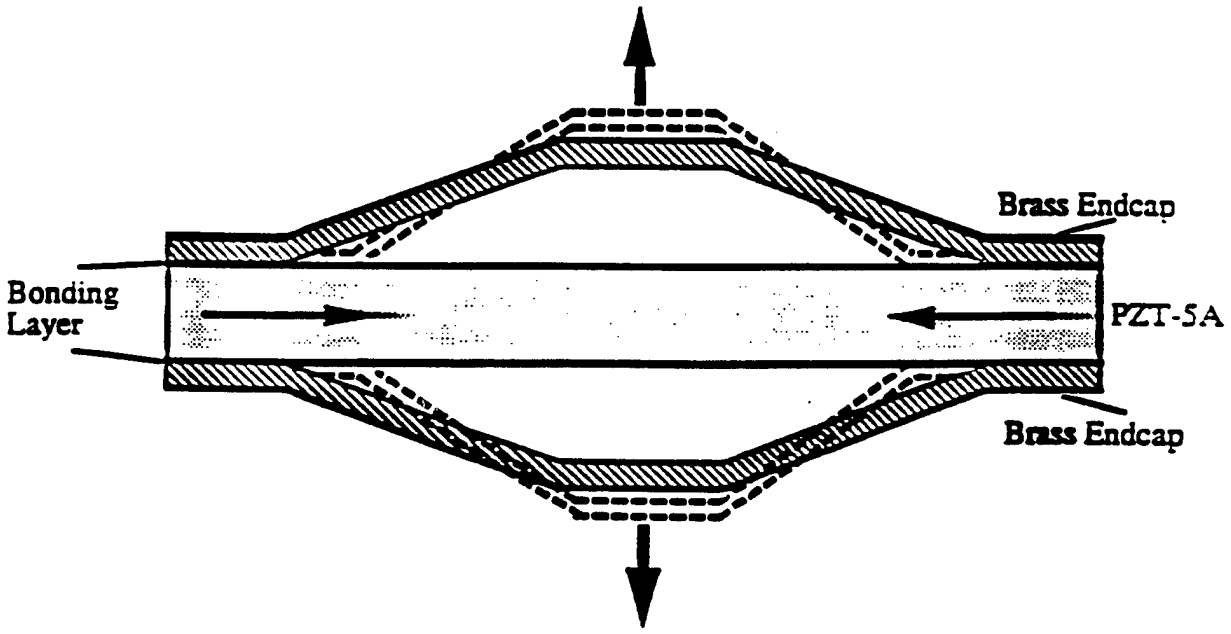

F 10

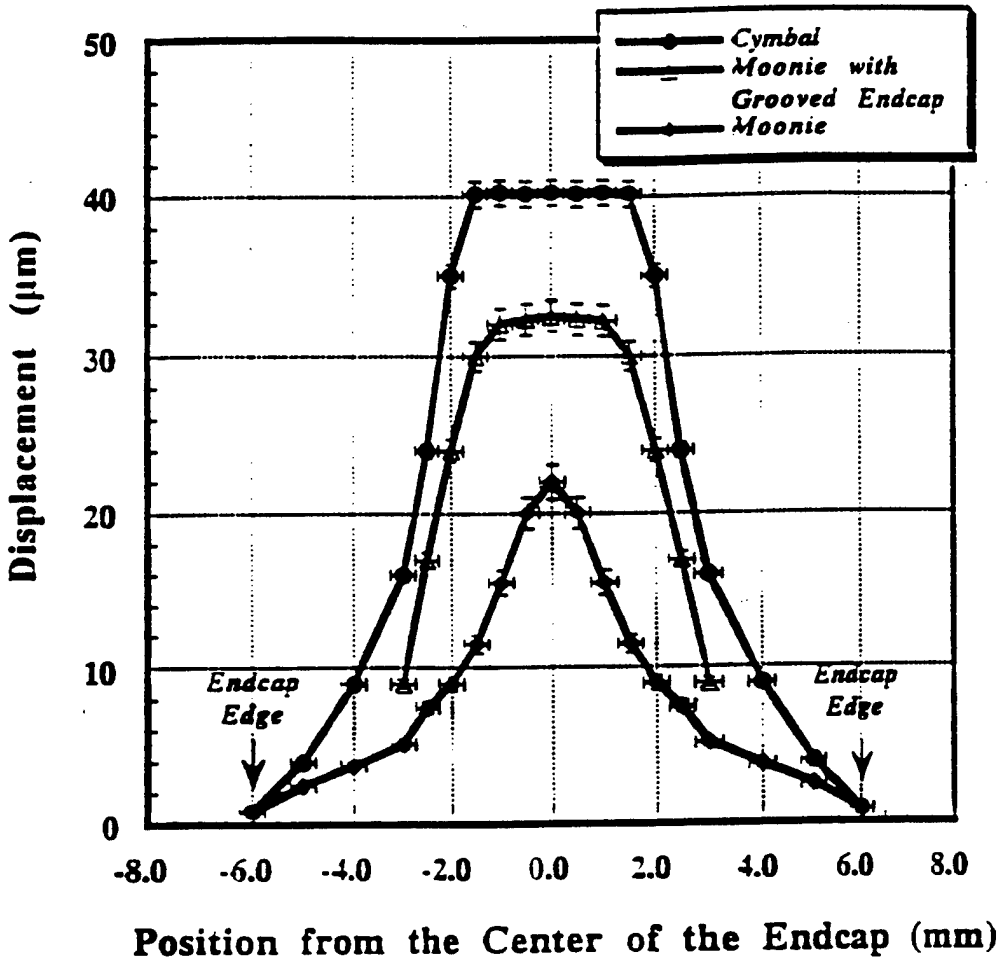

Dimensions: d_m= 12.7, d_p= 12.7, d_c= 9.0, h= 0.2, t_p=1.0, t_m=0.30 (all in mm)

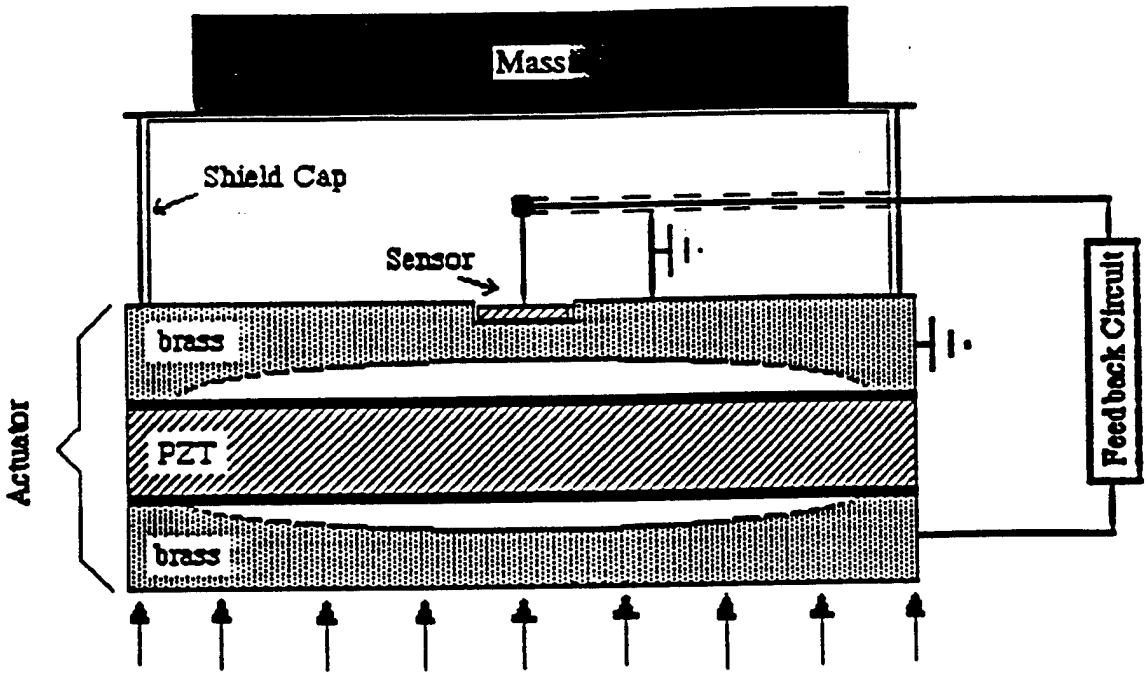
Mass
Shield Cap
Sensor
brass
PZT
brass
Actuator
Feedback Circuit
Vibration Normal to Actuator Surface

F. 12

APPENDIX 39

FOURTH EURO CERAMICS · Vol 5 pp 39–46
Electroceramics
Edited by G Gusmano, E Traversa
© Gruppo Editoriale Faenza Editrice S p A. · Printed in Italy

PIEZOELECTRIC COMPOSITES WITH ENCLOSED HOLLOW SPACES

J. F. Fernández*, A. Dogan, Q. M. Zhang, R. E. Newnham

Materials Research Laboratory, The Pennsylvania State University, University Park, PA 16802, USA
* (Current address: Electroceramics Department, Instituto de Cerámica y Vidrio, CSIC, 28500 Arganda del Rey, Madrid, Spain)

ABSTRACT

Current research activity on piezoelectric sensors and actuators is moving toward achieve better resolution and higher power densities. High resolution and small sizes are needed in applications such a biomedical ultrasound, probes for invasive procedures, flow noise control, non-destructive testing, and automotive instrumentation. Piezoelectric transducers with enclosed hollow space offer several special advantages including low acoustic impedance, reduced mass, sensitivity to weak hydrostatic waves, and enlarged displacements through flextensional and rotational motions.

This paper describes recent advances in the processing and properties of five types of hollow transducers based on composites with connectivity patterns of 0(0)-3, 1(0)-3, 2(0)-2-2 and 2-0-2. Piezocomposites with hollow space included within the structure clearly demonstrate the advantages of functional composites in the field of smart systems.

1. INTRODUCTION

PZT is widely used as a transducer material because of its high piezoelectric coefficients. However, for hydrophones applications, PZT is a poor material for several reasons. The hydrostatic piezoelectric coefficient, d_h ($=d_{33}+2d_{31}$), is very low. The piezoelectric voltage coefficients, g_{33} and g_h, are also low because of the high dielectric constant of PZT (1800). Moreover, the acoustic matching of PZT with water is poor because of its high density (7.9 g/cm^3), ans the mechanical properties leave much to be desired because it is a brittle, unflexible ceramic.

In the last decade, a number of investigators have fabricated composites of PZT and polymers to overcome the aforementioned problems of PZT [1-7]. The manufacture of piezoelectric composites requires careful replacement of a portion of the ceramic with polymer. This replacement reduce the acoustic impedance of the piezoelectric ceramic, bringing it closer to that of water and the human body. It has been shown that it is possible to improve upon the piezoelectric properties of homogeneous PZT by the composite approach [8]. The concept that the connectivity of the individual phases controls the resulting properties has been demonstrated in a number of composites with different geometry and different connectivity patterns of the individual phases. The hydrostatic piezoelectric properties of these composites are far superior to those of single-phase PZT. However, some of the earlier composites are difficult to prepare and suffer a reduction in hydrostatic sensitivity with increasing pressure

Thus, there still exists a need for further improvement in the piezoelectric properties of these composites.

2. HOLLOW PIEZOCOMPOSITES

Current research on piezoelectric sensors and actuators is moving toward miniaturized devices to achieve better resolution and higher power densities. High resolution and small sizes are needed in applications such as biomedical ultrasound, ultrasonics, probes for invasive procedures, flow noise control, nondestructive testing evaluation of composites, and automotive instrumentation. Higher frequencies and better impedance matching are advantageous in underwater transducers and biomedical ultrasonics. The introduction of open space in piezocomposites meets both of these criteria. In most of the cases, careful design of piezocomposites with open spaces leads to the development of reliable, robust, low cost transducers with improved piezoelectric properties. Table I summarizes recent trends in the design of piezocomposites with open spaces.

TABLE I
New trends in piezocomposite design with open spaces

Previous			New design		
Connectivity pattern	Type	Name	Connectivity pattern	Type	Name
0-3	PT/PZT in polymer	Piezorubber	0(0)-3	PZT hollow spheres	BBs
1-3	PZT fiber in polymer	PZT spaghetti	1(0)-3	PZT tubules in polymer	PZT macaroni
3-1	PZT with drilled holes	Perforated PZT	3-1(0)	PZT honeycomb skeleton	Honeycomb
2-2	Cantilever	PZT bimorph	2-0-2	split bimorph	Zig Zag
2-2	Tape cast PZT multilayer	PZT actuator	2(0)-2-2(0)	Capped PZT	PZT moonie and cymbal

3. BBs TRANSDUCERS

BBs are hollow spherical transducers a few millimeters in diameter, about the same size as the metallic pellets used in air rifles (BB guns). PZT BBs are mass produced, by a patented forming process in which air is blown through a PZT slurry of carefully controlled viscosity [9]. The hollow spheres are 1-6 mm in diameter with wall thickness of 0.1 mm. Densities are about 1.3 g/cm^3 giving the BB a low acoustic impedance close to that of water and human tissue.

When embedded in a polymer matrix to form a 0-3 composite the BB spheres are surprisingly strong, and able to withstand large hydrostatic pressure without collapse. Close-packed transducer arrays are easily assembled [10]. Hydrostatioc piuezoelectric coeffiucients well in excess of 1000 pC/N have been measured

When electroded inside and out, and poled radially the BB becomes an omnidirectional transducer suitable for underwater or biomedical applications. For spheres with a 2.6 mm diameter and 90 µm thick walls, the resonant frequencies are 700 kHz for the breathing mode (d) and 10 Mhz for the wall thickness mode (d) [10] BB's are small enough to be used in

4.PZT MACARONI

Poling is sometimes difficult for the long, slender PZT fibers used in 1-3 composites. Electric breakdown often occurs before poling is complete, and the transducer is ruined. Lower poling and driving fields are obtained when the spaghetti-like PZT fibers are replaced with macaroni-like PZT tubules [12]. When electroded inside and outside, the thin-walled tubes are poled and driven radially at relatively modest voltages. The effective piezoelectric constant in the radial direction can be tuned to positive, zero, and negative values by varying the ratio of the outer radius (R) to the inner radius (r) of the tube. For a suitable ratio of R/r, this effective constant can also be adjusted in sign and magnitude with a DC bias field for tubes made of electrostrictive materials [12]. Endcapped thin wall tubes also exhibit exceptionally high hydrostatic response with effective d_h coefficient of -14.000 pC/N and effective figure of merit, $d_h g_h$, higher than 10^{-11} m^2/N. For large area applications, these tubes can be readily integrated into 1-3 composite structure to provide low acoustic density and high piezoelectric activity.

5. ZIG- ZAGS

Zig-zag actuators are split bimorphs in which two ceramic legs are driven independently to generate synchronized horizontal and vertical displacements. The legs are joined in a teepee-like configuration which imparts a rolling motion to the load. Typical motions are in the 1-30 μm range and look to be useful in piezomotor and conveyor belt applications due to the ability to drive a load in two directions [13]. The mechanical impedance can be optimized by changing the angle between the legs, and the actuator's working parameter controlled by changing the driving voltage and frequency.

6. HONEYCOMB CERAMIC COMPOSITES

The basic structure of this composite is schematically illustrated in figure 1, where the ceramic is poled perpendicular to the z-direction as indicated [14]. The transducer is operated in the transverse piezoelectric mode (TP). It should be mentioned that two forms of honeycomb composite transducers were investigated earlier [15-16]. The earlier honeycomb composite transducers are operated in the longitudinal piezoelectric mode. Due to the limitations of this operation mode, the effective hydrostatic piezoelectric response of the earlier honeycomb composite transducers are an order of magnitude smaller than that of the TP honeycomb transducers. An endcapped honeycomb structure was made by placing thin layers of epoxy over the two ends to block the openings. When this endcapped honeycomb is subjected to hydrostatic pressure, the d_{33} response is eliminated and the piezoelectric response comes from the d_{31} component of the piezoelectric. This is due to fact that the stress component perpendicular to the wall is zero because the interior is filled with air. The stress field in the x-, y- and z-direction induces three d_{31} responses in the corresponding ceramic plates. Exceptionally high hydrostatic piezoelectric d_h values were obtained up to -4700 pC/N. One of the biggest advantages of such a composite is the extrusion process that permitss the development of complex geometries by a cost effective procedure.

7. MOONIES AND CYMBALS.

In recent years, piezoelectric and electrostrictive ceramics have been used in many actuator applications. To meet these needs a new type of composite actuator based on a flextensional transducer has been developed [17-21]. This ceramic-metal composite actuator, or "moonie", consists of either a piezoelectric ceramic disc or a multilayer stack, sandwiched between two specially designed metal end caps. The basic configuration of the moonie is shown in figure 2.

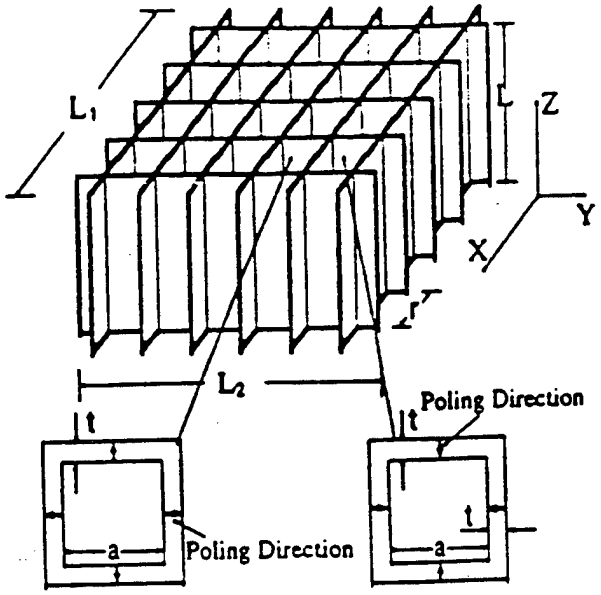

Figure 1 Schematic drawing of a honeycomb ceramic structure. Poling directions are indicated in the insert of the figure. Notice the difference in the poling directions between neighboring cells.

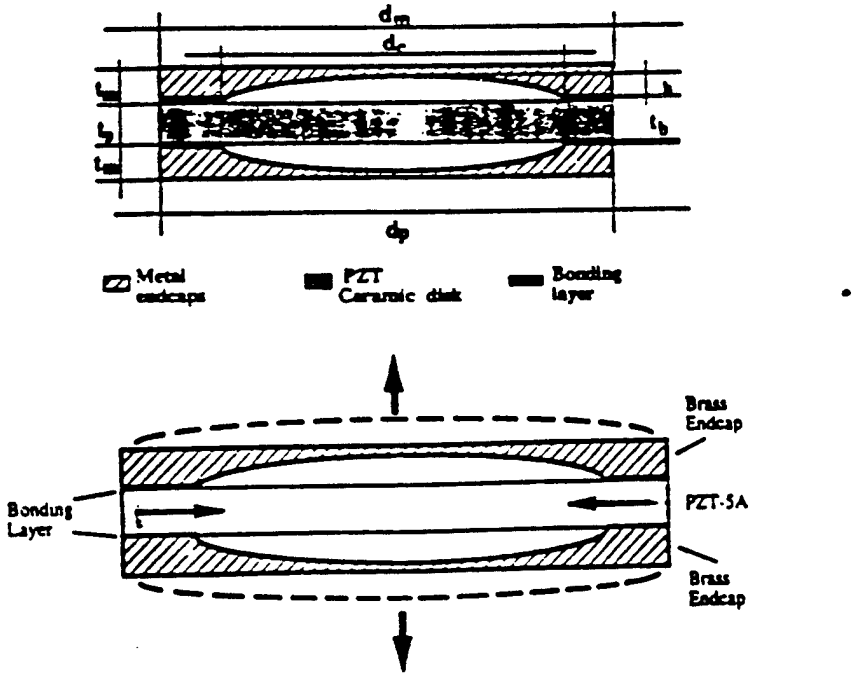

Figure 2. The geometry of the ceramic-metal composite actuator "Moonie". The arrows describe the displacement directions when the moonie is driven by a field paralled to the poling direction of the ceramic.

The metal endcaps serve as mechanical transformers for converting and amplifying the lateral motion of the ceramic into a large axial displacement normal to the end caps. Both the d_{31} ($=d_{32}$) and d_{33} coefficients of the piezoelectric ceramic contribute to the axial displacement of the composite. Figure 3 shows the enhanced displacement of the moonie actuator compared to that of a PZT ceramic. This design provides a sizable displacement, as well as a large

generative force. In other words, it bridges the gap between the two most common types of actuators, the multilayer and the bimorph [22]. The shallow spaces under the end caps produce a substantial increase in strain by combining the d_{33} and d_{31} coefficients of the ceramic. It is attractive for hydrophone, transceiver and actuator applications, and is especially advantageous for use as a non-resonant, low frequency projector in deep water.

Hydrophone sensitivity depends on d_h, the hydrostatic piezoelectric charge coefficient, and g_h, the hydrostatic piezoelectric voltage coefficient. The moonie transducer was introduced as a hydrophone having the highest figure of merit, $d_h \times g_h = 50,000 \times 10^{-15}$ m^2/N [23], about 500 times larger than the uncapped PZT ceramic. The moonie also possesses high capacitance and excellent pressure tolerance. The stress distribution within the moonie hydrophone under a hydrostatic pressure was determined using FEA. Extensional stresses along the radial and tangential directions are generated under a hydrostatic pressure, and contribute significantly to the very high figure of merit of the moonie.

Moonie actuators also have very high effective d_{33} coefficients depending on the geometry. Effective d_{33} coefficients as large as 13,000 pC/N were obtained with brass caps 0.3 mm thick, but the value decreased rapidly toward the edge of the transducer. This is approximately thirty times higher than the d_{33} of a PZT-5A ceramic. The characteristics of the moonie actuator depend markedly on both the geometry and the choice of materials. Among the geometric parameters, cavity diameter, cavity depth, and cap thickness are the main parameters which controls the displacement of a moonie actuator. An applied 1 kV/mm electric field produces a displacement of 22 μm at the center of a carefully designed brass capped moonie actuator. By stacking two identical single moonies with these dimensions, the double stacked moonie actuator exhibits a 40 μm displacement, (figure 3).

The generative force of the moonie was measured experimentally and calculated by FEA. The calculated maximum force (30 N) at the effective working area of 3 mm^2 agrees with that obtained by the extrapolation of the experimental data.

For actuators, however, the stress concentration on the brass endcap just above the bonding layer reduces the effective force transfer from the PZT to the cap. It is possible to eliminate part of the stress concentration by removing the portion of the endcap just above the bonding region where the maximum stress concentration is observed. An enhacement in properties has been obtained by introducing a ring shaped groove on the exterior of the end caps [23]. The largest displacement was achieved when the groove was positioned above the

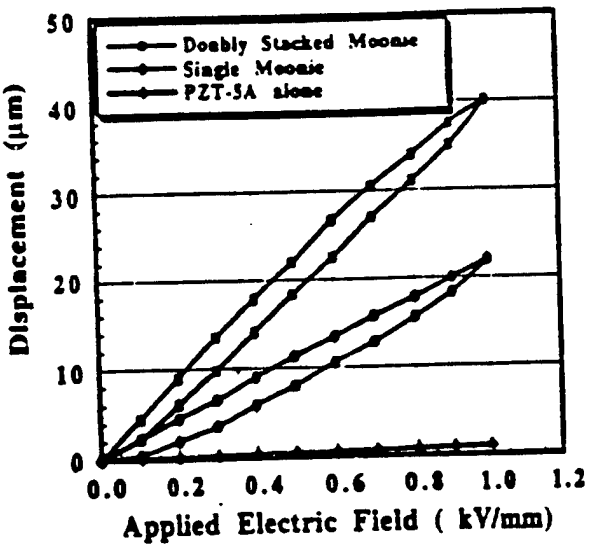

Figure 3. The displacement characteristics of the moonie actuator as a function of the applied electric field.
Dimensions: d_m=12.7, d_p=12.7, d_c=9.0, h=0.2, t_p=1.0, t_m=0.3 (all in mm).

bonding layer. The deeper and wider the groove, the higher the displacement. Since the stress concentrates at the groove edges, this becomes a potential source of fatigue and may eventually produce failure under long term usage.

A new design of moonie with "cymbal" shaped endcaps has recently been developed [24]. The endcaps are fabricated by punching metal sheets. The cymbal design removed most of the region with stress concentration, and yields higher and more reproducible displacements. Even though this new design looks similar to the earlier moonie design, it has a different displacement mechanism. Displacement is a result of the pure flexural motion of the endcap for the moonie. For the cymbal, the displacement is created by the combination of flexural and rotational motion. Figure 4 shows the displacement values and the position dependence of the different endcap designs with with fixed cavity depth (0.2 mm) and cavity diameter (0.9 mm). The cymbal actuator generated a 40 μm displacement which is about twice the moonie displacement. Flexural motion of the endcaps is the principal motion mechanism of the original moonie actuator. For this reason the displacement of the moonie actuator is highly dependent on position. Displacement decreases dramatically away from the center of the endcap, where the maximum displacement is observed, to the edge, where the displacement is equal to that of the PZT. A moonie with grooved endcaps show significately less position dependence of displacement. The cymbal actuator exhibits a more homogeneous displacement over a wider section about 4 mm in diameter at the center of the endcap. The large flat contact surface of the new endcap design makes it more practical for stacking the individual actuators together to reach higher displacement. Additionally, the new multistacked cymbal structure is more stable under uniaxial external loading. This actuator consists of five elements, 12.7 mm in diameter, 10 mm total thickness, and exhibits a displacement of 175 μm.

Properties and perfomance of metal-ceramic composites, moonie and cymbal, can be tailored through the geometrical design and the selection of the adequate materials [25]. Because of their large displacement and charge, moonie and cymbal composites show great potential for many applications [23-26], including hydrophone sensors, transceivers for fish finders, positional actuators and highly sensitive accelerometers.

8. SMART MATERIALS

Smart materials [27] have the ability to perform both sensing and actuating functions. Passively smart materials respond to external change in a useful manner without assistance, whereas actively smart materials have a feedback loop which allows them to both recognize the change through an actuator circuit. Many smart materials are analogous to biological

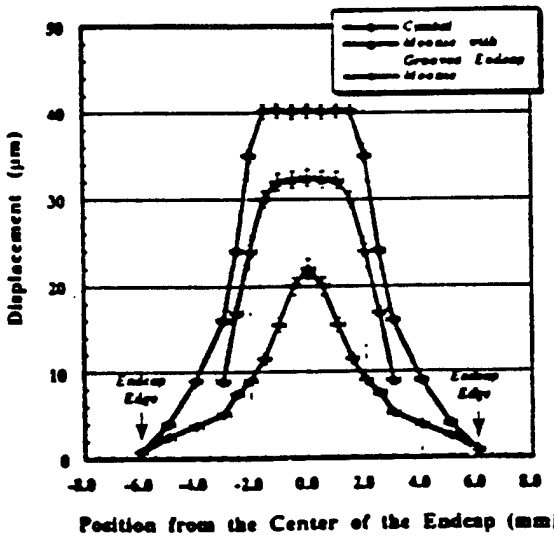

Figure 4. The position dependence of displacement for different endcap designs.

systems: piezoelectric hydrophones mentioned earlier are similar in mechanism to the "ears" by which a fish senses vibrations. Piezoelectrics with electromechanical coupling, shape memory materials that can "remember" their original shape, electrorheological fluids with adjustable viscosities, and chemical sensors which act as synthetic equivalents to the human nose are examples of smart electroceramics. "Very smart" materials, in addition to sensing and actuating, have the ability to "learn" by altering their property coefficients in response to the environment. Integration of these different technologies into compact, multifunction packages is the ultimate goal of research in the area of smart materials. Hollow piezoelectric composites introduce new tools in the search of smart and very smart materials. The capability of integrating different structures in piezoelectric composites with open spaces make possible to develop advances systems with complex functions.There are several recently applications and materials that open the big changes to occur in this field during the coming decades.

A new vibration control device based on the moonie actuator has been developed by Tressler [28]. The actuator portion of the device consist of the standard (11 mm diameter, 2 mm thick) moonie, and a small piezoelectric ceramic embedded in the upper end cap that serves as a sensor (0.1 mm thick). This protoptype sensor/actuator piezocomposite is capable of detecting and suppressing in real time, small vibration displacements (< 1 μm), with low force (< 100 gf). The dynamic frequency range of the device spans from 100 Hz to at least 2500 Hz. The sensor detects sinusoidal vibrations normal to the actuator surface, via a feedback loop, and send a signal of appropiate amplitude and phase shift to the actuator so that if effectively cancel is the external vibration. Potential aplications for this device include active optical systems, rotor suspension systems, and other low level vibration suppression devices

ACKNOWLEDGEMENTS

The authors would like to express their gratitude for the support to the following agencies and organizations: Office of Naval Research Contract no. N00014-92 J 1510, National Science Foundation Grant no. DMR-9223847, Spanish Science Ministry (CICYT MAT94-807 and DGICYT PR94-028), Turkish Science and technology Council and Middle East Technical Ankara University.

REFERENCES

[1] R. E. Newnham, D. P. Skinner and L.E. Cross, "Connectivity and Piezoelectric-Pyroelectric Composites", *Mat. Res. Bull.*, 13, 525-536(1978).

[2] D. P. Skinner, R. E. Newnham and L. E. Cross, "Flexible Composite Transducers", *Mat. Res. Bull.*, 13, 599-607(1978).

[3] T. R. Shrout, W. A. Schulze and J. V. Biggers, "Simplified Fabrication of PZT/polymer composites", *Mat. Res. Bull.* 14, 1553-59(1979).

[4] K. A. Klicker, J. V. Biggers and R. E. Newnham, "Composites of PZT and Epoxy for Hydrostatic Transducer Applications", *J. Am. Ceram. Soc.*, 64, 5-9, 1981.

[5] H. P. Savakus, K. A. Klicker and R. E. Newnham, "PZT Epoxy Piezoelectric Transducers: A Simplified Fabrication Procedure", *Mat. Res. Bull.*, 16, 6, 677-680(1981).

[6] T. R. Gururaja, W. A. Schulze, L. E. Cross, R. E. Newnham, B. A. Auld and Y. J. Wag, "Piezoelectric Composite Materials for Ultrasonic Transducer Applications. Part I: Resonant Modes of Vibration of PZT Rod-Polymer Composites", *IEEE Transactions on Sonics and Ultrasonics*, vol. 32, no. 4, pp. 481-498, 1985.

[7] T. R. Gururaja, W. A. Schulze, L. E. Cross, R. E. Newnham, B. A. Auld and Y. J. Wang, "Piezoelectric Composite Materials for Ultrasonic Transducer Applications. Part II: Evaluation of Ultrasonic Medical Applications", *IEEE Transactions on Sonics and Ultrasonics*, 32, 4, 499-513(1985).

[8] R. E. Newnham, "Composite Electroceramics," *J. Mat. Education*, 7,605-651(1985).

[9] L.B. Torobin, "Methods of Making Hollow, Porous Microspheres", U.S. Patent #4,671,909, 1987.
[10] R. Meyer Jr, H. Weitzing, Q. Xu, Q. Zan and R. E. Newnham, "Lead Titanate hollow Sphere Transducers", *J. Am. Ceram. Soc.* 77,6,1669-72(1994).
[11] D. Kilkomerson, B. Gardineer and H. Hojeibane, " Quasi-Omnidirectional Transducers for Ultrasonic Electro-Beacon Guidance of Invasive Devices", *Proceedings of SPIE* 1733,154-65(1992).
[12] Q. M. Zhang, H. Wang and L. E. Cross, "Piezoelectric Tubes and Tubular Composites for Actuator and Sensor Applications", *J. Mater. Sci.* 28,3962-68(1993).
[13] M.G. Matsko, Q. C. Xu and R. E. Newnham, "Zig-Zag Piezoelectric Actuators: Geometrical Control of Displacement and Resonance", *J. of Intelligent Mat. Systems and Structures*, (in press).
[14] Q. m. Zhang, H. Wang, J. Zhao, J. T. Fielding, R. E. Newnham and L. E. Cross, " A High Sensitivity Piexzoelectric Transducer Based on Transverse Piezoelectric Mode Honeycomb Ceramic Composites", *IEEE Transactions on Ultrasonics, Ferroelectric and Frequency Control* (in press).
[15] T. R. Rhrout, L.J. Bowen and W. A. Shulze, "Extruded PZT-Polymer Composites for Electromechanical Transducer Applications", *Mater. Res. Bull.* vol 15, 1371-80(1980).
[16] A. Safari, A. Halliyal, R. E. Newnham and I. M. Lachman, "Transverse Honeycomb Composite Transducers", *Mater. Res. Bull.* vol 17, 301-9(1982).
[17] R. E. Newnham, Q. C. Xu and S. Yoshikawa, Transformed stress direction-acoustic transducer, U.S. Patent # 4,999,819, March 12, 1992.
[18] Q. C. Xu, S. Yoshikawa, J. Belsick and R. E. Newnham, "Piezoelectric Composites with High Sensitivity and High Capacitance for Use at High Pressures", *IEEE Transactions on Ultrasonics, Ferroelectrics and Frequency Control*, 38, 6, 634-639(1991).
[19] Y. Sugawara, K. Onitsuka, S. Yoshikawa, Q. Xu, R. E. Newnham, and K. Uchino, Metal-Ceramic Composite Actuators", *J. Am. Ceram. Soc.*, 75, 4, 996-998(1992).
[20] A. Dogan, Q. C. Xu, K. Onitsuka, S. Yoshikawa, K. Uchino and R. E. Newnham, "High Displacement Ceramic-Metal Composite Actuators (Moonie)", *Ferroelectrics* 156,1-6(1994).
[21] K. Onitsuka, A. Dogan, Q.C. Xu, J. Tressler, S. Yoshikawa, and R.E. Newnham, "Design Optimization for Ceramic-Metal Composite Actuators (Moonie)", *Ferroelectrics* 156,37-42(1994).
[22] K. Uchino, "*Piezoelectric and Electrostrictive Actuators*", Morikita Publication,3
[23] K. Onitsuka, "Effects of Bonding and Geometry on the Flextensional Transducer, "Moonie"", Ph.D. Thesis, The Pennsylvania State University, University Park, PA (1993).
[24] A. Dogan, "Flextensional "Moonie and Cymbal" Actuators", Ph.D. Thesis, The Pennsylvania State University, University Park, PA (1994).
[25] J. F. Fernandez, A. Dogan, J. Tressler, J. T. Fielding, K Uchino and R. E. Newnham, "Temperature Dependence of High Displacement Ceramic-Metal Composite Actuators", *97 Am. Ceram. Soc. Meeting*, April 1995, Cinncinati, OH, USA.
[26] R. E. Newnham, A. Dogan, J. T. Fielding, J. F. Fernandez, D. Smith, J. Tressler, J. Wallis, K. Uchino, W. Zhu, "Moonies, Cymbals and BB's", *Office of Naval Research transducer Materials and Transducers Workshop*, April 1995 State College, PA, USA.
[27] R. E. Newnham and G. Ruschau, "Smart Electroceramics", *J. Am. Ceram. Soc.*, 74, 3, 463-480(1991).
[28] J. F. Tressler, "Smart Ceramic-Metal Composites for Active Vibration Control", M.S. Thesis, The Pennsylvania State University, University Park, PA (1993).
[29] J. F. Tressler, Q. C. Xu, S. Yoshikawa, K. Uchino and R. E. Newnham, "Composite Flextensional Transducer for Sensing and Actuating", *Ferroelectrics* 156,67-72(1994).

APPENDIX 40

FOURTH EURO CERAMICS - Vol. 5 - pp. 133-138
Electroceramics
Edited by G. Gusmano, E. Traversa
© Gruppo Editoriale Faenza Editrice S.p.A. - Printed in Italy

TEMPERATURE DEPENDENCE OF NEW DESIGN CERAMIC-METAL PIEZOCOMPOSITE ACTUATORS

J. F. Fernández*, A. Dogan, J. T. Fielding, K. Uchino, R. E. Newnham

International Center for Actuators and Transducers, Materials Research Laboratory, The Pennsylvania State University, University Park, PA 16802, USA
* (Current address: Electroceramics Department, Instituto de Cerámica y Vidrio, CSIC, 28500 Arganda del Rey, Madrid, Spain)

ABSTRACT

The unique design of metal-ceramic actuators exhibits very high displacement and large generative forces. This new design metal-ceramic composite actuators consists of a piezoelectric disk sandwiched between two cone-truncated shaped metal endcaps. The radial motion of the piezoelectric ceramic is converted into a flextensional and roto-flextensional motion in the metal endcap. There is a Thermally Induced Displacement (TID) of the piezocomposite with temperature that is related to the thermal expansion mismatch between the metal endcaps and the ceramic. By selecting appropriate materials it is possible to avoid this TID. Very low or negligible temperature dependence of the displacement was attained by using PZT ceramics with low temperature dependence on its properties or by using metal with higher stiffness and lower thermal expansion coefficients than the ceramics.

1. INTRODUCTION

In recent years, piezoelectric and electroestrictive ceramics have been used in many actuator applications. A new type of metal-ceramic composite actuator, which is based on the concept of flextensional transducer has been reported [1-2]. In this metal-ceramic composite the PZT ceramic is sandwiched between metalic endcaps with shallow cavities. Because the shallow cavities have a moon shape, the composites is named "moonie". The radial motion of the piezoelectric ceramic is converted into a flextensional motion in the metal endcap. As a result, a large displacement is obtained at the device center in the direction perpendicular to the ceramic disk.

Due to large difference in the thermal expansion coefficient between the metal, brass, 20 x 10^{-6} /°C, and the ceramic, PZT, 6 x 10^{-6} /°C, a significant thermally-generated stress is produced in the composite during the cooling process when silver paste bonding is used. If no stress relaxation occurs below the glass softening temperature, typically 400 °C, thermally induced compressive stresses are generated in the PZT, while tensile stresses are generated in the endcaps [3]. These prestresses help to maintain the PZT polarization during exposure to high hydrostatic pressure, which is required for hydrophone applications. However this tensile stress concentration can easily damage the outer edge of the PZT. The dimensional change produced during the poling process of the PZT increases this tensile stress concentration, reaching values close to the fracture strength of the ceramic.

As actuators, metal-ceramic composites need to achieve higher displacement and reduce the stress concentration in order to attain higher generative force and reliability. It was found that the introduction of a ring-shaped groove on the endcaps enhanced markedly the displacement [4]. At the same time, assembly techniques using room temperature bonding curing epoxies with prepoled ceramic were successfully developed. However, because the polymers have a low melting point, the epoxy bonding method is only useful for low temperature applications. In addition, the temperature characteristics of the moonie are related to those of the ceramic elements [5-6]. The thermal expansion coefficient mismatch between the metal and ceramic is the origin of the Thermal Induced Displacement or TID [6].

New metal-ceramic designs using truncated-cone shaped endcap, called "cymbals" [7], have demonstrated higher displacements, effective piezoelectric coefficients, and generative forces [6]. In cymbal actuators the radial motion of the ceramic is converted into flextensional and rotational motion of the metal endcap. In this paper different parameters affecting the temperature dependence of the new design metal-ceramic "cymbal" actuators, were investigated in order to avoid the temperature dependence of properties.

2. EXPERIMENTAL PROCEDURE.

Poled disks, having 12.7 mm in diameter and 1 mm in thickness, of three different commercial composition were investigated, Table I. Different metals and alloys were selected according to the thermal expansion coefficient and the stiffness, table II. Truncated-cone shape of the cymbal design [7], was achieved by punching first and then pressing (up to 100 MPa) metal sheets of approximately 250 μm. After pressing, the cavity depth of the endcap is 270 μm, for zirconium, brass, low carbon steel and kovar; 250 μm for molybdenum and 175 μm for tungten. All metal endcaps show a well defined ring shaped bonding layer of 2 mm and a cavity diameter of 8.7 mm.

Table I. Piezoelectric properties of ceramics used as a drive element in cymbals.

CERAMIC	ε'	tg δ	d_{31} (pC/N)	d_{33} (pC/N)
PZT 8D	1104	0.003	-107	289
PZT 5A	1802	0.016	-208	429
PZT 5H	3500	0.016	-285	581

Table II. Metal endcap characteristics

METAL ENDCAP	Density (g/cm^3)	v_s (Km/s)	α (10^{-6} K^{-1})	E (GPa)
Zirconium	6.49	3.44	5.9	77
Brass	8.33	3.59	19.9	110
Kovar	8.36	4.00	5.5	138
Low Carbon Steel	7.86	5.13	11.7	207
Molybdenum	10.22	5.63	5.1	324
Tungsten	19.30	4.58	4.6	405

The ceramic disk and the endcaps were bonded together around the circumference with two different epoxies, listed in table III. Both are two component epoxies with similar strength

characteristics. Eccobond is a black color epoxy that contains dispersed $CaCO_3$ particles. Masterbond is a clear yellow pure epoxy phenolic with a wide temperature range of operation and needs to be cured at moderately elevated temperatures.

The displacement of a composite actuator was measured at 0.1 Hz in frequency under and applied field of 1 kV/mm with a Linear Voltage Differential Transducer, LVDT, at room temperature or with a photonic non contact sensor as a function of temperature. In both cases the resolution was 0.05 μm. Temperature dependence experiments were performed in a specially designed temperature chamber in the range of -5° C to +95°C. Borosilicate Glass Standard Reference Materials 731 from NIST, was uses as a temperature standard.

Table III. Characteristics of epoxies

EPOXY	Curing Process	Temperature Range
Eccobond	24 h RT	-40 +90 °C
Masterbond	20 h RT + 4 h 70 °C	-55 +175 °C

3. RESULTS AND DISCUSSION.

Figure 1 shows the effect of Young's modulus of metal encaps and hardness-softness of ceramic materials on the displacement of composite cymbal actuators. For the same metal endcap, there is dependence of the displacement on the d_{31} piezoelectric coefficient of the ceramic. The higher the contraction of the PZT in the radial direction is, and thereafter the contraction of the cavity, the higher the displacement is. The decrease of the displacement with the increase of the stiffness of the metal endcap is related to higher mechanical losses in the roto-flextensional motion (monolithic hinge type plus flextensional motion) of the endcap. That behavior is almost linear for cymbals bonded at room temperature with eccobond. The displacement of the stiffest metal is approximately 52-57% of that achieved using least stiff metal endcaps, and it is practically independent of the ceramic type. In the case of composites bonded with masterbond a different behavior was exhibited. In general the lower displacement values was observed than for the room temperature cured, epoxy bonded cymbals. And it seems that this decrease is significant for the cymbals made with PZT 5H, that shows the highest displacement. The reason for such behavior is attributed to the rigidity of the epoxy. Even though both epoxies have similar strength, masterbond is a pure phenolic epoxy.

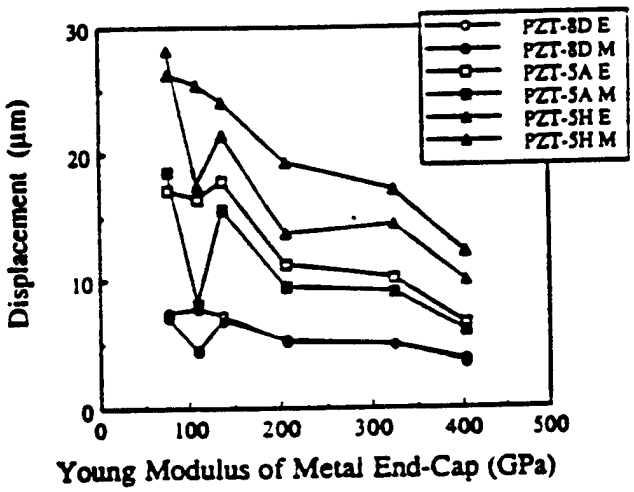

Figure 1 Displacement of cymbals actuators for different ceramics and metal endcaps.

while eccobond, having dispersed particles, possesses a higher flexibility. The thickness of the bondline using masterbond is slightly thinner than for the eccobond, with ranges on 10-15 μm and 20-25 μm respectively. On the other hand, for cymbals assembled with endcaps having larger thermal expasion coefficient than the ceramic, stresses generated during the elevated temperatured epoxy curing resulted in a pronounced decrease in attained displacement. In the case of brass, which has the highest mismatch of thermal expansion coefficient in relation to the ceramic, the displacement is drastically reduced.

TID measured data in table IV shows that by the reduction of the mismatch between the metal and the ceramic it is possible to avoid or to get a negative TID. From the point of view of practical application, negative TID's are very interesting because the metal produces a compressive stress on the ceramic that can reduce the depolarization process due to the increasing of the temperature. At the same time, negative TID could easily overcome in the final device by combining the cymbal with carefully tailored materials.

Table IV. TID (μm) of different metal endcap PZT 5H cymbal actuators (from -5°C to 95°C).

EPOXY	Tungten	Molybdenum	Kovar	Zirconium	LC Steel	Brass
Eccobond	-8.1	-0.5	-0.5	-0.5	4.8	48.9
Masterbond	-2.0	-2.0	-0.3	1.0	8.4	60.5

Figure 2 shows the thermal dependence of the displacement for different endcap materials bonded to PZT 5H with eccobond. There is a drastically decrease of the displacement for temperatures higher than 50°C attributed to the bonding layer that became more flexible at higher temperatures. The linear operation region of the actuator is restricted to temperatures between 15°C to 45°C for the materials with low mismatch of thermal expansion coefficient between metal and ceramic elements. For temperatures below 15°C, the increasing of the displacement with the temperature is related to the temperature dependence of the piezoelectric ceramic, in particular of the d_{31} variation with temperature [8].

With masterbond it is possible to extend the operating temperature range of the cymbal actuator (figure 3). In that case it is observed that the temperature dependence of the displacement is very close to that of the d_{31} of the ceramic in all the temperature range. That dependence is higher for the least stiff metal endcaps. Some deviations to such a behavior are observed for the metals with higher thermal expansion coefficient than the ceramic. Figure 4 shows various measured curves for brass, kovar and tungsten metal endcaps bonded with masterbond to several PZT ceramic types. From these curves it is possible to determine different ways to eliminate the thermal dependence of the cymbal actuators:

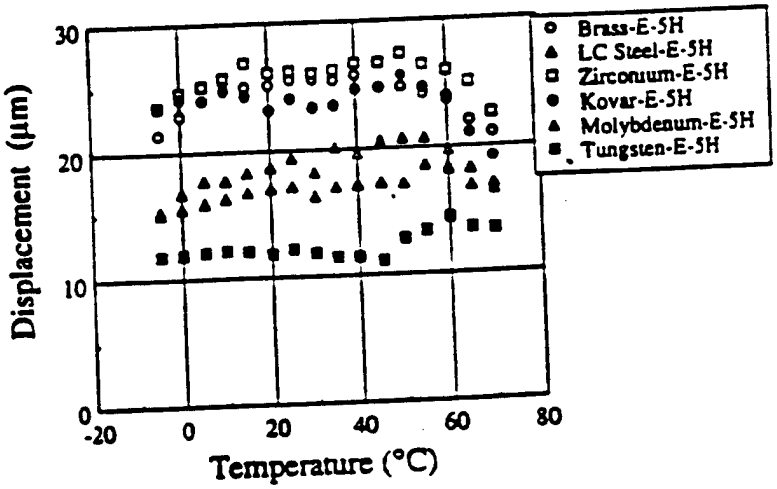

Figure 2. Displacement as a function of temperature for cymbals bonded with eccobond.

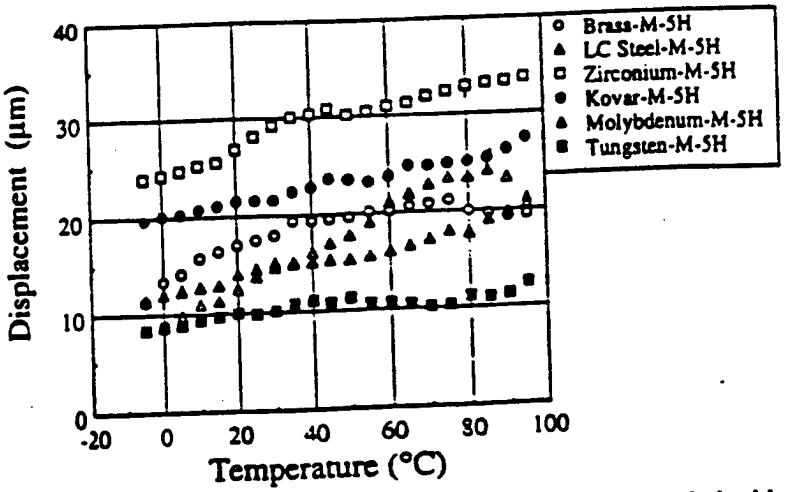

Figure 3. Displacement as a function of temperature for cymbals bonded with masterbond.

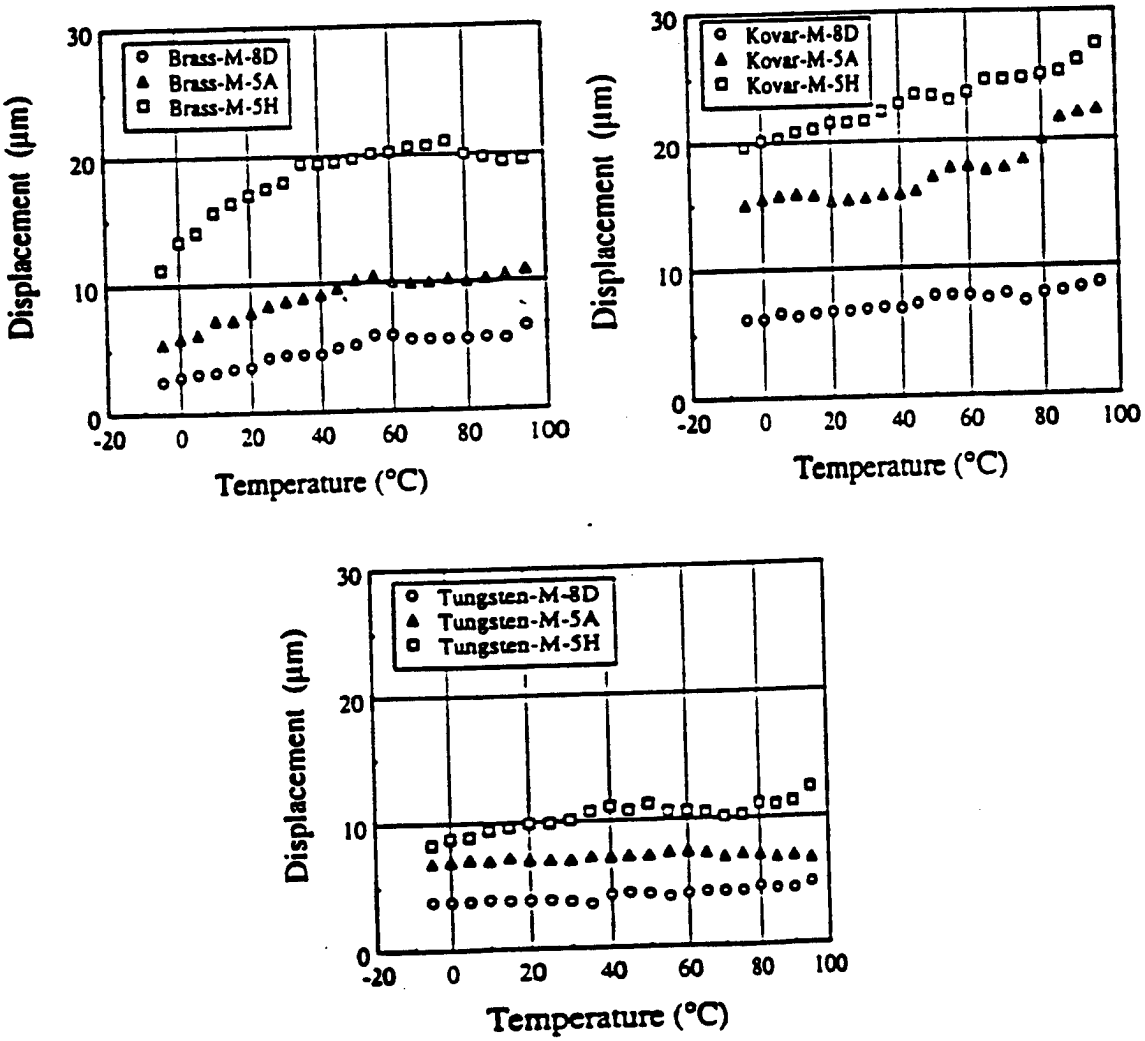

Figure 4 Displacement as a function of temperature for the cymbal bonded with masterbond showing the behaviour of different PZT types for brass, kovar and tungten endcaps.

a) Reducing the temperature dependence of the radial coefficients of the PZT ceramic. If the bonding has no significant effect on the temperature characteristics and the stiffness of metal is low, the metal-ceramic composite follows the thermal characteristics of PZT ceramics, meaning that the cymbal works as a displacement amplifier. In such a case, piezoelectric ceramics with low temperature dependence are more powerful for temperature applications, such as PZT 8D and even PZT 5A.

b) Changing the cavity size: In the case of brass, it is possible to observe a very low temperature dependence for temperatures higher than 40°C. In such a case, the mismatch of thermal expansion coefficients between the metal endcaps and the ceramic produces a positive and high TID or in other words, the cavity size changes. It is possible to consider that the cavity size is changing slowly in relation to the cavity depth. As the cavity depth increases the displacement decreases [9]. Inconvenient is that the net position of the actuator is increasing continuously because of the TID, even though the temperature dependence could be cancelled for a fixed temperature range.

c) Using higher stiffness metal: The mechanical losses cause a reduction of the displacement, however tungsten endcaps provide a temperature independent behavior. One of the most important characteristics of that composite is the existence of a slightly negative TID that can be easily compensated.

d) Combining multistack structures constructed using the above mentioned effect, it is possible to have very high displacement and negligible TID and temperature dependence.

ACKNOWLEDGMENTS

The authors would like to express their gratitude for the support to the following agencies and organizations: Office of Naval Research Contract no. N00014-92 J 1510, National Science Foundation Grant no. DMR-9223847, Spanish Science Ministry (CICYT MAT94-807 and DGICYT PR94-028), Turkish Science and Technology Council (TUBITAK) and Middle East Technical University, Ankara-TURKEY.

REFERENCES

[1] R. E. Newnham, Q. C. Xu and S. Yoshikawa, Transformed Stress Direction-Acoustic Transducer, U.S. Patent # 4,999,819, March 12, 1992.

[2] Q. C. Xu, A. Dogan, J. Tressler, S. Yoshikawa and R. E. Newnham, "Ceramic-Metal Composite Actuators", *Ferroelectrics* 160,337-46(1994).

[3] K. Onitsuka, "Effects of Bonding and Geometry on the Flextensional Transducer, "Moonie"", Ph.D. Thesis, The Pennsylvania State University, University Park, PA (1993).

[4] K. Onitsuka, A. Dogan, Q.C. Xu, J. Tressler, S. Yoshikawa and R.E. Newnham, "Design Optimization for Ceramic-Metal Composite Actuators (Moonie)", *Ferroelectrics* 156,37-42(1994).

[5] A. Dogan, S. Yoshikawa, K. Uchino and R. E. Newnham, "The Effect on the Characterics of the Moonie Transducer and Reliability Issue", *IEEE Transactions on Ultrasonics, Ferroelectrics and Frequency Control*, Proceeding V.II pp 935-9, France (1994).

[6] A. Dogan, "Flextensional "Moonie and Cymbal" Actuators", Ph.D. Thesis, The Pennsylvania State University, University Park, PA (1994).

[7] A. Dogan, J.F. Fernandez, K. Uchino and R. E. Newnham, "New Piezoelectric Composite Designs for Displacement Amplification" IV ECERS, this volume.

[8] D. Berlincourt; "Piezoelectric Crystal and Ceramics" Ultrasonic Transducer Materials, O. E. Mattiat ,Plenum Press, New York (1971)

[9] Q. C. Xu, S. Yoshikawa, J. Belsick and R. E. Newnham, "Piezoelectric Composites with High Sensitivity and High Capacitance for Use at High Pressures", *IEEE Transactions on Ultrasonics, Ferroelectrics and Frequency Control*, 38, 6, 634-639(1991).

APPENDIX 41

COMPOSITE SENSORS AND ACTUATORS

ROBERT E. NEWNHAM*

Composite materials have found a number of structural applications but their use in the electronics industry has been relatively limited. As the advantages and disadvantages of electroceramic composites are better understood, we can expect this picture to change.

In this paper we review some of the composite sensor and actuator studies carried out in our laboratory during the past two decades. These functional composites make use of a number of underlying ideas including connectivity patterns leading to field and force concentration; the use of periodicity and scale in resonant structures; the symmetry of composite structures and its influence on physical properties; polychromatic percolation and coupled conduction paths; varistor action and other interfacial effects; sum, combination, and product properties; coupled phase transformation phenomena; and the important role that porosity and inner composites play in composite materials. These ideas provide a basic understanding of functional composites and have been discussed previously [1]. In the present paper, we describe several composite piezoelectrics and their applications. Several of these transducers mimic the geometries of the sound-sensing organs of fish: elongated feelers, vibrating air bladders, and spherical inner ears.

Early investigators concentrated on polymer-ceramic composites for use as hydrophones. Several interesting connectivity patterns [2] were developed including 3-3 structures made by the replamine process [3] and by fugitive phase technique [4]. Then came the more useful 1-3 composites consisting of parallel PZT fibers embedded in a polymer matrix. These structures were made by extrusion [5], by dicing [6], and more recently by injection molding [7] and lithographic lost-wax techniques [8]. The coupling between the ceramic fibers and the polymer matrix is important [11]. In optimizing hydrophone performance, the $d_h g_h$ product was chosen as a figure of merit. The 1-3 composite increases d_h and g_h by reducing the d_{31} piezoelectric coefficient and the dielectric constant while maintaining the large d_{33} coefficient.

The usefulness of the 1-3 composite in high frequency applications for non-destructive testing and medical diagnostics was recognized later [9]. Biomedical transducers require resonant frequencies in the 1-10 MHz range, high electromechanical coupling coefficients, low acoustic impedance, and broad bandwidth. The 1-3 transducers manufactured by Siemens [8] have thickness resonances of 5-10 MHz, coupling coefficients $k_t = 0.67$, $K = 600, \tan\delta < 0.025$, and a mechanical Q about 10.

* Intercollege Materials Research Laboratory, Pennsylvania State University, University Park, PA 16802-4801, USA.

Poling is sometimes difficult for the long, slender PZT fibers used in 1-3 composites. Electric breakdown often occurs before poling is complete, and the transducer is ruined. Lower poling and driving fields are obtained when the spaghetti-like PZT fibers are replaced with macaroni-like PZT tubules. When electroded inside and out, the thin-walled tubes are poled and driven radially at relatively modest voltages. Radial motions are coupled to length-wise displacements through the d_{31} coefficient. Effective piezoelectric constants of about 8000 pC/N and large $d_h g_h$ products are achieved with these composites [10]. Other variants on the basic 1-3 structure include the 1-2-3 composite with transverse load bearing fibers [11], and the 1-3-0 composite with a foamed polymer matrix [12], and the interesting woven fiber composites devised by Safari and co-workers [13].

Perhaps the simplest piezoelectric composite is the 0-3 transducer made by dispersing ceramic particles in a polymer matrix. The NTK Piezo-Rubber films and cables are used as flexible hydrophones, keyboards. blood pressure cuffs, and musical instruments. They are made by hot-rolling $PbTiO_3$ particles into a chloroprene rubber matrix [14].

Composites with 1-3 and 3-2 connectivity were prepared by drilling either circular or square holes in prepoled PZT blocks. Drilling was carried out in a direction perpendicular to the poled axis and by filling the drilled holes with epoxy [15]. On samples optimized for hydrophone performance, the g_h and $d_h g_h$ coefficients were about 4 and 40 times greater, respectively, for the 1-3 composites; and 25 and 150 times greater for the 2-3 composites compared to those of solid PZT.

BB transducers are made from hollow spheres of PZT a few millimeters in diameter, about the same size as the metallic pellets used in air rifles (BB guns). PZT BBs are mass produced by a patented forming process [16] in which air is blown through a PZT slurry of carefully controlled viscosity. The hollow spheres are 1-6 mm in diameter with wall thickness of 0.1 mm. Densities are about 1.3 g/cm^3 giving the BB a low acoustic impedance close to that of water and human tissue. When embedded in a polymer matrix to form a 0-3 composite the BB spheres are surprisingly strong, and able to withstand large hydrostatic pressure without collapse. Close-packed transducer arrays are easily assembled.

When electroded inside and out, and poled radially the BB becomes an omnidirectional transducer suitable for underwater or biomedical applications. For spheres 2.6 mm is diameter with 90 mm thick walls, the resonant frequencies are 700 kHz for the breathing mode (d_{31}) and 10 MHz for the wall thickness mode (d_{33}). BBs are small enough to be used in catheters for non-invasive surgery to act as beacons, sensors, and actuators.

In recent years, piezoelectric and electrostrictive ceramics have been used in many actuator applications [17]. To meet these needs a new type of composite actuator based on a flextensional transducer has been developed [18]. This ceramic-metal composite actuator, or "moonie" consists of either a piezoelectric ceramic disc or a multilayer stack, sandwiched be-

tween two specially designed metal end caps. This design provides a sizable displacement, as well as a large generative force. In other words, it bridges the gap between the two most common types of actuators, the multilayer and the bimorph. The shallow spaces under the end caps produce a substantial increase in strain by combining the d_{33} and the d_{31} contributions to the ceramic. It is attractive for hydrophone, transceiver and actuator applications, and is especially advantageous for use as a non-resonant, low frequency projector in deep water [19].

REFERENCES

[1] R.E. NEWNHAM, J. Mat. Edu. **7** (1985) 601.
[2] R.E. NEWNHAM, D.P. SKINNER AND L.E. CROSS. Mat. Res. Bull. **13** (1978) 525.
[3] D.P. SKINNER, R.E. NEWNHAM AND L.E. CROSS. Mat. Res. Bull. **13** (1978) 599.
[4] T.R. SHROUT, W.A. SCHULZE AND J.V. BIGGERS. Mat. Res. Bull. **14** (1979) 1553.
[5] K.A. KLICKER, J.V. BIGGERS AND R.E. NEWNHAM. J. Am. Ceram. Soc. **64** (1981) 5.
[6] H.P. SAVAKUS, K.A. KLICKER AND R.E. NEWNHAM. Mat. Res. Bull. **16** (1981) 677.
[7] C.P. BOWEN, T.R. SHROUT, R.E. NEWNHAM AND C.A. RANDALL, Journal of Int. Mat. Syst. & Struct. **6** (1995) 159-168.
[8] G. PREU, A. WOLFF AND D. CRAMES, U. Bast Euro-Ceramics II **3** (1991) 2005.
[9] T.R. GURURAJA, W.A. SCHULZE, L.E. CROSS, R.E. NEWNHAM, B.A. AULD AND Y.J. WANG, EKE Transactions on Ultrasonics **32** (1985) 481, 499.
[10] W. PAN, Q.M. ZHANG, A. BHALLA AND L.E. CROSS. J. Am. Ceram. Soc. **72** (1989) 571.
[11] M.J. HAUN, R.E. NEWNHAM AND W.E. SCHULZE. Adv. Ceram. Mat. **1** (1986) 361.
[12] M.J. HAUN AND R.E. NEWNHAM, Ferroelectrics **68** (1986) 123.
[13] V.F. JANAS AND A. SAFARI, J. Am. Ceram. Soc. **78** (1995) 2945.
[14] H. BANNO, Ferroelectrics **50** (1983) 329.
[15] A. SAFARI, S. DAVANZO AND R.E. NEWNHAM, Ferroelectrics **50** (1983) 257.
[16] R. MEYER, H. WEITZING, Q.C. XU, Q.M. ZHANG. R.E. NEWNHAM AND J.K. COCHRAN, J. Amer. Ceram. Soc. **77** (1994) 1669.
[17] K. UCHINO, Mat. Res. Soc. Bull. **18** (1993) 42.
[18] Y. SUGAWARA, K. ONITSUKA, S. YOSHIKAWA, Q. XU, R.E. NEWNHAM, AND K. UCHINO, J. Am. Ceram. Soc. **75** (1992) 996.
[19] Q.C. XU, S. YOSHIKAWA, J. BELSICK, AND R.E. NEWNHAM, IEEE Transactions on Ultrasonics, Ferroelectrics and Frequency Control, **38** (1991) 634.

APPENDIX 42

DOUBLY RESONANT CYMBAL-TYPE TRANSDUCERS

James F. TRESSLER and Robert E. NEWNHAM

Materials Research Laboratory, The Pennsylvania State University

University Park, PA 16802 USA

Abstract **- A doubly resonant cymbal-type transducer has been developed by capping a poled piezoceramic disk asymmetrically. It is intended for use in the frequency range between 10 kHz and 50 kHz. The two resonance frequencies can be easily manipulated by selecting appropriate cap materials and/or geometry. The prominent feature of this device is the ability to obtain two resonances at desired frequencies without the need for electrical tuning. In addition, proper placement of the resonance frequencies may also allow for the broadening of the operational bandwidth as well as the generation of difference frequencies.**

I. INTRODUCTION

Multiple resonant acoustic projectors can exhibit a number of advantages over their singly resonant counterparts, namely the potential for wider operational bandwidths and difference frequency generation. Typically, multiple resonances are generated through the use of electronics and/or the use of acoustic matching plates. Steel, et al. [1] developed a continuously tunable two-plate high-frequency (240 kHz) transducer in which one piezoceramic disk was used as the driver and the second was used to control the resonance condition through the use of appropriate inductors and resistors in the electrical circuitry. Jain and Smith [2] applied this same concept to their low frequency (30 kHz) continuously tunable sandwich transducer which consisted of four PZT rings (2 drive, 2 control) sandwiched between two metal masses. Loading the control

ceramics with an inductive load made the structure resonate at two frequencies. Inouye, et al. [3] achieved dual resonance conditions by attaching an acoustic matching plate to a tapered piezoceramic resonator. This configuration had resonances at 23 kHz and 32 kHz. Similarly, a constant area Langevin transducer consisting of a quarter wave front (head) layer, a ceramic stack, and a steel tail was found to exhibit two distinct resonance peaks in its conduction response (at 73 kHz and 119 kHz). This dual resonance behavior was only observed, though, when the characteristic impedance of the head material exceeded 4 MRayls [4]. Doubly resonant longitudinal vibrations have been obtained in tonpilz transducers by using three masses instead of the conventional two, where the additional mass is inserted within the piezoelectric stack [5]. This type of transducer has two mechanical resonances that can be used for both transmitting and receiving operations. By proper design, it is possible to use the entire frequency band from the lower resonance frequency to somewhat above the upper resonance frequency. Very high frequency dual mode transducers are also being investigated as ultrasonic probes for the carotid artery [6]. In this application, a dual frequency probe made from a multilayer ceramic is used to obtain a mode image simultaneously with a high resolution B mode scan. The ceramic consists of two layers of different thickness poled in opposite directions. A thickness ratio of 1 to 0.7 gave dual resonances at 3.75 MHz and 7.5 MHz.

The patented moonie and cymbal-type transducers [7,8] have been shown to be excellent electroacoustic transducer candidates. Their operational principles have been reported previously [9,10]. The cymbal design consists of a piezoelectric ceramic disk (typically PZT) poled in the thickness direction which is sandwiched between two thin metal endcaps, each of which contains a truncated cone-shaped cavity on its inner surface. The moonie style cap, on the other hand, consists of a metal disk with a shallow conical cavity machined into its inner surface. When the ceramic contracts radially under the application of an applied AC electric field, the endcaps flex to give an amplified strain (displacement) in the direction normal to the cap surface. In addition, the moonie, and especially the cymbal, are characterized as being of small size, thin profile, and perhaps most importantly, easy and inexpensive to fabricate.

A doubly resonant cymbal-type transducer has been constructed by capping a PZT driving element asymmetrically. The focus of this paper is to demonstrate the ease by which it is possible to generate distinct resonances at any two desired frequencies between 10 kHz and 50 kHz through proper design engineering without the need for electronic tuning or matching plates. Two configurations will be considered: (1) two identically shaped cymbal caps of different metals, and (2) two caps of the same material, but with different shapes.

II. EXPERIMENTAL PROCEDURE

The doubly resonant cymbal transducers were made by first shaping the metal caps to the desired geometry. In the case of the cymbal caps, a die punch simultaneously cut and shaped the caps from a sheet of metal foil 0.25 mm thick. The dimensions of the cymbal caps were: diameter = 12.7 mm, thickness = 0.25 mm, the cavity diameter was tapered from 9.0 mm at the bottom of the cap to 3.0 mm at the top, and the maximum cavity depth ranged from 0.12 mm to 0.47 mm. The flange of each of the caps was bonded to a PZT-5A disk (Piezokinetics, Bellefonte, PA) poled in the thickness direction which was 12.7 mm in diameter and 1.0 mm thick. The adhesive was a thin layer ($\approx$ 20 μm thick, 1.5 mm wide) of Emerson and Cuming Insulating Epoxy (45LV epoxy resin, 15LV resin hardener). Great care must be taken to insure that no epoxy leaks into the air-filled cavity and that the layer is thin enough to ensure a good metal/PZT electrode contact. The capacitance of the transducer and its admittance (or conductance) spectrum are simple and effective techniques that can be used to characterize the quality of the bonding layer, with the latter doubling as a means to observe the dual resonances. The Ansys® (Swanson Analysis Systems, Inc.) finite element software program was also used as a guide in designing the transducers. Modal analysis was used to obtain the resonance frequencies and mode shapes for a two dimensional axisymmetric model.

III. EXPERIMENTAL RESULTS

The fundamental resonance frequency of a 12.7 mm diameter cymbal transducer is governed by the elastic constants of the endcap material [11], as well as the cap thickness and cavity dimensions. Fig. 1 shows the FEA calculated first resonance frequency of a cymbal transducer capped with different metals of varying cavity depth (cap thickness and cavity diameter held constant at 0.25 mm and 9.0 mm, respectively). As can be seen, by the appropriate selection of cap materials and cap geometry, the fundamental resonance frequency can be easily tailored from 15 kHz to about 45 kHz. These data imply that capping the PZT driving element asymetrically should result in a double resonance.

The first asymetrically capped cymbal transducer used two identically shaped caps of different materials, steel and brass. The measured conductance vs. frequency spectrum is shown in Fig. 2. The dual resonance behavior is quite apparent. The first resonance, at 23.1 kHz, is the (0,1) mode associated with the brass cap and the second resonance, at 32.9 kHz, is the (0,1) mode of the steel cap. This conclusion was arrived at from the mode shapes at these two frequencies as calculated by the Ansys® finite element program (Fig. 3). This shows that the dual resonance behavior of the steel/brass cap combination is a direct result of the individual vibrations associated with each cap. The use of two different cap types also results in a double resonance. Fig. 4 compares the measured admittance spectra of (a) the moonie-type transducer, (b) the cymbal-type transducer, and (c) the moonie/cymbal cap combination. These results experimentally verify the argument that the dual resonance behavior derives from the fundamental resonance mode of each individual cap.

As evidenced by Fig. 1, the cap geometry also strongly affects the resonance frequency. Therefore, obtaining dual resonance behavior with cymbal caps of a single material can also be accomplished by using two caps with different dimensions. The admittance spectra of cymbal transducers with brass caps each with a different cavity depth is shown in Fig. 5. The dual

resonance behavior is again visible, where the first resonance, at 17.3 kHz, 18.1 kHz, or 24.3 kHz is due to the (0,1) mode of the cap with the shallower cavity, 0.12 mm, 0.18 mm, or 0.32 mm, respectively. The second resonance, at 30 kHz, is due to the (0,1) mode of the cap with the deeper cavity, 0.47 mm. Utilizing caps with nearly the same shape can drive the two resonances close enough that they can couple together (Fig. 6). When this occurs, it is possible to increase the operational bandwidth by lowering the mechanical Q. From this result, it appears as though the operational bandwidth of the doubly resonant cymbal is roughly twice that of the singly resonant device.

Being able to fix two individual resonances at the desired frequencies in a cymbal transducer of a given diameter by simply either capping it asymmetrically with different materials and/or with differently shaped caps provides the transducer designer the capability of working with a very simple structure and being able to manipulate the working frequency range of the device without the need for sophisticated electronics.

IV. CONCLUSIONS

A dual resonance transducer has been developed simply by capping a PZT disk driving element asymmetrically. The simple construction, small size, thin profile, inexpensive fabrication procedure, and ability to easily tailor the two resonances by changing the cap materials and/or manipulating their dimensions are the striking features of this device. It is expected that capping the ceramic driving element asymmetrically with caps of two different thicknesses or with two different cavity diameters will also generate dual resonance behavior.

REFERENCES

[1] G.A. Steel, B.V. Smith, and B.K. Gazey, "Tunable Sonar Transducers," *Electronics Lett.*, vol. 22, pp. 758-759, July 1986.

[2] S.K. Jain and B.V. Smith, "Tunable Sandwich Transducer," *Electronics Lett.*, vol. 24, pp. 311-312, March 1988.

[3] T. Inouye, T. Nada, A. Kameyama, K. Sugiuchi, S. Takahashi, and M. Konno, "Investigation for Wide-Band Underwater Ultrasonic Transducers," *Trans. of the IEICE*, vol. E 70, pp. 723-734, August, 1987.

[4] B.V. Smith, R.L. Mansfield, D.T.I. Francis, and J.R. Dunn, "The Design of a 100-kHz Wideband Sonar Transducer," in *Proceedings of the Third International Workshop on Transducers for Sonics and Ultrasonics*, M.D. McCollum, B.F. Hamonic, and O.B. Wilson, Eds. Lancaster, PA: Technomic, 1993, pp. 231-238.

[5] S.C. Thompson, M.P. Johnson, E.A. McLaughlin, and J.F. Lindberg, "Performance and Recent Developments with Doubly Resonant Wideband Transducers," in *Proceedings of the Third International Workshop on Transducers for Sonics and Ultrasonics*, M.D. McCollum, B.F. Hamonic, and O.B. Wilson, Eds. Lancaster, PA: Technomic, 1993, pp. 239-249.

[6] S. Saitoh, M. Izumi, and Y. Mine, "A Dual Frequency Ultrasonic Probe for Medical Applications," *IEEE Trans. Ultrason., Ferroelec., Freq. Contr.*, vol. 42, pp. 294-300, March 1995.

[7] R.E. Newnham, Q.C. Xu, and S. Yoshikawa, "Transformed Stress Direction Acoustic Transducer," United States Patent no. 4,999,819, March 12, 1991.

[8] A. Dogan and R.E. Newnham, "Metal-Electroactive Ceramic Composite Actuator," United States Patent Pending.

[9] Q.C. Xu, S. Yoshikawa, J.R. Belsick, and R.E. Newnham, "Piezoelectric Composites with High Sensitivity and High Capacitance for Use at High Pressures," *IEEE Trans. Ultrason., Ferroelec., Freq. Contr.*, vol. 38, pp. 634-639, November 1991.

[10] Q.C. Xu, A. Dogan, J. Tressler, S. Yoshikawa, and R.E. Newnham, "Ceramic-Metal Composite Actuator," *Ferroelectrics*, vol. 160, pp. 337-346, 1994.

[11] J.F. Tressler, A. Dogan, J.F. Fernandez, J.T. Fielding, Jr., K. Uchino, and R.E, Newnham, "Capped Ceramic Hydrophones," in *1995 IEEE Ultrasonics Symposium Proceedings*, M. Levy, S.C. Schneider, B.R. McAvoy, Eds., Piscataway, NJ: Inst. Electrical and Electronics Engineers, 1995, pp. 897-900.

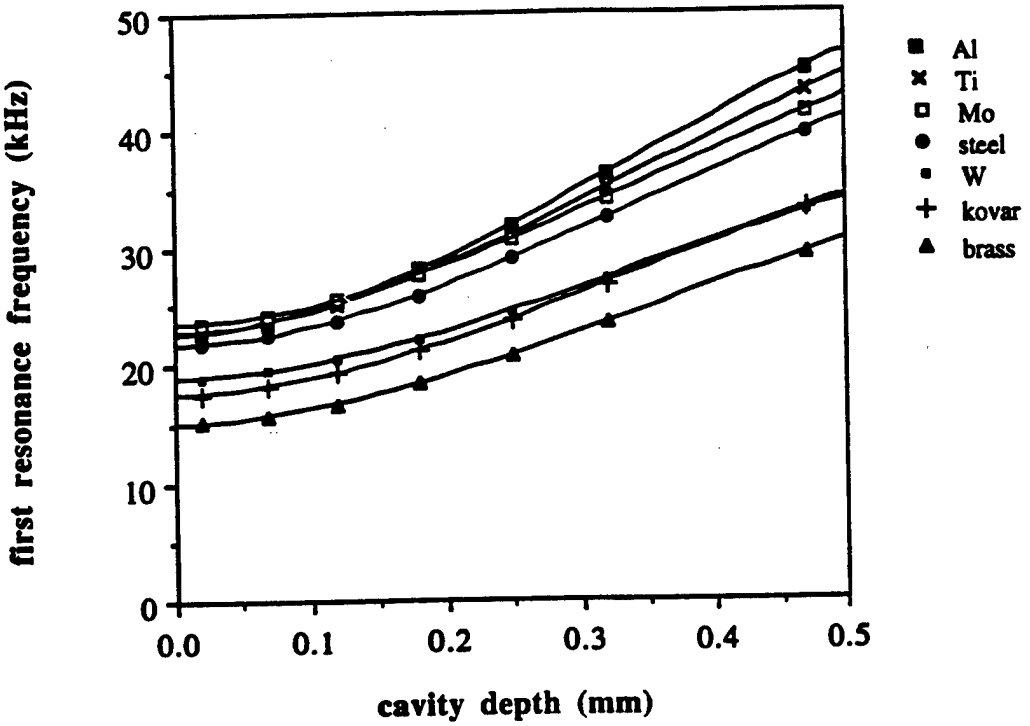

Fig. 1. Effect of cap material and cavity depth on the first resonance frequency of a standard size cymbal transducer (values calculated from Ansys® program). The key shows the element symbols or alloy names used as cap materials.

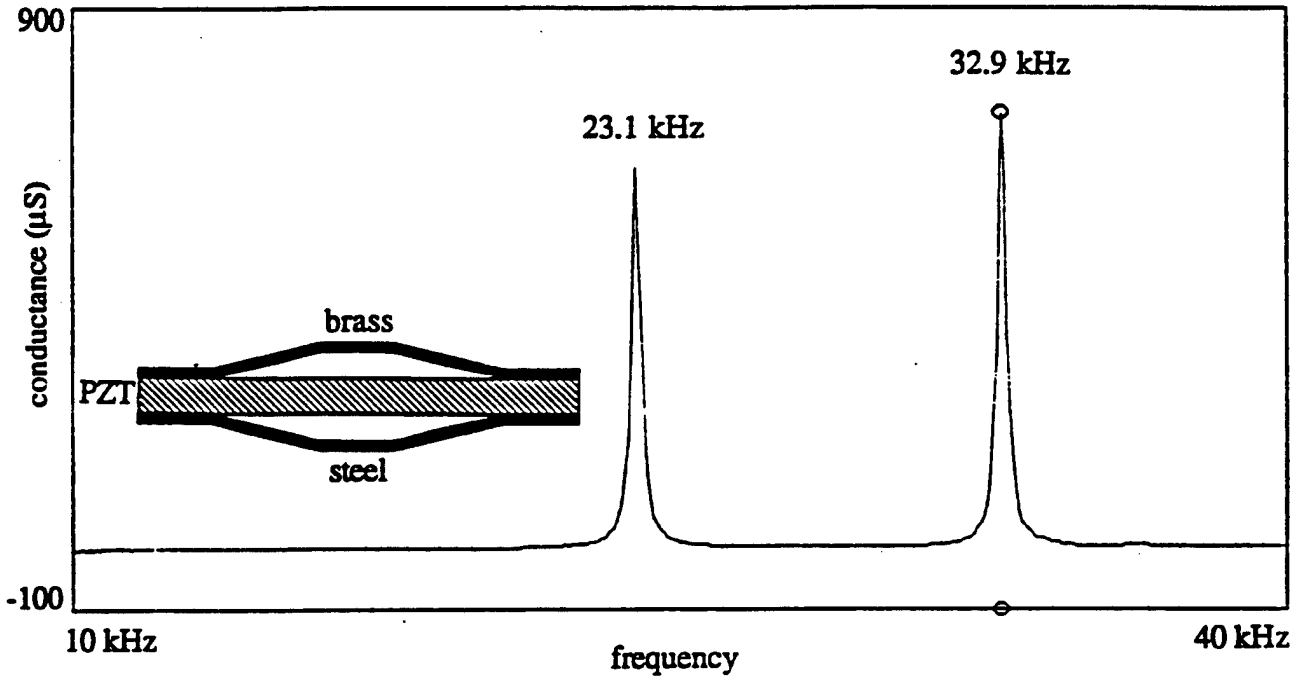

Fig. 2. Conductance vs. frequency for a cymbal transducer with a brass/steel endcap combination as measured in air.

(a) brass cap (0,1) mode at 23.1 kHz

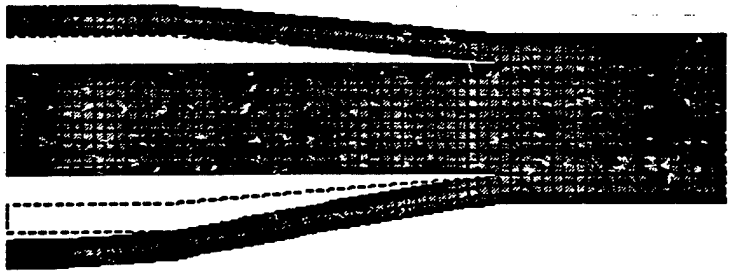

(b) steel cap (0,1) mode at 32.9 kHz

Fig. 3. Vibration mode shapes calculated by FEA for the brass/steel cap combination at (a) 23.1 kHz, and (b) 32.9 kHz. The dashed lines indicate the undeformed shape.

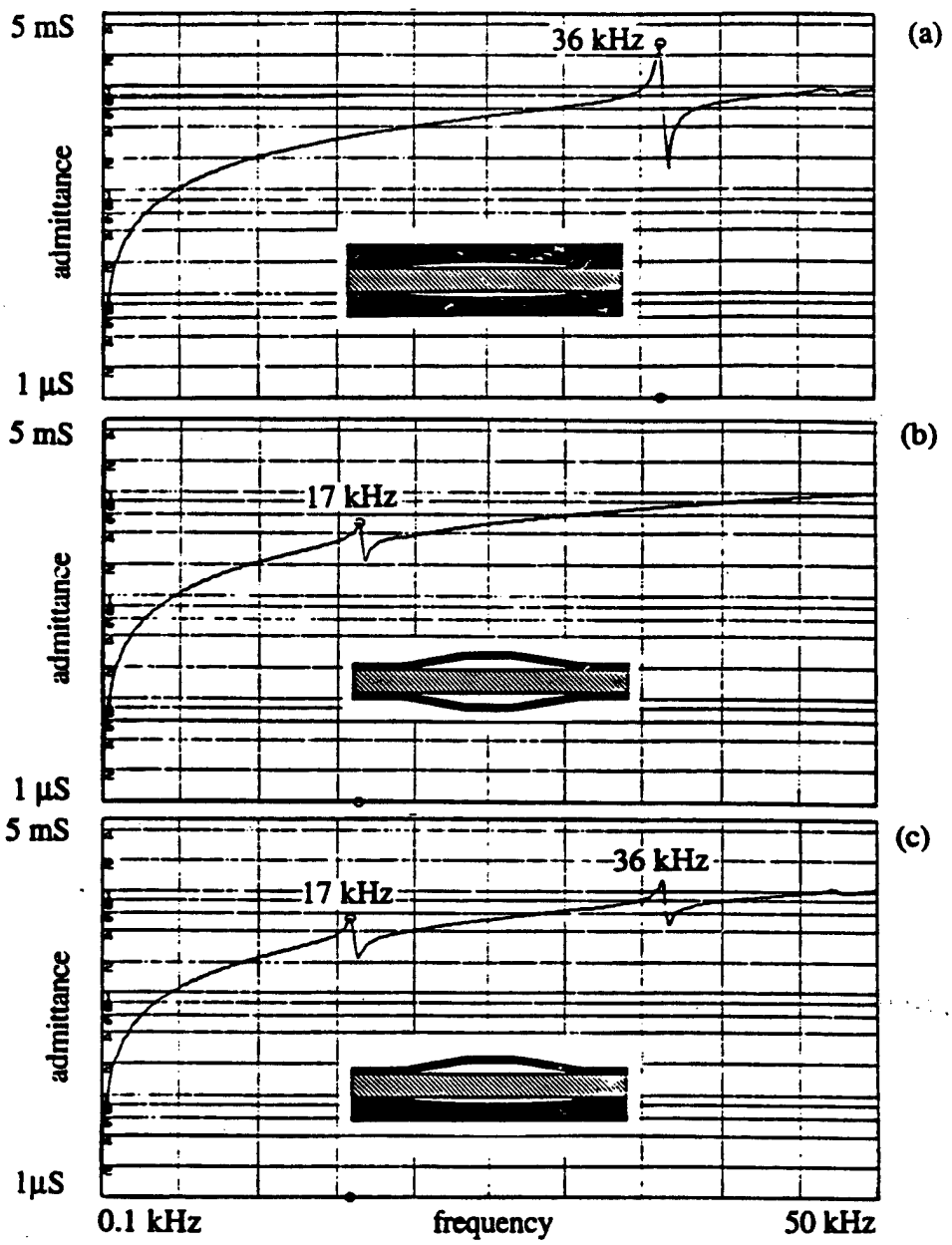

Fig. 4. Measured admittance spectra of (a) the standard brass-capped moonie transducer, (b) the standard brass-capped cymbal transducer, and (c) the moonie/cymbal cap combination transducer.

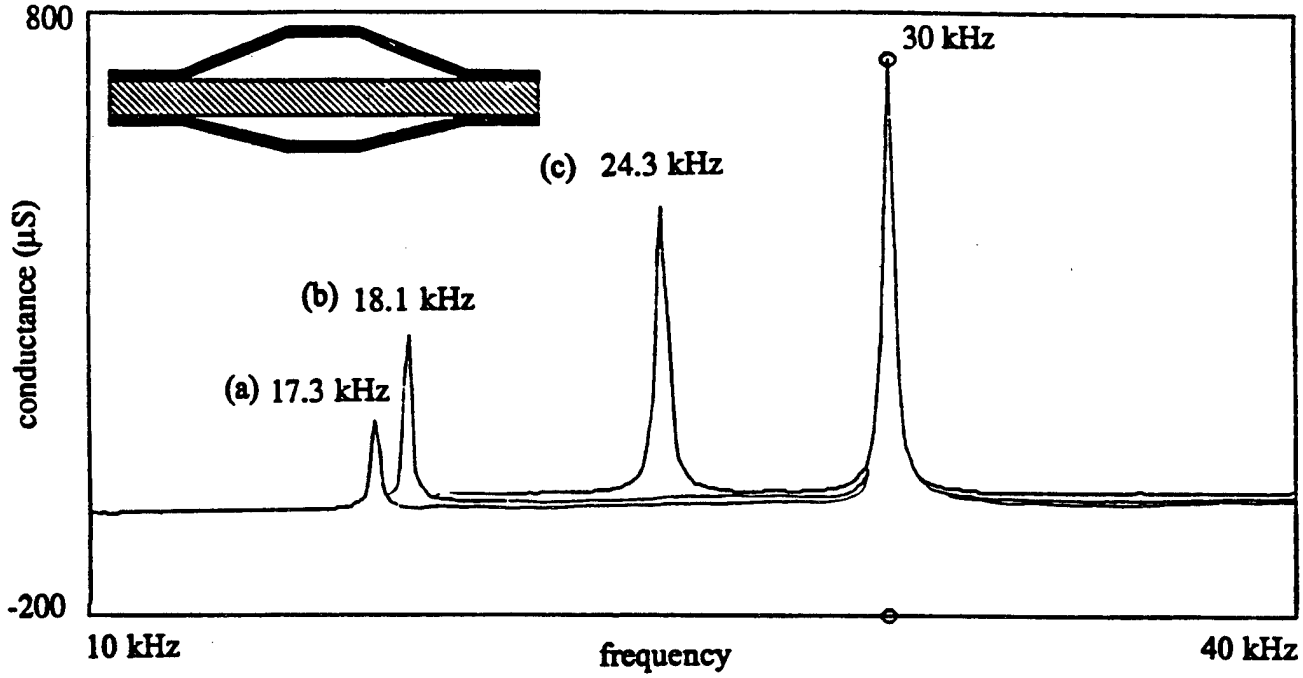

Fig. 5. Conductance vs. frequency for a cymbal transducer with two brass caps, one of which has a cavity depth of 0.47 mm and the other having a cavity depth of (a) 0.12 mm, (b) 0.18 mm, and (c) 0.32 mm. All were measured in air.

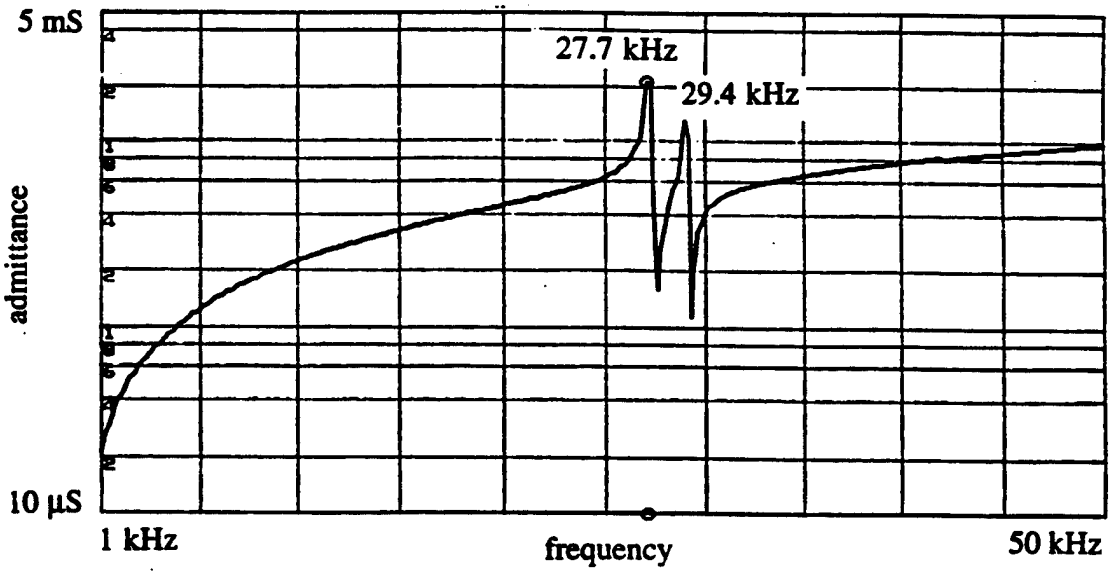

Fig. 6. Measured admittance spectrum of a brass-capped cymbal transducer showing the ability to couple the two resonances.

APPENDIX 43

Ceramic-Metal Composite Transducers for Underwater Acoustic Applications

James F. Tressler, Wenwu Cao, Kenji Uchino, and Robert E. Newnham
International Center for Actuators and Transducers, Materials Research Laboratory
Pennsylvania State University, University Park, PA 16802 USA

Abstract--A ceramic-metal composite electro-acoustic transducer has been developed for use as an underwater projector or receiver. Its resonance frequency ranges from 10 kHz to 40 kHz and its effective coupling coefficient is around 20%. Finite element analysis has been performed to ascertain how the transducer dimensions and the materials that comprise it effect aforementioned parameters.

I. INTRODUCTION

A. The Cymbal Transducer

The new cymbal-type transducer [1], like the patented moonie transducer [2], is based on the concept of the flextensional transducer. Both the cymbal and moonie utilize either a poled piezoelectric, electrostrictive, or ferro- to antiferroelectric phase change material in the form of a ceramic disk (fully electroded on each face). This disk is sandwiched between two specially shaped metal electrode endcaps, each of which contains a shallow air-filled cavity on its inner surface. In the case of the moonie transducer, the cavities are in the shape of a half moon, whereas the cymbal contains a truncated cone-shaped cavity (see Fig. 1). The presence of these cavities allows the metal caps to serve as mechanical transformers for converting a portion of an incident axial direction stress into radial and tangential stresses of opposite sign. Alternatively, the caps can also couple an extensional vibration mode of the ceramic to a flexural vibration motion of the cap to produce a large displacement in the axial direction.

B. Finite Element Analysis

The finite element method is a powerful tool for the design and analysis of electroacoustic transducers. There are a host of high quality references that detail the theory of FEM so it will not be discussed here. A number of software packages are currently available which perform FEA. The two most common which have the capability to perform piezoelectric analysis are Atila® and ANSYS®. The latter can do static, harmonic, transient, or modal analyses [3]. Static analysis is used to determine displacements, stresses, etc., under static loading conditions. Harmonic analysis determines the steady state response of a structure under a sinusoidal external drive. Transient dynamic analysis ascertains the response due to arbitrarily time-varying loads, and modal analysis calculates the natural frequencies and mode shapes of the structure.

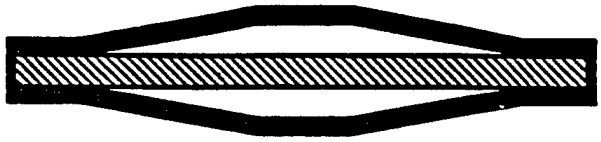

Fig. 1. Cross sectional view of the cymbal transducer (not to scale)

C. Transducer Characterization

When a transducer is used to detect sound underwater, it is commonly referred to as a source or projector. Conversely, when it is used to detect underwater sound, it is called a receiver or hydrophone. It is typically desirable to use a hydrophone at frequencies well below its fundamental resonance so that its response (i.e. output voltage per unit incident pressure) will be independent of frequency over a wide range. Projectors, on the other hand, are generally driven in the neighborhood of the resonance frequency in order to achieve the maximum volume velocity and output power.

The effective coupling coefficient, k_{eff}, is a measure of the transduction process. Its definition, based on energy conservation, is:

$$k_{eff} = \sqrt{\frac{\text{stored mechanical energy}}{\text{input electrical energy}}} \qquad (1)$$

This coefficient can be calculated easily from the resonance (f_r) and anti-resonance frequencies (f_a) as:

$$k_{eff} = \sqrt{1 - \left(\frac{f_r}{f_a}\right)^2} \qquad (2)$$

This paper will focus on how the geometry and materials affect the resonance frequency and effective coupling coefficient of the cymbal transducer.

II. EXPERIMENTAL PROCEDURE

A. Cymbal Transducer Fabrication

Using metal foil between 120 μm and 380 μm thick, 12.7 mm diameter caps were simultaneously cut and shaped using a die punch. The cavity diameter was tapered from 3.0 mm at the top of the cap to 9.0 mm at the bottom. The depth of the cavity, as measured from the top of the cap, ranged from 120 μm to 470 μm. These caps were then adhered to 1.00 mm thick, 12.7 mm diameter poled PZT-552 disks (Piezokinetics) using Emerson and Cuming insulating epoxy. To ensure proper alignment of the caps, the entire assembly was kept under pressure in a special die during the 24 hour, room temperature curing step.

B. Finite Element Analysis

The ANSYS® software package version 5.1 (Swanson Analysis Systems, Inc.) was used to calculate the resonance and antiresonance frequencies, as well as the vibration modes of the cymbal transducer. A two-dimensional axisymmetric model was analyzed and it consisted of three parts: (1) a piezoelectric (PZT) disk, (2) two metal caps, and (3) epoxy layers between the cap and ceramic as well as surrounding the structure.

The PZT disk was fixed at a radius of 6.35 mm and a thickness of 1.0 mm. Equipotential surfaces were placed on both the top and bottom surfaces of the PZT disk to represent the electrodes. The epoxy layer between the cap and ceramic had a thickness of 20 μm and a width of 1.50 mm. The outer epoxy layer had a width of 0.20 mm and a height equal to that of the outer rim of the transducer. The radius of the cavity was fixed at 4.5 mm at the cap/PZT interface and was tapered to 1.5 mm at the top of the cap. Both the thickness of the cap as well as the maximum cavity depth were used as variables in the model.

The resonance frequencies of the transducer were obtained using the short circuit elastic stiffness matrix, $[c^E]$, in the model; whereas the antiresonance frequencies were calculated using the open circuit stiffnesses $[c^D]$. The coupling coefficients were then found by inserting the aforementioned values into Equation (2) [4]. Resonance and antiresonance frequencies were also obtained experimentally in air from the cymbal's admittance spectra using an HP 4194A Impedance Analyzer. The calculated values were then compared to those obtained experimentally.

III. EXPERIMENTAL RESULTS

The results presented in this paper will focus on the cymbal transducer as an underwater projector, as its pressure tolerance and performance as a hydrophone has been reported previously [5]. Fig. 2 shows the first vibration mode of the cymbal transducer as calculated by the ANSYS® program. This mode is the (0,1) or "umbrella" flexural mode of the caps. The dashed lines indicate the undeformed shape.

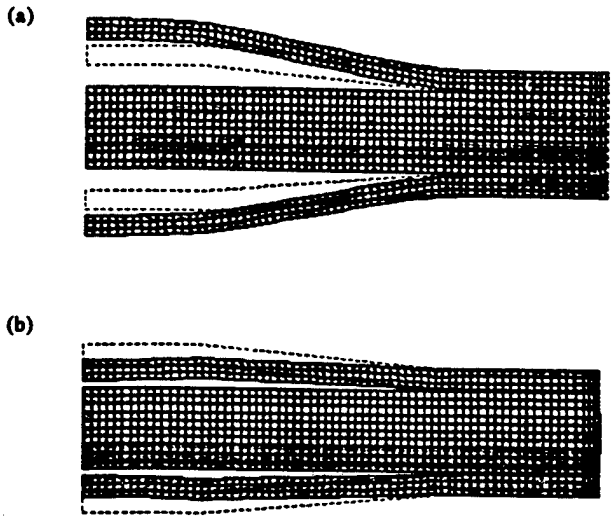

Fig. 2. First vibration mode of the cymbal transducer showing the cap deflection when (a) the ceramic is contracting, and (b) when the ceramic is expanding. The mesh size is also shown here.

Fig. 3 shows the experimentally measured admittance and phase as a function of frequency for a brass capped cymbal in the neighborhood of its fundamental resonance. The cap was 250 μm thick and had a maximum cavity depth of 320 μm. A sharp, smooth peak is indicative of a good quality metal-to-ceramic bond. The resonance at 21 kHz is due to the (0,1) vibration mode of the cap, as described above.

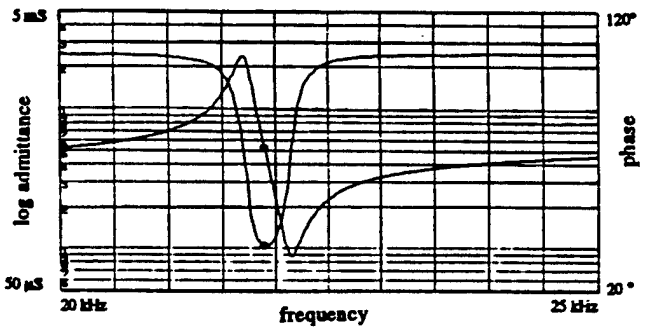

Fig. 3. Admittance and phase as a function of frequency for a brass capped cymbal transducer.

The first resonance frequency of a fixed size cymbal transducer but with different cap materials is shown in Fig. 4. It appears to be a linear function of the ultrasonic velocity of the cap material. The quantity $[E/\rho(1-\sigma^2)]^{1/2}$ is proportional to the resonance frequency of a thin circular plate clamped around its edge [6], which is approximately the boundary condition present in the cymbal. Experimentally obtained results are included for comparison. Discrepancies are attributed to the inability to precisely control the bonding layer width, cavity diameter, and cavity depth (all of which influence the resonance frequency) when fabricating the samples. These results do show, however, that for a given size cymbal transducer, the fundamental resonance frequency can be varied simply by changing the cap material.

The effective coupling coefficients for cymbals with different cap materials, both calculated and experimentally determined, are shown in Fig. 5. The coefficient is solely a function of the Young's modulus of the cap material, as opposed to the resonance frequency, which also depends upon the density and Poisson's ratio. The model underestimates the experimentally obtained value by as much as 20%. This is most likely due to the inability to adequately model the bonding layer. The experimentally determined coupling coefficients are probably more accurate because they are nearly equal to the reported value for a class V flextensional [4].

Fig. 6 shows how the cap thickness influences the resonance frequency of the cymbal transducer. These results show that as the cap thickness increases, the resonance frequency also increases. This is because the caps effectively become "stiffer" as they become thicker.

The effect of the cavity depth (i.e. the cap shape) on the resonance frequency is presented in Fig. 7. As the cavity depth increases, a corresponding increase in the resonance frequency is also observed. This is attributed to the fact that the nodal ring associated with the (0,1) vibration mode of the cap moves toward the center of the cap as the cavity depth increases, thus reducing the actively vibrating surface area.

Fig. 8 shows how the cap thickness and cavity depth affect the effective coupling coefficient (as calculated by the ANSYS® program). The data show that the cap thickness has relatively little effect on k_{eff}, whereas it is strongly influenced by the cavity depth.

Figs. 9 and 10 show the effect of PZT type on the resonance frequency and effective coupling coefficient, respectively. These calculated results show that the PZT type has little effect on the resonance frequency of the cymbal transducer. However, the transducers with softer PZT's exhibit slightly higher coupling coefficients than those which are made of hard PZT.

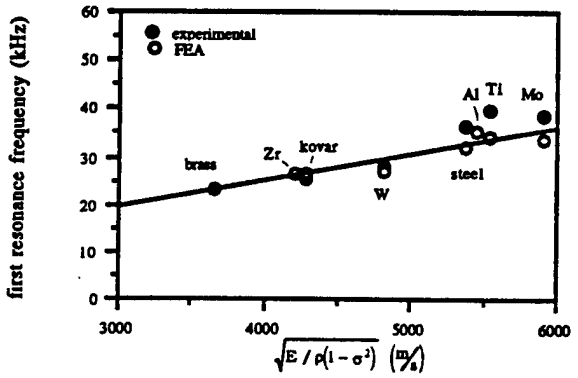

Fig. 4. Effect of cap materials on the first resonance frequency of the cymbal transducer. Metal names or elemental symbols are shown.

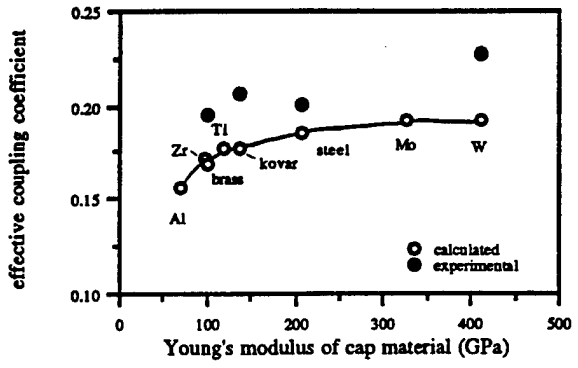

Fig. 5. Effect of cap materials on the effective coupling coefficient of the cymbal transducer. Metal names or elemental symbols are shown.

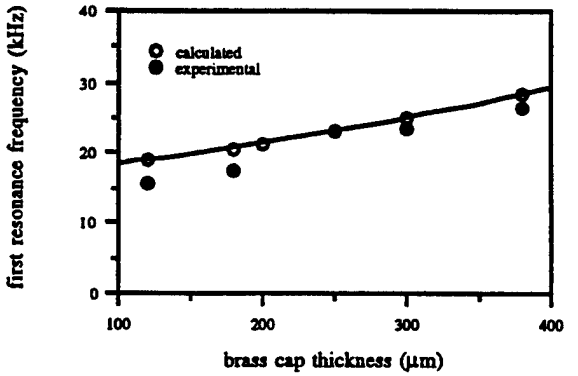

Fig. 6. Effect of brass cap thickness on the first resonance frequency of a cymbal transducer.

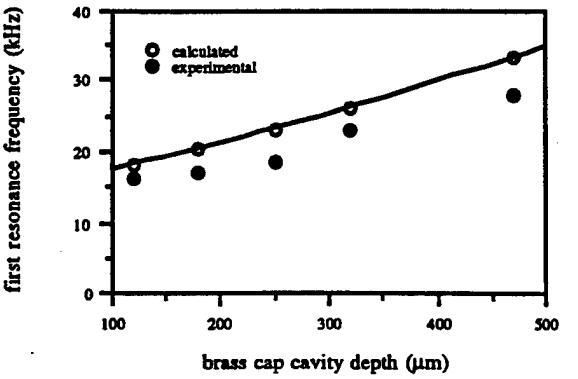

Fig. 7. Effect of brass cap cavity depth on the first resonance frequency of a cymbal transducer.

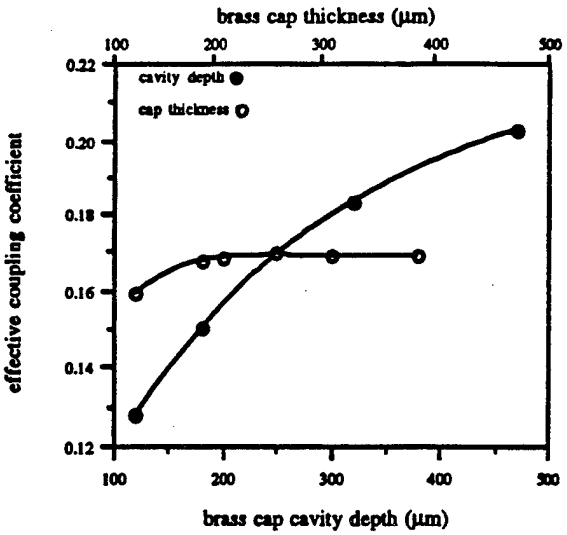

Fig. 8. Effect of brass cap thickness and cavity depth on the effective coupling coefficient of a cymbal transducer.

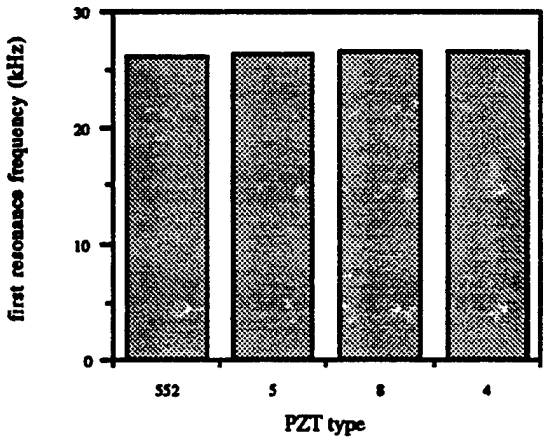

Fig. 9. Effect of PZT type on the resonance frequency of a cymbal transducer (with brass caps). Results are from FEA calculations.

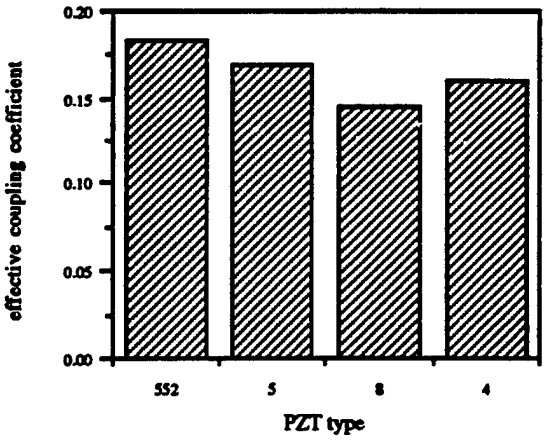

Fig. 10. Effect of PZT type on the effective coupling coefficient of a cymbal transducer (with brass caps). Results are from FEA calculations.

IV CONCLUSIONS

Both the fundamental resonance frequency and effective coupling coefficient of a cymbal transducer can be easily tailored either by changing its endcap material or varying the cap dimensions. This capability gives the transducer designer wider flexibility if constrained by size or materials limitations. Studies are currently underway to determine the effect of water loading on the performance and properties of the transducers.

ACKNOWLEDGMENT

This work was funded through the Office of Naval Research grant #N0001492J1510.

REFERENCES

[1] A. Dogan and R.E. Newnham, "Metal-electroactive ceramic composite actuator," United States Patent pending.

[2] R. E. Newnham, Q. C. Xu, and S. Yoshikawa, "Transformed Stress Direction Acoustic Transducer," United States Patent 4,999,819, March 12, 1991.

[3] *ANSYS User Manuals for revision 5.0*, Swanson Analysis Systems, Inc., Houston, PA, 1992.

[4] K. D. Rolt and J. L. Butler, "Finite element modulus substitution method for sonar transducer effective coupling coefficient," in *Proceedings of the Third International Workshop on Transducers for Sonics and Ultrasonics*, M. D. McCollum, B. F. Hamonic, and O. B. Wilson, Eds., Lancaster, PA: Technomic, 1993, pp. 344-352.

[5] J. F. Tressler, A. Dogan, J. F. Fernandez, J. T. Fielding. Jr., K. Uchino, and R. E. Newnham, "Capped ceramic hydrophones," in *1995 IEEE Ultrasonics Proceedings*, M. Levy, S. C. Schneider, B. R. McAvoy, Eds., Piscataway, NJ: Inst. Electrical and Electronics Engineers, 1995, pp. 897-900.

[6] L. E. Kinsler, A. R. Frey, A. B. Coppens, and J. V. Sanders, *Fundamentals of Acoustics*, 3rd ed., New York: John Wiley & Sons, 1982, ch. 4, pp. 92-95.

APPENDIX 44

Vibration Modes of PZT Hollow Sphere Transducers

Sedat Alkoy, Aydin Dogan, Anne-Christine Hladky [1], Joe K. Cochran [2] and Robert E. Newnham

IMRL, The Pennsylvania State University, University Park, PA 16802 USA

[1]IEMN-Departement I.S.E.N., 41 Boulevard Vauban, 59046 LILLE Cedex, France

[2] Georgia Institute of Technology, Atlanta, GA 30332 USA

Abstract - Millimeter size hollow green spheres have been formed from PZT-5 powder slurries with a coaxial nozzle process. After binder burnout and sintering, the spheres were poled tangentially with top-to-bottom external electrode caps. Principal modes of vibration were found to be an ellipsoidal, a higher order circumferential and a breathing mode near 230 kHz, 350 kHz and 700 kHz, respectively. Coupled modes were also determined at higher frequencies depending on the electrode configuration. These same modes with similar frequencies were obtained from the finite element analysis of the spheres using the ATILA finite element code, and experimental results were shown to be consistent with the modeling study. Hydrostatic piezoelectric charge coefficients of the spheres were measured and the results were found to vary between 600 - 1,000 pC/N, with hydrophone figure of merit ($d_h \times g_h$) between $70{,}000 \times 10^{-15}$ - $135{,}000 \times 10^{-15}$ m^2/N for tangentially poled spheres. Previous results indicates even higher values for radially poled spheres.

I. Introduction

For over 40 years lead zirconate titanate has been used as the main piezoelectric material in many electromechanical transducer applications [1]. However, bulk PZT ceramics were unable to satisfy the requirements of the underwater hydrophones and biomedical ultrasound applications due to their low hydrostatic piezoelectric charge coefficient, d_h ($= d_{33} + 2\,d_{31}$) and high density (7.9 g/cm^3), which causes an acoustic impedance mismatch between the transducer and the water, or human body (density $\approx$ 1.0 g/cm^3). Those problems have been overcome by coupling the ceramic material with polymers [2] which causes a decrease in the density of the structure and an increase in the sensitivity, as well as with metals [3], which introduces hollow spaces into the structure and amplify the sensing and actuating characteristics of the ceramic by redesigning the transducer.

In addition to the sensing and actuating characteristics, and acoustic impedance matching, the directionality of these properties, as well as the size of the transducer has often been an issue for certain applications. The intravascular image catheters, today widely used in medicine for both diagnostic and surgical purposes, are appropriate examples, where ultrasonic transducers are utilized for both guiding the catheter and forming the image. In such an application the size of the transducer must correlate with the size of the catheter and the vessel that is going to be imaged. A smaller size is also needed to achieve improved resolution and higher power densities. Another requirement of the catheter applications reveals itself with the problems encountered by using a flat piece of transducer element. Such an elements ability to receive an ultrasound pulse is limited to a small range of angles around 90° to the receiver. This problem was addressed by Vilkomerson et al. [4] and tried to be solved by using a quasi-omnidirectional PVDF transducer with a spherical geometry deposited on a spherical brass bead, which can both receive and transmit signals independent of direction. Similarly, Lockwood et al. [5] prepared a high frequency transducer from a thin hemispherical ceramic dish to obtain an inherently focused ultrasound beam.

A spherical transducer with omnidirectional properties has been a research interest for other applications as well such as, Navy-USRD series of F-42 omnidirectional standard ceramic transducers [6]. Smaller sizes of these transducers can be used in flow noise studies for complex surface structures in underwater ultrasound. Recently, Fujishima et al. [7] reported larger size spherical air transducers to be used as omnidirectional speakers.

Millimeter size piezoelectric hollow sphere transducers, so-called bucking balls (BBs), described in this paper and reported elsewhere by Meyer et al. [8], not only satisfy the size, omnidirectionality and density (~1.3 g/cm^3) requirements but they were shown to have orders of magnitude higher hydrostatic sensitivities over bulk PZT [9].

In this paper, results of the dielectric and hydrostatic piezoelectric charge coefficient measurements of three types of non-symmetric electrode configurations of tangentially poled hollow sphere transducers are presented. Vibration modes and their resonance frequencies are identified using ATILA finite element code, and the results of the modeling study are compared with that of the experiments.

Proceedings of the IEEE International Symposium on the Application of Ferroelectrics, August 1996, East Brunswick, NJ, in press

II. Fabrication of Piezoelectric Hollow Sphere Transducers

Thin wall hollow green spheres were fabricated at room temperature using a coaxial nozzle process by extruding a liquid through an annular-cross-section nozzle with a gas jet providing a ballooning effect. This process was originally developed by Torobin [10] to mass produce large numbers of ceramic and metal spheres. In the fabrication of BBs a fine-grained slurry of PZT is prepared from PZT-501A (Ultrasonic Powders, Inc.) powders, and Poly(methyl methacrylate), PMMA is used as the binder and acetone as the dispersant. The Torobin process is shown to be a flexible fabrication technique for mass production of hollow spheres with various compositions and dimensions.

Firing of the green spheres includes a binder burnout step at 550°C for 30 minutes and a sintering step at 1285°C for 90 minutes. A previous physical characterization study on the sintered spheres by Fielding et al. [11] concluded that thin wall spheres contain microcracks and substantial porosity. The wall thickness was also found to be larger than expected. However, improvements in the process will be undertaken to minimize these defects.

A thin layer of gold was deposited as the external top and bottom electrodes with electrode gaps between them. Silver electrical lead wires were attached to the electrodes using E-solder #3021 (Insulating Materials, Inc). Spheres were then dip-coated with polyurethane (Dexter Hysol us-0089) for insulation and to provide strength for the hydrostatic measurements. Poling was carried out with a tangential (top-to-bottom) poling field of 20 kV/cm at 120°C for 4 minutes in a silicone oil bath. Three types of non-symmetric electrode configurations were investigated (see figure-1). Four samples for each electrode configuration were prepared and evaluated in order to increase the accuracy of the results of the measurements. The results reported in this paper are average values of the measurements taken from several samples and vary within 15 % range.

III. The Finite Element Code "ATILA"

ATILA is developed at the Acoustics Department at ISEN specifically for modeling sonar transducers [12]. A static analysis can be performed which provides information concerning prestresses, and the behavior under hydrostatic pressure. A modal analysis can be done where vibration modes, their resonance frequencies and associated coupling factors can be determined. Finally, the in-air or in-water impedance and displacement field, the Transmitting Voltage Response and the directivity patterns of a sonar can be modeled through a harmonic analysis.

In this study, ATILA is used to determine the modes of vibration for each electrode configuration, along with the resonance and antiresonance frequencies of these modes. Calculated results were presented as admittance vs. frequency spectra, and compared with the experimental results.

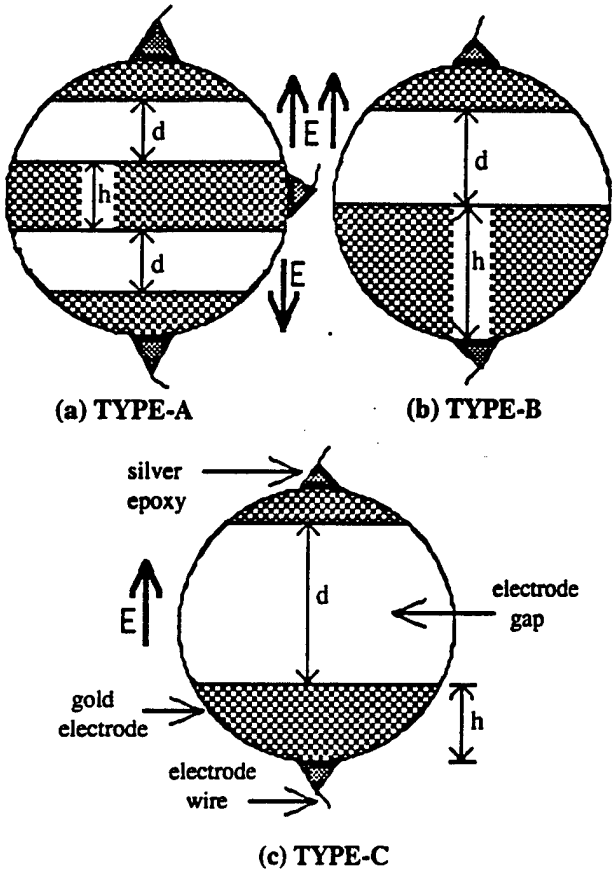

Fig.1. Electrode configurations of the tangentially poled piezoelectric hollow sphere transducers

IV. Results and Discussion

A. *Dielectric Characterization*

Dielectric property measurements were performed at 1.0 kHz and 1.0 Volt using an HP 4275-A Multi-frequency LCR Meter. Average capacitance values of 2.5 to 10 pF are measured, (see table-1). Considering the fact that the sphere walls are not free of defects those values are in fair agreement with the calculated values of 6 to 10.5 pF using a cylindrical tube approximation [8] :

$$C = \varepsilon_r \varepsilon_0 \frac{\pi t (r_i + r_o)}{d} \qquad (1)$$

The capacitance of the tangentially poled spheres were found to be highly dependent on the electrode size and uniformity.

B. *Modes of Vibration of Tangentially Poled Transducers*

The evaluation of the polarization behavior of a tangentially poled sphere with finite element method clearly indicates that only the unelectroded region between the electrode caps is tangentially poled, and the material under the

electrodes is unpoled and inactive .From this result the size of the electrode gap is expected to control the dielectric and acoustic properties of the transducer.

The finite element analysis of the tangentially poled spheres indicates that the principal modes of vibrations are : an *ellipsoidal mode* -ellipsoidal distortion of the sphere- with a resonance frequency of around 240 kHz, a *higher order circumferential mode* -buckling of the sphere wall- at frequencies between 300 to 400 kHz and a *breathing mode* -volumetric contraction and expansion of the sphere- at around 600 kHz. Higher frequency coupled modes were also obtained from the finite element analysis. Comparison of the admittance vs. frequency spectra calculated by ATILA and obtained from the measurements for a type-C sphere is shown in figure-3 as an example.

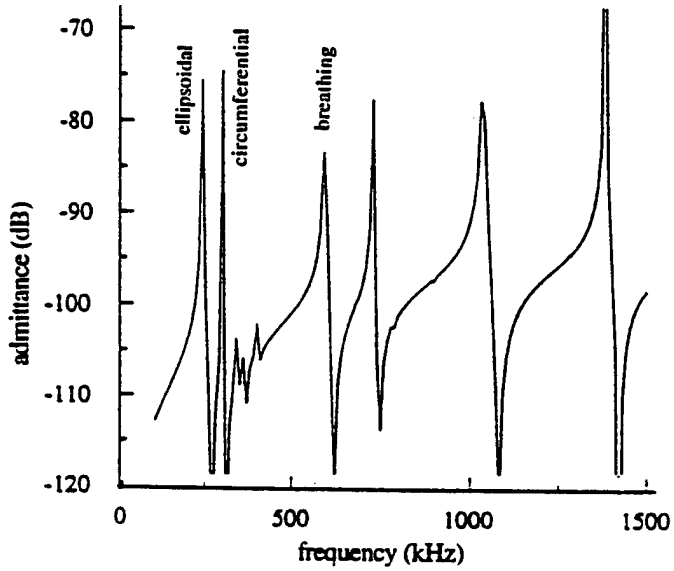

(a) calculated

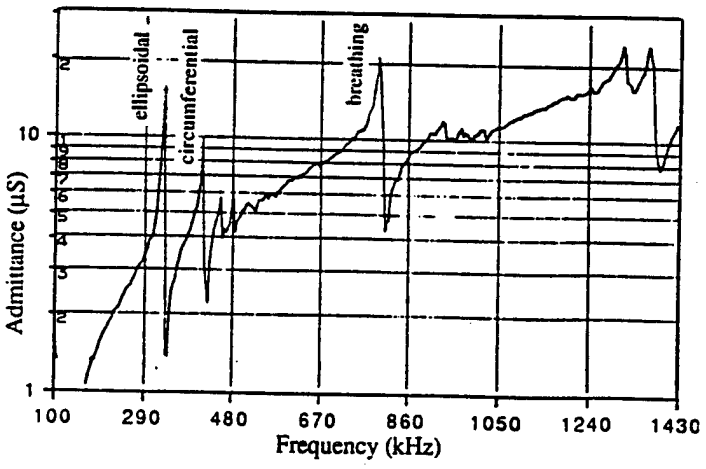

(b) observed

Fig.2. Admittance spectra of a tangentially poled PZT hollow sphere (electrode configuration : Type-C)

The calculated and measured resonance and antiresonance frequencies are also given in table-2 for all three types of electrode configurations. It is clearly seen from the figure and the results that there is a close match between the model and the experimental results for the three main modes of vibration. However, this is not true for the coupled modes. The discrepancies between the model and the measurements are attributed to the non-uniform wall thickness of the spheres. Since these higher frequency modes results from a coupling between either the ellipsoidal and thickness mode, or the circumferential and the thickness mode, a non-uniform wall thickness can be expected to influence the resonance frequency of that particular mode and yield broad, smooth admittance peaks. Each major peak in the admittance spectra was also studied using ATILA and the displacement fields of the main vibration modes are shown in figure-3. In the figure the dashed lines shows the rest position and the solid lines shows the drive position.

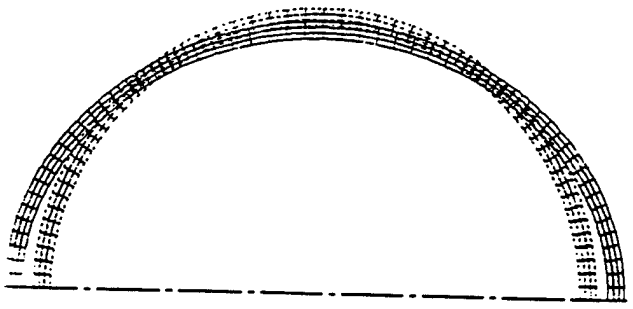

(a) Ellipsoidal mode (f_r ~ 240 kHz)

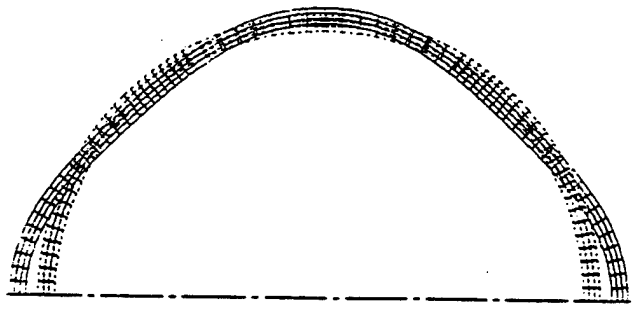

(b) Higher order circumferential mode (f_r = 300 - 400 kHz)

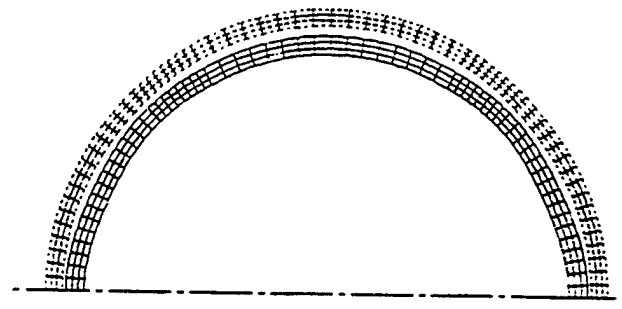

(c) Breathing mode (f_r ~ 600 kHz)

Fig.3. Main modes of vibration of a tangentially poled PZT hollow sphere (displacements with an arbitrary amplitude)

C. *Hydrostatic Sensitivity Measurements*

In order to evaluate the hollow sphere transducers for possible underwater applications as hydrophones the hydrostatic piezoelectric charge coefficient (d_h) of the spheres were measured in an oil pressure chamber under hydrostatic pressures from 100 to 1,000 psi with a 30 Hz stimulus. A PZT disc was also measured to compare the BBs with bulk material. From these results hydrostatic piezoelectric voltage coefficient (g_h) and hydrophone figure of merit of the spheres were calculated using the following equations. The results are given in table-1 and plotted in figure-4

$$g_h = \frac{d_h}{\varepsilon_{33}} \tag{2}$$

$$\textit{figure of merit} = d_h \times g_h \tag{3}$$

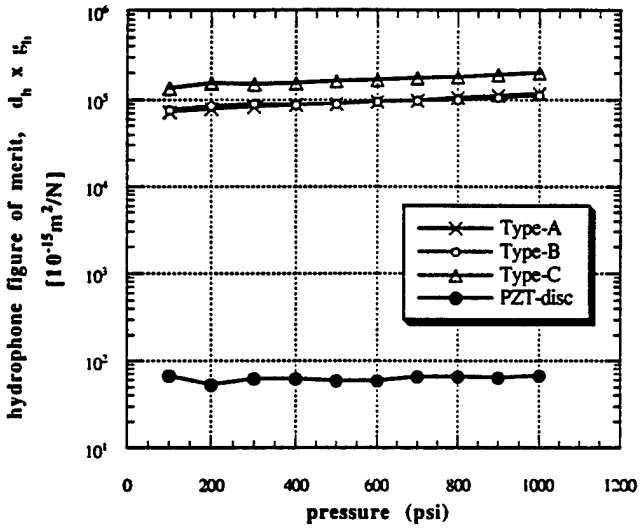

Fig.4. Hydrostatic sensitivity of the PZT hollow spheres

Evaluation of the results indicates that tangentially poled BBs possess 3 orders of magnitude higher hydrophone figure of merit. Even higher values have been reported by Alkoy et al. [9] for radially poled spheres. The amplification of d_h and figure of merit results from the spherical geometry and the unique electrode designs. A detailed discussion along with a simplified model is given elsewhere [9]

TABLE-1.
COMPARISON OF THE DIELECTRIC AND PIEZOELECTRIC PROPERTIES

Property \ Type	Bulk PZT-5A	Tangentially poled spheres Type-A	Type-B	Type-C
electrode gap d (mm)	n/a	0.77	1.06	1.81
electrode height, h (mm)	n/a	0.75	1.38	0.84
Capacitance, C (pF)	131.0	9.73	4.5	2.6
Dielectric loss, tan δ	0.017	0.017	0.022	0.014
Dielectric constant, ε_r	1,622	628	800	789
Hydrostatic piezoelectric charge coefficient @, d_h (pC/N)	30	630	736	966
Hydrophone figure of merit, $d_h \times g_h$ (10^{-15} m^2/N)	60	71,354	76,464	133,640

TABLE-2.
COMPARISON OF THE CALCULATED AND MEASURED RESONANCE FREQUENCIES

Type / Vibration mode and resonance frequency (kHz)	Type-A FEA	Type-A Exp.	Type-B FEA	Type-B Exp.	Type-C FEA	Type-C Exp.
Ellipsoidal mode	240	199	240	220	240	234
Higher order circumferential	320	330	290	312	300	315
Breathing mode	590	651	590	704	590	716
Ellipsoidal + thickness coupled	1,000	not found	980	1,264	1,030	1,300
Higher order circumferential + thickness coupled	1,660 2,520	1,966 2,870	710 1,300 1,660 1,980	1,583	730 1,380 1,840 2,210	1,708

V. CONCLUSIONS

Miniature, hollow sphere piezoelectric transducers were prepared using an inexpensive, flexible slurry-coaxial nozzle process. Three different electrode configurations for tangential poling of the spheres were examined through dielectric, piezoelectric measurements, and using ATILA finite element code. The main modes of vibration, regardless of the electrode configuration, were determined to be ellipsoidal, higher order circumferential and breathing modes. Higher frequency coupled modes were also observed. Compared to bulk PZT, much higher d_h and hydrophone figure of merit are obtained .

ACKNOWLEDGMENTS

This study is partly funded by ONR through contract # N0001492J1510.

REFERENCES

[1] B. Jaffe, W.R. Cooke & H. Jaffe, *Piezoelectric Ceramics* , Academic Press, 1971, pp.135-83

[2] T.R. Gururaja, R.E. Newnham, K.A. Klicker, S.Y. Lynn, W.A. Schulze, T.R. Shrout & L.J. Bowen, "Composite piezoelectric transducers" in *Proc. IEEE Ultrason. Symp.*, 1980, pp.576-581

[3] A. Dogan, "Flextensional moonie and cymbal actuators", *Ph.D. Thesis*, The Pennsylvania State University, University Park, 1994

[4] D. Vilkomerson, B. Gardineer, and H. Hojeibane, "Quasi-Omnidirectional Transducers for Ultrasonic Electro-Beacon Guidance of Invasive Devices." *SPIE* , 1733, pp 154-165, 1992

[5] G. R. Lockwood, D. H. Turnbull and F. S. Foster,Fabrication of high frequency spherically shaped cermaic transducers", *IEEE Trans. Ultrason. Ferroelec. Freq. Cont.*, 4 , [2], pp. 231-235, Mar. 1994

[6] L. E. Ivey, "NRL-USRD Series F42 Omnidirectional Standard Transducers," *Underwater Sound Reference Detachment*, 1979, Naval Research Laboratory, Orlando, Florida

[7] S. Fujishima, T. Nakamura and T. Okada, "Characteristics of spherical piezoelectric ceramic speakers", *Proc. Acous. Soc. Jap.*, March 26-28, 1996

[8] R. Meyer, Jr., H. Weitzing, Q. Xu, Q. Zhang & R.E. Newnham, " Lead Zirconate Titanate hollow sphere transducers," *J. Amer. Ceram. Soc.*, 77, (6), pp. 1669-1672, 1994

[9] S. Alkoy, A.Dogan, A.C. Hladky, P. Langlet, J.K. Cochran and R.E. Newnham, "Miniature piezoelectric hollow sphere transducers", *Proc. IEEE Int. Freq. Cont. Symp.*, June 1996, in press

[10] L.B. Torobin, " Methods of making hollow, porous microspheres", *U.S. Patent* No. 4,671,909 , 1987

[11] J.T. Fielding, Jr., D. Smith, R. Meyer, Jr., S. Trolier-McKinstry & R.E. Newnham, "Characterization of PZT hollow sphere transducers", *IEEE Int. Symp. Appl. Ferroelec.*, 1994, pp.202-205

[12] A.C. Hladky-Hennion and J.N. Decarpigny, "Finite element modeling of active periodic structures: application to 1-3 piezocomposites", *J. Acous. Soc. Am.* , 94, pp.621-635, 1993

APPENDIX 45

1996 IEEE INTERNATIONAL FREQUENCY CONTROL SYMPOSIUM

MINIATURE PIEZOELECTRIC HOLLOW SPHERE TRANSDUCERS

Sedat Alkoy, Aydin Dogan, Anne-Christine Hladky*, Philippe Langlet*, Joe. K. Cochran** & Robert E. Newnham

IMRL, The Pennsylvania State University, University Park, PA 16802,USA
*IEMN-Departement ISEN, 41 Boulevard Vauban, 59046 LILLE Cedex, France
**Georgia Institute of Technology, Atlanta, GA 30332, USA

Abstract: Miniature piezoelectric transducers were prepared from millimeter size hollow spheres which have been formed from PZT-5A powder slurries with a coaxial nozzle process. After sintering, the spheres were poled in two ways: radially and tangentially. Principal modes of vibration were found to be a breathing mode near 700 kHz and a thickness mode near 13 MHz for the radially poled spheres, and an ellipsoidal, a circumferential and a breathing mode near 230 kHz, 350 kHz, 700 kHz, respectively for tangentially poled spheres. Coupled modes were also observed at higher frequencies. These same modes with similar frequencies were obtained from finite element analysis using the ATILA FEM code, and experimental results were shown to be consistent with the modeling study. Hydrostatic d_h coefficients were found to vary between 700 - 1,800 pC/N which are orders of magnitude higher than the d_h of bulk PZT. The hydrophone figure of merits (d_h*g_h) were calculated to be between 68,000 - 325,000 $*10^{-15}$ m^2/N for various types of poled spheres. These values are three orders of magnitude higher than the bulk PZT figure of merit. Potential applications include ultrasonic imaging, non-destructive testing and hydrophones.

Introduction

Lead zirconate titanate (PZT) based ceramics have been the leading piezoelectric materials for electromechanical transducers for the last 40 years. [1] However, for both underwater hydrophones and biomedical ultrasound applications bulk PZT is a poor material for several reasons. The hydrostatic piezoelectric charge coefficient, d_h ($=d_{33}+2d_{31}$) of PZT is very low due to the opposite signs of d_{33} and d_{31}. The hydrostatic piezoelectric voltage coefficient, g_h ($=d_h/\varepsilon_r*\varepsilon_o$) is also low because of the high dielectric constant, ε_r, of PZT. In addition to those drawbacks, the acoustic impedance matching of PZT with water and the human body (density = 1.0 g/cm^3) is poor due to the high density (7.9 g/cm^3) of bulk PZT.

Since the 1980's attempts have been made to overcome those problems by coupling the ceramic material with polymers [2,3] and metals [4,5], and introducing hollow spaces into the transducer structure. These studies succeeded in improving the hydrostatic piezoelectric properties by decreasing the density of the transducer, and by amplifying the sensing and actuating characteristics of the ceramic by redesigning the transducer. In developing new transducers, the biological world has often been used as the inspiration for innovative ideas and new designs. Sharks, fish and the other inhabitants of the underwater world - the way they talk and listen - can be imitated in piezoelectric transducer designs.

The piezoelectric hollow sphere transducers described in this paper and elsewhere [6] are modeled after the inner ear of a fish. The inner ear is made up of inertia-sensing chambers resembling accelerometers. Within each chamber is a dense ear stone (otolith) which vibrates in a near field sound wave. The inertia of the ear stone causes it to lag behind the motion of the fish, and to push against the hair cells lining the chamber (sacculus). On bending, the hair cell membranes deform, stimulating neural transmissions to the brain. Connections to the swim bladder of the fish further improve the sensitivity to far-field sound. [7]

Smaller sizes are needed to achieve improved resolution and higher power densities for intravascular image catheters in biomedical ultrasound, flow noise studies for complex surface structures in underwater ultrasound, and embedded sensors for nondestructive evaluation. Millimeter size piezoelectric hollow sphere transducers (BBs) not only satisfy these size requirements, but also possess omnidirectionality and low density (~1.3 g/cm^3), both of which are inherent to the unique structure and design of the transducer, and both has been cited as advantages for a transducer for certain applications. [8,9]

In this paper, several poling and electroding configurations for the hollow sphere transducers are introduced. Results of the dielectric and hydrostatic piezoelectric charge coefficient measurements are presented. Vibration modes and their resonance frequencies are identified by the ATILA finite element analysis code and the results of the modeling study are compared with the experimentally obtained admittance spectra.

Fabrication of PZT hollow sphere transducers

Green PZT spheres are prepared using a fabrication technique, which was developed by Torobin [10] to produce large numbers of ceramic and metal hollow spheres. A fine-grained slurry of PZT-501A (Ultrasonic Powders, Inc.) is prepared and injected through a coaxial nozzle with air passing through the center tube. The slurry exits the nozzle in a hollow cylindrical form, but the bottom later closes due to the surface

0-7803-3309-8/96 $5.00

tension and hydrostatic pressure. The closed cylinder is inflated into a bubble by the inner air pressure untill the pressure equals that of the cylinder. At this critical pressure the bubble closes, and the sphere breaks free. The Torobin process is shown to be a flexible fabrication technique for hollow spheres with various compositions [11,12]. It also allows us to tailor the size (1 to 6 mm in diameter) and the wall thickness (12 to 150 μm) of the spheres by changing the viscosity and air jet velocity.

The green spheres are fired at 550°C for 30 minutes for binder burnout, followed by sintering at 1285°C for 90 minutes. Sintering is performed in a closed alumina crucible in a bed of PZT powder to minimize lead loss from the spheres. A physical characterization study by Fielding et.al. [13] concluded that spheres with a sintered diameter of ~ 2.76 mm and a mean wall thickness of 80 μm, contain microcracks and substantial porosity. The wall thickness variation was also found to be larger than expected, ranging from 40 to 100 μm. Improvements in the fabrication process will be undertaken to minimize these defects and wall thickness variations, since they degrade the dielectric properties and disturb the vibrations of the transducer.

Two poling configurations have been studied: radial poling with inside and outside electrodes, and top-to-bottom poling with two external cap electrodes, (see figure-1). For the top-to-bottom poling three symmetric electrode configurations, with electrode gap dimensions (d): d = 0.79 mm (Type-1), d = 1.38 mm (Type-2) and d = 1.71 mm (Type-3) were investigated. The effect of increasing the poled regions on the capacitance, vibration modes and hydrostatic sensitivity of the transducer was examined.

For radial poling Conductive Silver 200 (Demetron GmbH) was used as the inner electrode after drilling an electrode hole with a diameter of about 450 μm prior to the binder burnout step. Silver electrical lead wires were attached and the electrode hole was sealed using E-solder # 3021 (Insulating Materials, Inc.) silver epoxy adhesive. A thin layer of gold was deposited as the external electrode for both configurations. Spheres were then dip-coated with polyurethane (Dexter Hysol us-0089) for insulation and to provide strength for the hydrostatic measurements. Poling was carried out with an electric field of 20 kV/cm at 120°C in a silicone oil bath.

Three samples for each electrode configuration were prepared and evaluated in order to increase the accuracy of the results of the dielectric, piezoelectric and hydrostatic property measurements. The results reported in this paper are average values, and they are within ± 15 % range of the results of the measurements taken from several samples.

ATILA finite element code

ATILA is a finite element code developed by the Acoustics Department at ISEN for the modeling of sonar transducers. It can provide information concerning prestresses, and the behavior under hydrostatic pressure (static analysis), together with the resonant frequencies and modes and the associated coupling factors (modal analysis), the in-air or in-water impedance and displacement field, the Transmitting Voltage Response and the directivity patterns (harmonic analysis). [14-16]

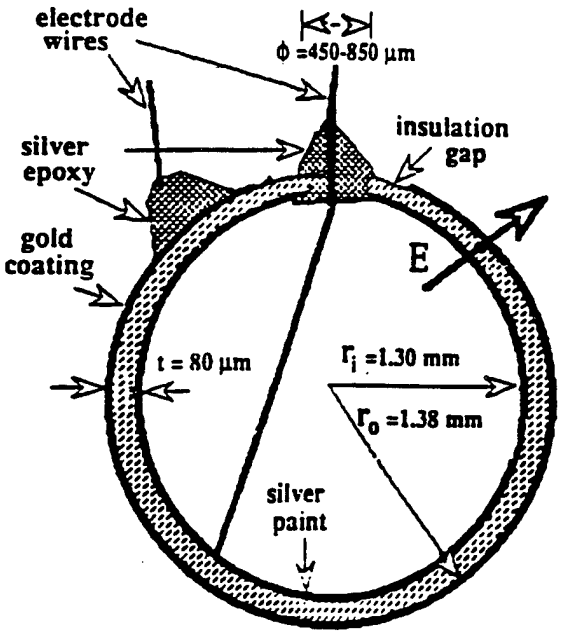

Figure-1(a). Radial poling configuration

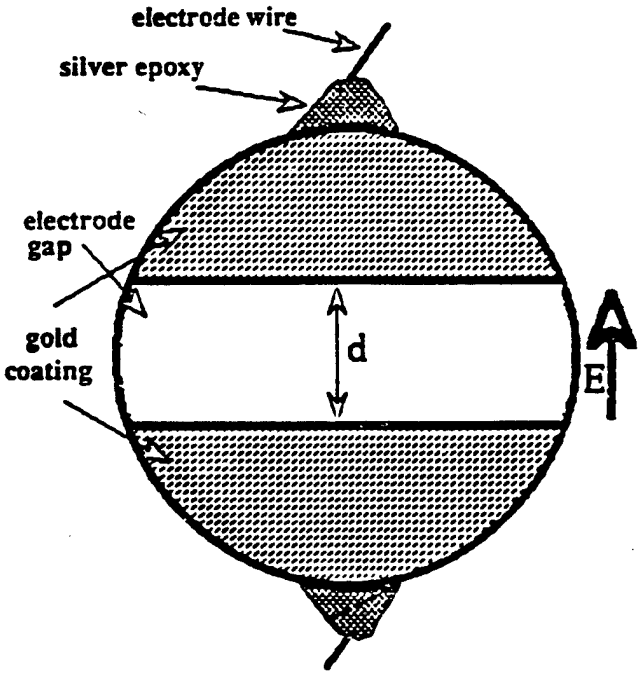

Figure-1(b). Top-to-bottom poling configuration

In our study, ATILA is used to identify the modes of vibration and, to determine the resonance and antiresonance frequencies of these modes for different electrode configurations. The resultant calculated admittance vs. frequency spectra are compared with the experimental measurements obtained using an HP 4194-A Impedance/Gain Phase Analyzer.

Results and Discussion

Dielectric Characterization : Dielectric properties of the transducers were measured using a HP 4275-A Multi-frequency LCR Meter at 1.0 kHz and 1.0 Volt. For radially poled spheres a typical capacitance value of 2.900 pF , and a dielectric loss of 0.020 were measured. An average dielectric constant (ε_r) of about 1.000, somewhat lower than the typical value of 1.850 for UPI 501A powders, was calculated from the capacitance using the following equation for a spherical capacitor [6] :

$$C = 4\pi\varepsilon_r\varepsilon_o\left(\frac{r_i r_o}{r_o - r_i}\right) \qquad (1)$$

This lower than expected dielectric constant can be attributed to wall thickness variations, incomplete inner electrode, and the defects observed in the sphere wall [13]. In the case of top-to-bottom poled spheres, capacitance values ranging from 3 to 7 pF is measured, (see table-1). Those values are in fair agreement with the calculated values of 9 to 11 pF using a cylindrical tube approximation [6] :

$$C = \varepsilon_r\varepsilon_o\frac{\pi (r_i + r_o)}{d} \qquad (2)$$

As expected, the capacitance of top-to-bottom poled spheres is highly dependent on the electrode size and uniformity.

Modes of vibration of radially poled transducers: Finite Element Analysis (FEA) of a radially poled hollow sphere suggests two principal modes of vibration, shown in figure-2(a) in the calculated admittance spectra. The first mode is a volumetric expansion and contraction of the sphere, the so-called breathing mode utilizing d_{31}. The resonance and antiresonance frequencies of the mode are calculated as 620±10 kHz and 780±10 kHz, respectively. Using the relation [17]

$$k_p^2 = 1 - \frac{f_r^2}{f_a^2} \qquad (3)$$

the planar coupling factor (k_p) is calculated as 0.61 from the FEA results. The second vibration mode is identified as the wall thickness mode of the sphere, and the predicted frequencies are f_r = 21.5 MHz and f_a = 24.0 MHz.

In comparison to the FEA results, an admittance spectra obtained from radially poled sphere transducer with a ~ 650 µm diameter electrode hole, and with an inner radius (r_i) = 1.30 mm, outer radius (r_o) = 1.38 mm, and an average wall thickness (t) =80 µm is shown in figure-2(b). The experimental measurements agree well with the FEA results. For the breathing mode the average resonance and antiresonance frequencies are 633 kHz and 686 kHz, respectively. Since the breathing mode frequency is mainly controlled by the diameter of the sphere [6], the close agreement between the calculated and measured values indicates fairly uniform dimensions for the spheres. The planar coupling factor is calculated as 0.38 from these measurements. The difference between the calculated and observed values of k_p is attributed to the electroding problems of the inner sphere surface. However, the resonance and antiresonance frequencies of 13.4 MHz and 13.8 MHz, respectively, for the thickness mode vibration - which is determined from the sample given in figure-2.(b) - is quite different from the values suggested by FEA. The

Table-1. Comparison of the dielectric and piezoelectric properties

Type / Property	Bulk PZT-5A	Top-to-bottom poled type-1	Top-to-bottom poled type-2	Top-to-bottom poled type-3	radially poled
electrode gap #, d (mm)	n/a	0.79	1.38	1.71	n/a
Capacitance, C (pF)	131.0	6.9	3.7	3.0	2.900
Dielectric loss, tan δ	0.017	0.027	0.071	0.026	0.020
Dielectric constant, ε_r	1,622	909	861	869	1,000
Hydrostatic piezoelectric charge coefficient @, d_h (pC/N)	30	743	788	870	1,800
Hydrophone figure of merit $d_h \times g_h$, (10^{-15} m^2/N)	60	68,677	81,659	98,610	324,000

valid only for top-to-bottom poled transducers

@ determined at 100 psi and 30 Hz

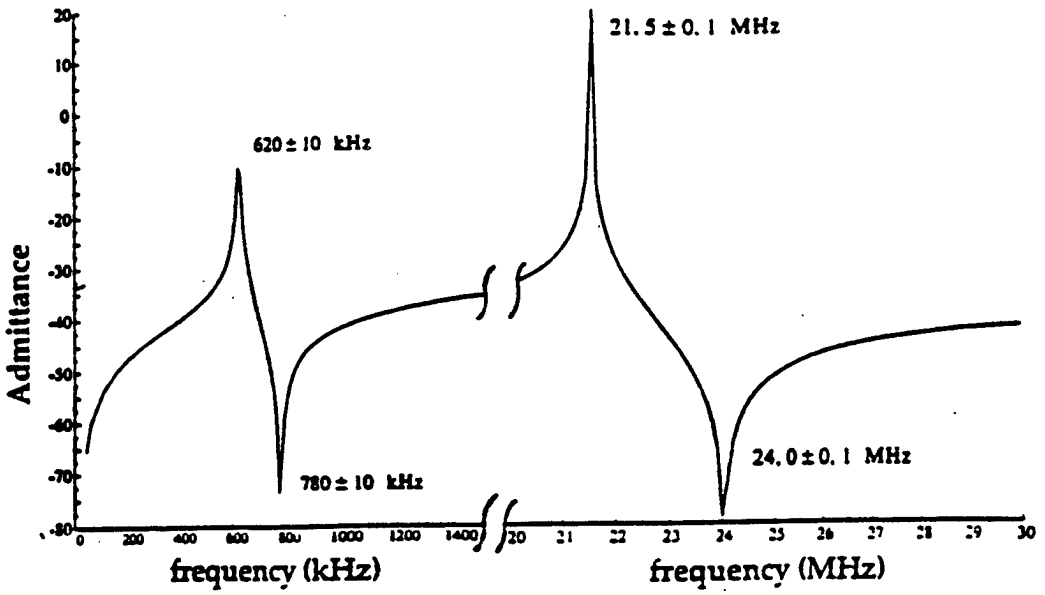

(a) calculated

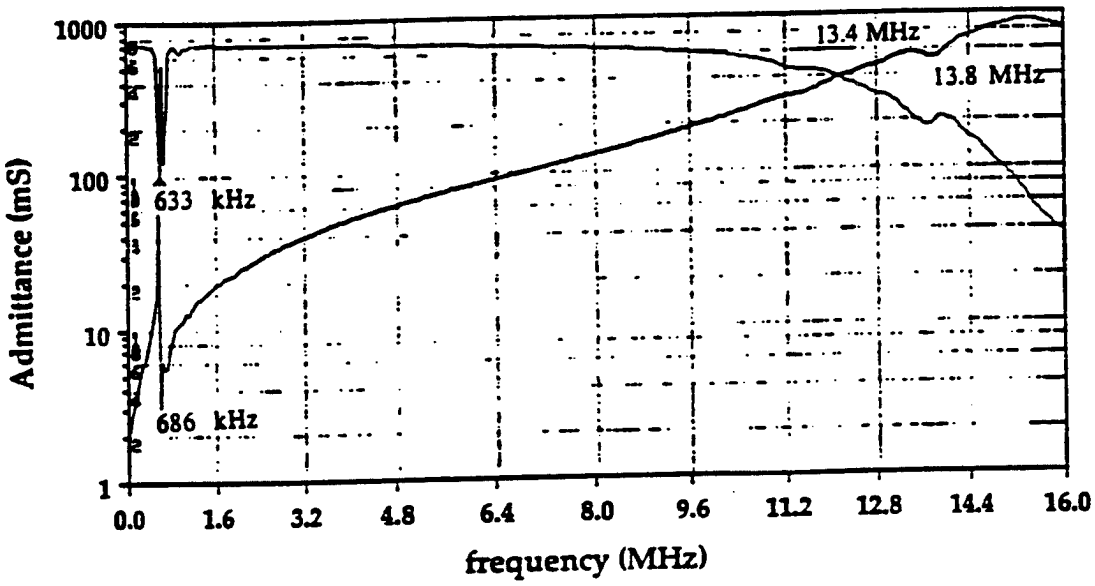

(b) observed

Figure-2. Admittance spectra of a radially poled PZT hollow sphere transducer

thickness mode itself has only been detected in a few of the samples, and the samples which possess a detectable thickness mode reveal this response as a smooth, broad peak in the admittance spectra. This discrepancy between the calculated and observed values is due to the large wall thickness variations within each sphere as reported previously [13].

Modes of vibration of top-to-bottom poled transducers : Finite element analysis of the top-to-bottom poling configuration indicates that only the unelectroded region between the electrode caps is tangentially poled, and the regions under the electrodes are unpoled, inactive regions (see figure-3). Therefore, the electrode gap is expected to control the

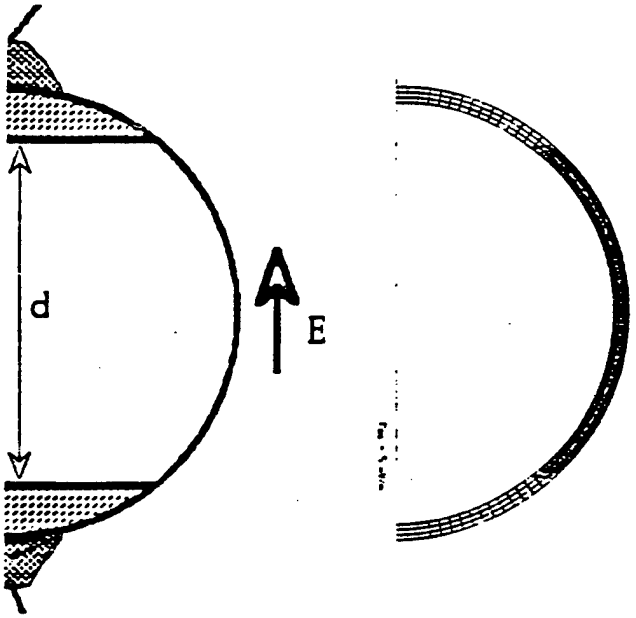

Figure-3. Polarized region of a top-to-bottom poled sphere

dielectric and acoustic properties of the transducer. Three types of top-to-bottom poled spheres with increasing electrode gap dimensions were studied. The principal mode of vibration under investigation for top-to-bottom poling configuration is the ellipsoidal distortion of the sphere. However, FEA results indicate the presence of two other modes in addition to the ellipsoidal mode, namely a higher order circumferential mode and a breathing mode, together with higher frequency coupled modes. The admittance spectra obtained from FEA for a Type-3. sphere with the largest electrode gap is compared with the experimentally obtained spectra in figure-4. Each major peak in the spectra was studied by FEA and the displacement fields of these vibrations are shown in figure-5.

The calculated and experimental resonance and antiresonance frequencies of all three types of transducers are given in table-2 . It is clear from these values that there is a close match between the modeling and the measurements for the three main vibration modes. However, in the case of the coupled vibration modes, the measured frequencies differ significantly from the values calculated by FEA. This is attributed to the non-uniform wall thickness of the spheres. Since these vibrations are a result of the coupling between either the ellipsoidal and thickness modes, or circumferential and thickness modes, the wall thickness variation is expected to strongly influence these coupled modes.

Another result obtained from the experiments and confirmed by the FEA is the introduction of new higher order circumferential-thickness coupled modes created by decreasing the electrode separation (see table-2).

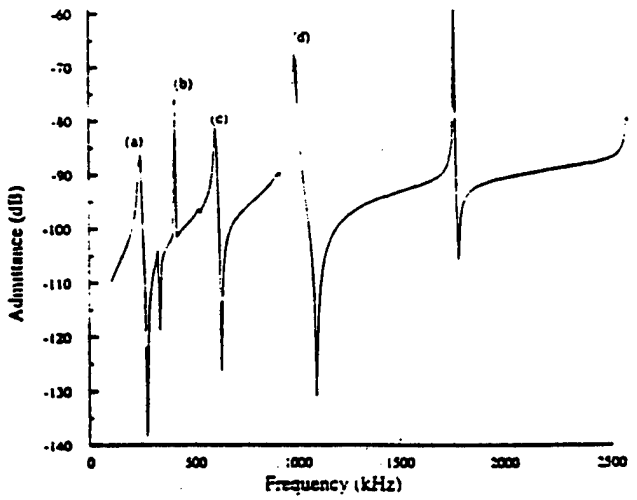

(a) calculated

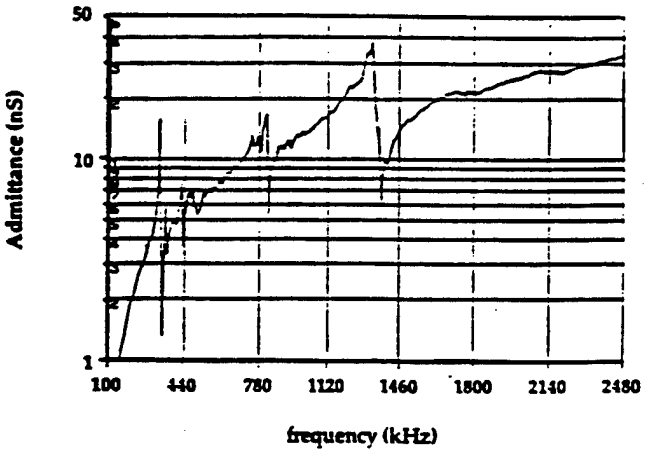

(b) observed

Figure-4. Admittance spectra of a top-to-bottom poled PZT hollow sphere transducer

Effect of Polymer Coating : Prior to the hydrostatic measurements the spheres are dip-coated with polyurethane. Admittance spectra of a radially poled sphere recorded before and after the polymer coating are shown in figure-6. It is found that the polymer coating has a clamping effect on the spheres, which shows itself as a decrease in the peak amplitude of the breathing mode, and a smoothing of the spectrum. A similar effect is observed for the top-to-bottom poled spheres accompanied by a slight shift of ellipsoidal and breathing modes to lower frequencies. This shift is about 10 kHz for the ellipsoidal mode, and 20-40 kHz for the breathing mode.

Hydrostatic sensitivity measurements : As part of the transducer characterization, hydrostatic measurements were carried out on poled and coated hollow spheres for possible application as underwater hydrophones. The hydrostatic piezoelectric charge coefficient (d_h) was measured in an oil bath

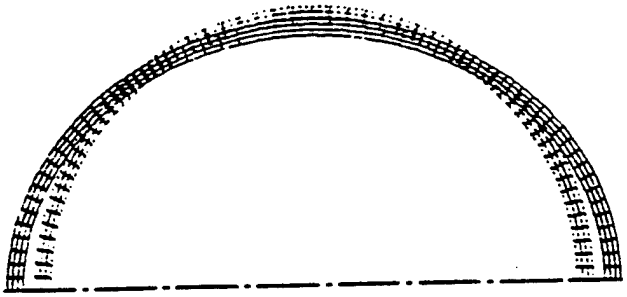

(a) Ellipsoidal mode (f_r ~ 240 kHz)

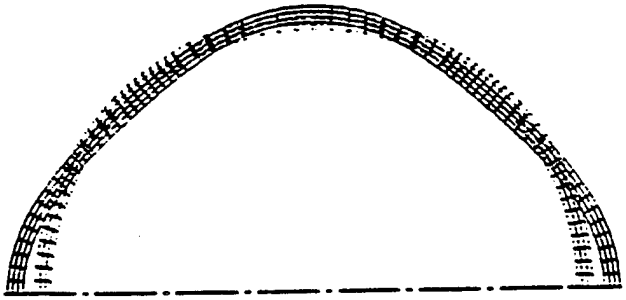

(b) Higher order circumferential mode (f_r = 300 - 400 kHz)

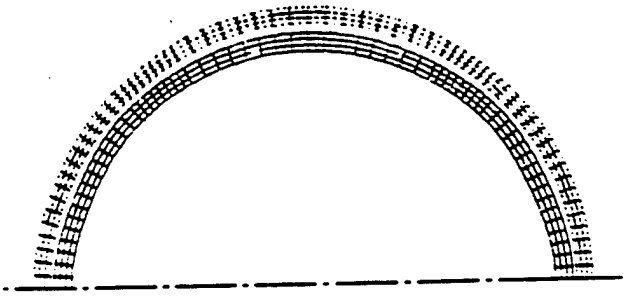

(c) Breathing mode (f_r ~ 600 kHz)

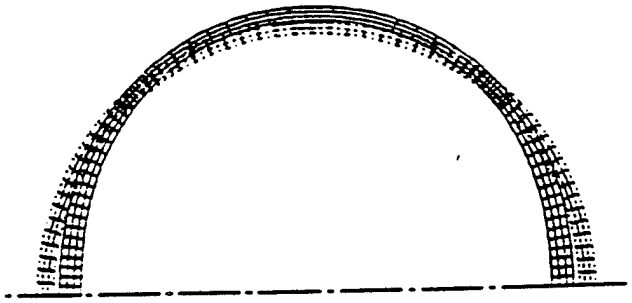

(d) Ellipsoidal + thickness coupled mode (f_r ~ 1.0 MHz)

Figure-5. Modes of vibration of a top-to-bottom poled piezoelectric hollow sphere

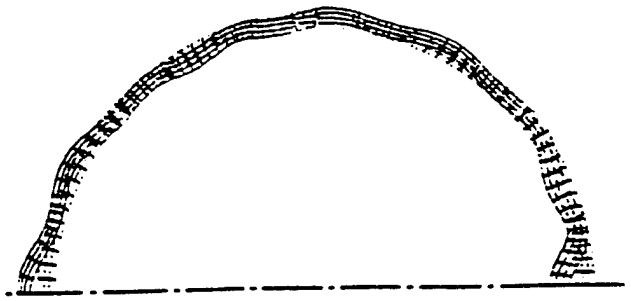

(e) Higher order circumferential + thickness coupled mode (f_r > 1.0 MHz)

Figure-5. (cont.) Modes of vibration of a top-to-bottom poled piezoelectric hollow sphere

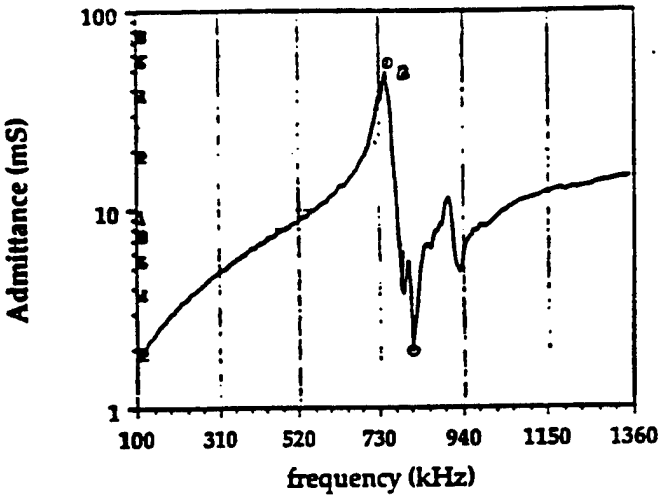

(a) before coating

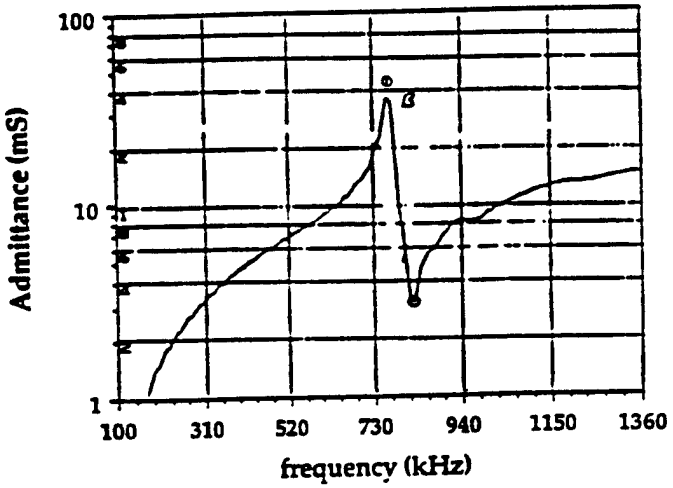

(b) after coating

Figure-6. Effect of polymer coating

Table-2. Comparison of the calculated and measured resonance frequencies

Type	Type-1		Type-2		Type-3		Radial	
Vibration mode & resonance frequency (kHz)	FEA	Exp.	FEA	Exp.	FEA	Exp.	FEA	Exp.
Ellipsoidal mode	240	235	240	221	240	233	n/a	n/a
Higher order circumferential mode	390	380	320	308	400	358	n/a	n/a
Breathing mode	590	712	590	701	590	708	620	633
Ellipsoidal + thickness coupled mode	980	1,272	980	1,226	980	1,280	n/a	n/a
Higher order circumferential + thickness coupled mode	1,630 2,330	2,005 2,866 3,751	1,680 2,480	1,987	1,750	not found	n/a	n/a

at hydrostatic pressures from 100 to 1,000 psi with a 30 Hz stimulus. A PZT disc is used to calibrate the measurements. The results are plotted in figure-7(a) for d_h vs hydrostatic pressure.

The hydrostatic piezoelectric voltage coefficient (g_h), and hydrophone figure of merit of the spheres are defined and calculated from the measured d_h values:

$$g_h = \frac{d_h}{\varepsilon_{33}} \tag{4}$$

$$figure\ of\ merit\ =\ d_h * g_h \tag{5}$$

The results are plotted in figure-7(b) for the hydrophone figure of merit vs. hydrostatic pressure. The measured and calculated values for both d_h and figure of merit are given in table-1. From these plots, the d_h values of the BBs are found to be one to two orders of magnitude higher than the d_h of bulk PZT, with the radially poled BBs displaying the highest d_h of all. Similarly the hydrophone figure of merit is found to be three orders of magnitude higher that of bulk PZT. Finally, evaluation of the results indicates that increasing the electrode separation for top-to-bottom poled spheres results in an increase in the hydrostatic sensitivity.

The amplification of the d_h and figure of merit lies in the geometry of the spherical BBs. A simplified explanation can be derived using Timoshenko's [18] argument for the transformation of an applied hydrostatic pressure on a spherical shell into a radial stress (σ_r) and two tangential stresses (σ_τ). This is schematically shown in figure-8. These stresses can be calculated using the following relations

$$\sigma_r = \frac{p_o r_o^3 (r^3 - r_i^3)}{r^3 (r_i^3 - r_o^3)} - \frac{p_i r_i^3 (r_o^3 - r^3)}{r^3 (r_i^3 - r_o^3)} \tag{6}$$

$$\sigma_\tau = \frac{p_o r_o^3 (2r^3 + r_i^3)}{2r^3 (r_i^3 - r_o^3)} - \frac{p_i r_i^3 (2r^3 - r_o^3)}{2r^3 (r_i^3 - r_o^3)} \tag{7}$$

where P_o is the outer hydrostatic pressure, P_i is the inner hydrostatic pressure and r is radius at which the stress is evaluated. For a thin-walled shell with the wall thickness ($t=r_o-r_i$), assuming $P_i = 0$, the above equations are simplified to give average stresses of:

$$\sigma_\tau = -8.89 * P_o = -0.50 * P_o * (r/t) \tag{9}$$

$$\sigma_r = -0.50 * P_o \tag{10}$$

where the ratio "r/t" is the stress amplification factor which makes hollow spheres important as a sensor. From the known relation between polarization (P) and stress (σ)

$$P_3 = d_{31} * \sigma_1 + d_{32} * \sigma_2 + d_{33} * \sigma_3 = -P_o * d_h \tag{11}$$

Using the stress configuration in figure-8, and combining equation (11) with equations (8) and (9), we obtain the following relations :

radial poling $\quad d_h = 0.5 * d_{33} + 17.8 * d_{31}$ (12)

top-to-bottom poling $\quad d_h = 8.89 * d_{33} + 9.39 * d_{31}$ (13)

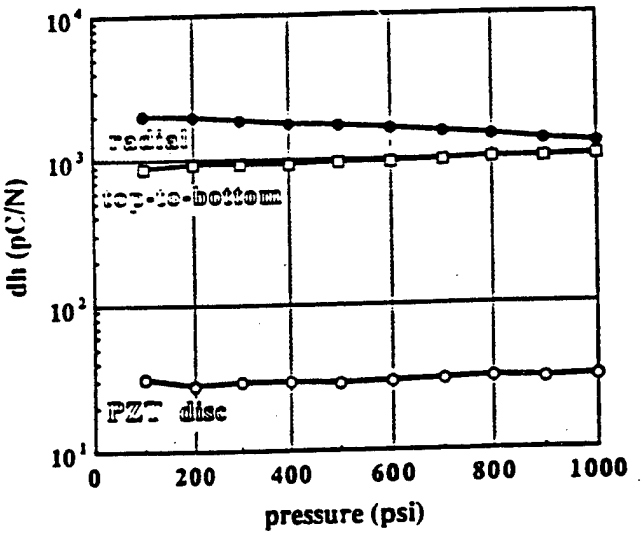

(a) effective hydrostatic piezoelectric charge coefficient (d_h) vs. hydrostatic pressure

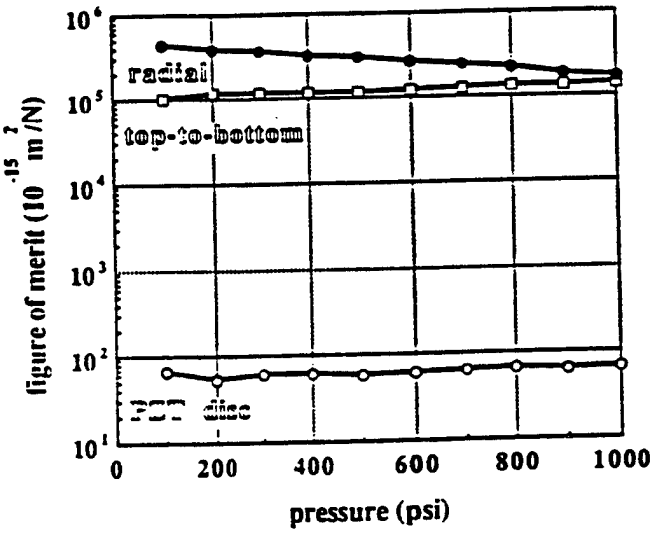

(b) hydrophone figure of merit ($d_h \times g_h$) vs. hydrostatic pressure

Figure-7. Hydrostatic sensitivity of the PZT hollow spheres

From equation (12) a d_h of about 2,600 pC/N is calculated for radial poling -with the assumption that 90 % of the sphere surface is electroded and poled effectively- whereas an average d_h of about 1800 pC/N was measured. This difference is attributed to the defects in the sphere wall and to the imperfect inner electrode. For the top-to-bottom poling configuration with only gold sputtered outher electrodes the model holds better, and equation (13) gives d_h values ranging from 550 pC/N to 1,190 pC/N for poled regions of 28.6 % for type-1 to 62 % for type-3, whereas average d_h values ranging from 743 pC/N to 870 pC/N were measured.

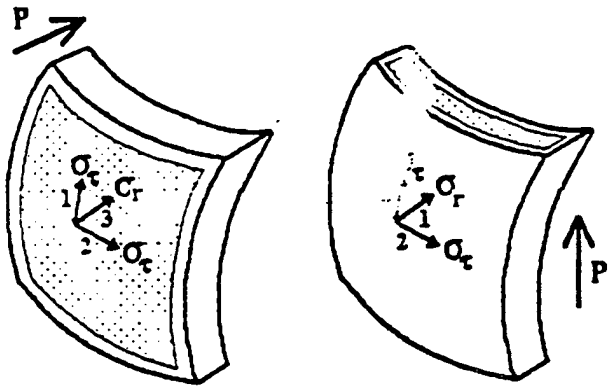

(a) radial poling case (b) top-to-bottom poling case

Figure-8. Transformation of an applied hydrostatic pressure into radial and tangential stresses

Conclusions

Small, hollow-sphere piezoelectric transducers can be prepared with an inexpensive and flexible manufacturing process. The main modes of vibration for radially poled PZT spheres are the breathing and thickness modes, which can be tailored over a frequency range of 200 kHz to 20 MHz by changing the diameter and the wall thickness. The main modes of vibration for top-to-bottom poled spheres are ellipsoidal, higher order circumferential and breathing modes. Higher frequency ellipsoidal and higher order circumferential modes coupled to a thickness mode are also observed. Compared to bulk PZT, much higher d_h and hydrophone figure of merits are obtained from the hollow sphere transducer design.

Acknowledgments

This study is partly funded by ONR through contract # N0001492J1510, and by Gebze Institute for Advanced Technology - Turkey. We thank Georgia Institute of Technology - USA and IEMN, Department ISEN - France for letting us use their facilities.

References

[1] B. Jaffe, W.R. Cooke & H. Jaffe, Piezoelectric Ceramics, Academic Press, 1971, pp.135-83

[2] K.A. Klicker, J.V. Biggers & R.E. Newnham, "Composites of PZT and epoxy for hydrostatic transducer applications", J. Amer. Ceram. Soc., 64, pp.5-9, 1981

[3] T.R. Gururaja, R.E. Newnham, K.A. Klicker, S.Y. Lynn, W.A. Schulze, T.R. Shrout & L.J. Bowen, "Composite piezoelectric transducers" in Proceedings of the IEEE Ultrasonics Symposium, 1980, 2, pp 576-581

"Piezoelectric composites with high sensitivity and high capacitance for use at high pressures". IEEE Transactions on Ultrasonics, Ferroelectrics and Frequency Control, 38, 6, pp.634-639, 1991

[5] A. Dogan, "Flextensional moonie and cymbal actuators", Ph.D. Thesis, The Pennsylvania State University, University Park, 1994

[6] R. Meyer, Jr., H. Weitzing, Q. Xu, Q. Zhang & R.E. Newnham", Lead Zirconate Titanate hollow sphere transducers." J. Amer. Ceram. Soc., 77, (6), pp. 1669-1672, 1994

[7] C.E. Bond, in Biology of Fishes, Saunders College Publishing Co., Philadelphia, 1979

[8] L. E. Ivey, "NRL-USRD Series F42 Omnidirectional Standard Transducers", Underwater Sound Reference Detachment, 1979, Naval Research Laboratory, Orlando, Florida

[9] D. Vilkomerson, B. Gardineer, and H. Hojeibane, "Quasi-Omnidirectional Transducers for Ultrasonic Electro-Beacon Guidance of Invasive Devices", SPIE, 1733, pp 154-165, 1992

[10] L.B. Torobin, " Methods of making hollow, porous microspheres", U.S. Patent No. 4,671,909 (1987)

[11] R.B. Clancy, T.H. Sanders, Jr. & J.K. Cochran, "Fabrication of hollow nickel spheres and low density syntatic foams", in Light Weight Alloys for Aerospace Applications II, Edited by E.W. Lee & N.J. Kim, The Minerals, Metals and Materials Society, Warrendale, PA, 1991, pp.477-85

[12] A.T. Chapman, J.K.Cochran, Jr., J.M. Britt & T.J. Hwang, " Thin-wall hollow spheres, from slurries". DOE-ECUT Program, ORNL Subcontent 86X-22043C, Annual reports, 1987,1988, 1989. Department of Energy, Washington, D.C

[13] J.T. Fielding, Jr., D. Smith, R. Meyer, Jr., S. Trolier-McKinstry & R.E. Newnham, "Characterization of PZT hollow sphere transducers", IEEE International Symposium on Application of Ferroelectrics, 1994, pp.202-205

[14] J. Assaad, B. Dubus, B. Hamonic, J.N. Decarpigny, J.C. Debus & R. Bossut, "Finite element modelling of ultrasonic transducers using the ATILA code" Ultrasonics International Conference Proceedings, 1991, pp.371-374

[15] B. Hamonic, J.C. Debus, J.N. Decarpigny, D. Boucher & B. Tocquet, "Analysis of a radiating thin-shell sonar transducer using the finite element method", J. Acous. Soc. Am., 86, (4), pp.1245-1253, Oct. 1989

of the finite element method to the modeling of 2D and 3D passive or active structures". Ultrasonics International Conference Proceedings, 1991, pp.415-418

[17] D.A. Berlincourt, D.R. Curran & H. Jaffe, "Piezoelectric and piezomagnetic materials and their function in transducers" in Physical Acoustics, Vol. 1, Part A, Edited by W.P. Mason, Academic Press, New York, 1964, pp.169-257

[18] S. Timoshenko and J.N. Goodier, in Theory of Elasticity, McGraw Hill Book Company Inc., New York, 1951

APPENDIX 46

PIEZOELECTRIC HOLLOW SPHERES

Sedat ALKOY, Aydin DOGAN, Anne-Christine HLADKY* and Robert E. NEWNHAM
IMRL, The Pennsylvania State University, University Park, PA 16802, USA
* IEMN - Departement I.S.E.N., 41 Boulevard Vauban, 59046 LILLE Cedex, France

Abstract

Lead zirconate titanate based green hollow spheres have been prepared with a coaxial nozzle process using fine grained slurry of PZT-5. Following the binder burnout and sintering, the spheres were poled radially and tangentially to be tested as piezoelectric transducers. For the radially poled spheres principal modes of vibration were found to be a breathing mode near 700 kHz and a thickness mode near 13 MHz. For the case of tangentially poled spheres those main modes of vibrations were determined as an ellipsoidal, a higher order circumferential and a breathing mode near 230 kHz, 350 kHz and 700 kHz, respectively. Higher frequency modes, which consist of coupling between ellipsoidal and thickness modes, or between circumferential and thickness modes were also determined for tangentially poled spheres. Hydrostatic piezoelectric charge coefficients (d_h) of the transducers were measured for their possible applications as hydrophones, and d_h values ranging from 700 to 1,800 pC/N were obtained. The hydrophone figure of merit ($d_h \times g_h$), calculated from d_h measurements were found to vary between 68,000 x 10^{-15} to 325,000 x 10^{-15} m^2/N. These values are substantially higher than the bulk PZT d_h and hydrophone figure of merit.

1. Introduction

Although lead zirconate titanate (PZT) based ceramics have been the leading piezoelectric material for electromechanical transducers for years, research in the last decade has intensified on coupling these ceramics with polymers and metals to overcome some of the problems associated with the bulk material. Those problems can be cited as the hydrostatic piezoelectric charge coefficient, d_h ($= d_{33} + 2\,d_{31}$) of PZT which is very low due to the opposite signs of d_{33} and d_{31}, the hydrostatic piezoelectric voltage coefficient, g_h ($= d_h / \varepsilon_r\ \varepsilon_0$) which is low due to the high dielectric constant, ε_r of PZT, and the acoustic impedance mismatch between bulk PZT and water, or human body (density $\approx$ 1.0 g/cm^3) because of the high density of PZT (7.9 g/cm^3). Some of the solutions presented include decreasing the density of the transducers by combining the ceramic with a polymer [1], and introducing hollow spaces into the transducer structure by using metal endcaps [2]. These designs were shown to amplify the sensing and actuating characteristics of the transducer. Nevertheless, directionality of those properties and the size of the transducer has often been cited as a crucial issue for some applications such as: intravascular image catheters[3], omnidirectional hydrophones [4] and speakers [5].

Miniature piezoelectric hollow sphere transducers, so called bucking balls (BBs), described here and reported elsewhere by Meyer et al. [6] were designed to satisfy the size, directionality and acoustic impedance matching requirements. In this paper results of the dielectric, piezoelectric and hydrostatic sensitivity measurements are presented for several types of radially and tangentially poled spheres.

2. Fabrication of the Hollow Sphere Transducers

Spheres were fabricated at the Georgia Institute of Technology using a coaxial nozzle process based on the Torobin patent [7]. The process is originally developed to mass produce thin-wall ceramic, metal and glass hollow spheres with diameters and wall thicknesses, ranging from 1 to 5 mm and 12 to 150 μm, respectively. The fabrication method used in producing the lead zirconate titanate based hollow spheres includes the preparation of a fine-grained slurry from PZT-501A powder (Ultrasonic Powders Inc.), Poly(methyl methacrylate), PMMA and acetone. This slurry is then injected through a coaxial nozzle with inert gas passing through the center. By the surface tension and hydrostatic forces a bubble forms and breaks free. The binder is then removed from the spheres by a binder burn-out step at 550°C for 30 minutes, furthermore the densification is achieved by a sintering step at 1285°C for 90 minutes.

A physical characterization study on the sintered spheres by Fielding et al.[8] indicated that the spheres contain microcracks and substantial porosity. The wall thickness variation was also found to be larger than expected, ranging from 40 to 100 μm. Improvements in the fabrication process will be undertaken to minimize these defects and wall thickness variations, since they degrade the dielectric properties and disturb the vibrations of the transducer.

Two poling configurations have been studied: radial poling with inside and outside electrodes, and top-to-bottom poling with two external cap electrodes, (see figure-1). For the top-to-bottom poling several symmetric and nonsymmetric electrode configurations were investigated, and the effect of increasing the poled regions on the capacitance, vibration modes and hydrostatic sensitivity of the transducer was examined.

For radial poling Conductive Silver 200 (Demetron GmbH) was used as the inner electrode after drilling an electrode hole with a diameter of about 450 μm prior to the binder burnout step. Silver electrical lead wires were attached and the electrode hole was sealed using E-solder # 3021 (Insulating Materials, Inc.) silver epoxy adhesive. A thin layer of gold was deposited as the external electrode for both configurations. Spheres were then dip-coated with polyurethane (Dexter Hysol us-0089) for insulation and to provide strength for the hydrostatic measurements. Poling was carried out with an electric field of 20 kV/cm at 120°C in a silicone oil bath.

Three samples for each electrode configuration were prepared and evaluated in order to increase the accuracy of the results of the dielectric, piezoelectric and hydrostatic property measurements. The results reported in this paper are average values, and they are within ± 15 % range of the results of the measurements taken from several samples.

3. ATILA Finite Element Code

ATILA is developed at the Acoustics Department at ISEN specifically for modeling sonar transducers [9]. A static analysis can be performed which provides information concerning prestresses, and the behavior under hydrostatic pressure. A modal analysis can be done where vibration modes, their resonance frequencies and associated coupling factors can be determined. Finally, the in-air or in-water impedance and displacement field, the Transmitting Voltage Response and the directivity patterns of a sonar can be modeled through a harmonic analysis.

In this study, ATILA is used to determine the modes of vibration for each electrode configuration, along with the resonance and antiresonance frequencies of these modes. Calculated results were presented as admittance vs. frequency spectra, and compared with the experimental results.

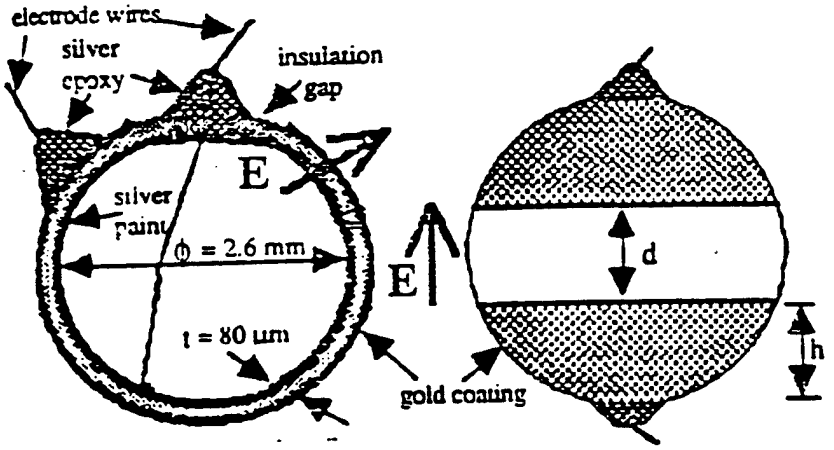

(a) Radially Poled (b) Symmetric Tangentially Poled (Type-1, 2 & 3)

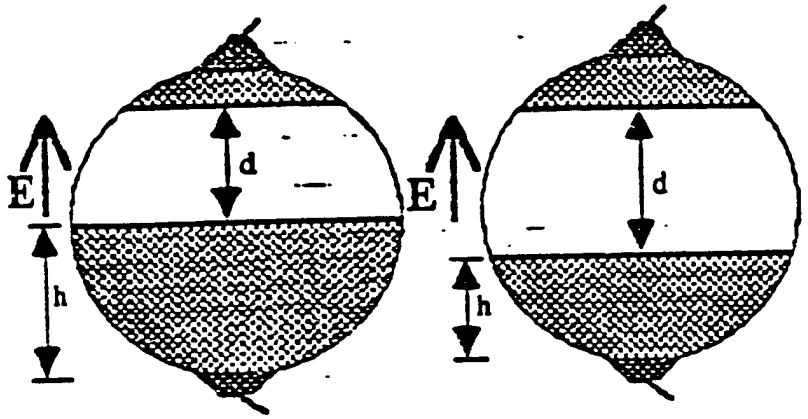

(Type-4) (Type-5)

(c) Non-symmetric Tangentially Poled

Figure-1. Electrode and poling configurations piezoelectric hollow sphere transducers

4. Characterization of Spheres

4.1. Dielectric properties

Dielectric characterization of the spheres were done using a HP 4275-A Multi-frequency LCR Meter at 1.0 kHz and 1.0 Volt. For radially poled spheres a typical capacitance value of 2,900 pF , and a dielectric loss of 0.020 were measured. An average dielectric constant (ε_r) of about 1,000, somewhat lower than the typical value of 1,850 for UPI 501A powders, was calculated from the capacitance using the following equation for a spherical capacitor [6] :

$$C = 4\pi\varepsilon_r\varepsilon_o\left(\frac{r_i r_o}{r_o - r_i}\right) \quad (1)$$

This discrepancy between the calculated and measured values are attributed to the wall thickness variations, inner electrode quality and the defects in the sphere wall [8]. Similarly, capacitance values ranging from 2.5 to 10 pF were measured for tangentially poled spheres (see table-1). Those values are in fair agreement with the calculated values of 6 to 11 pF using a cylindrical tube approximation [6]:

$$C = \varepsilon_r\varepsilon_o\frac{\pi t\,(r_i + r_o)}{d} \quad (2)$$

As expected, the capacitance of the tangentially poled spheres were found to be highly dependent on the electrode size and uniformity.

Table-1. Comparison of the dielectric and piezoelectric properties

Type / Property	Bulk PZT-5A	Top-to-bottom poled type-1	type-2	type-3	type-4	type-5	radially poled
electrode gap, d (mm)	n/a	0.790	1.380	1.710	1.060	1.810	n/a
electrode height, h (mm)	n/a	0.985	0.690	0.525	1.380	0.840	n/a
Capacitance, C (pF)	131.0	6.9	3.7	3.0	4.5	2.6	2,900
Dielectric loss, tan δ	0.017	0.027	0.071	0.026	0.022	0.014	0.020
Dielectric constant, ε_r	1,622	909	861	869	800	789	1,000
Hydrostatic piezoelectric charge coefficient @, d_h (pC/N)	30	743	788	870	736	966	1,800
Hydrophone figure of merit $d_h \times g_h$, (10^{-15} m^2/N)	60	68,677	81,659	98,610	76,464	133,640	324,000

@ determined at 100 psi and 30 Hz

4.2. Modes of vibration of radially poled spheres and effect of electrode hole

Results of the finite element analysis suggest two main modes of vibration for the radial poling configuration. These are the breathing mode and the thickness mode with resonance-antiresonance frequencies at 620-780 kHz and 21.5-24.0 MHz, respectively. Experimental measurements agree well with the calculations for breathing mode. The measured average resonance-antiresonance frequencies for this mode are 633-686 kHz. However, similar agreement could not been obtained for the thickness mode. This mode has only been detected in a few samples as a smooth, broad peak in the admittance vs. frequency spectra and the frequency range was 13.4-13.8 MHz for resonance and antiresonance frequencies, respectively. This discrepancy between the calculated and measured values is due to the large wall thickness variations within each sphere, as it has been reported by Fielding et al. [8].

The effect of the presence of an electrode hole on the vibration of the spheres was also investigated using the ATILA code and the results suggest that the hole introduces a new peak in the frequency range of the breathing mode at 750 kHz (see fig.-2/a). A similar secondary peak was also observed in the experimentally obtained admittance vs. frequency spectrum (see fig.-2/b). This secondary peak was studied using ATILA and the displacement field of the hollow sphere at 750 kHz is given in figure-3 with an arbitrary amplitude. In the figure the dashed lines correspond to the rest position and the solid lines shows the drive position.

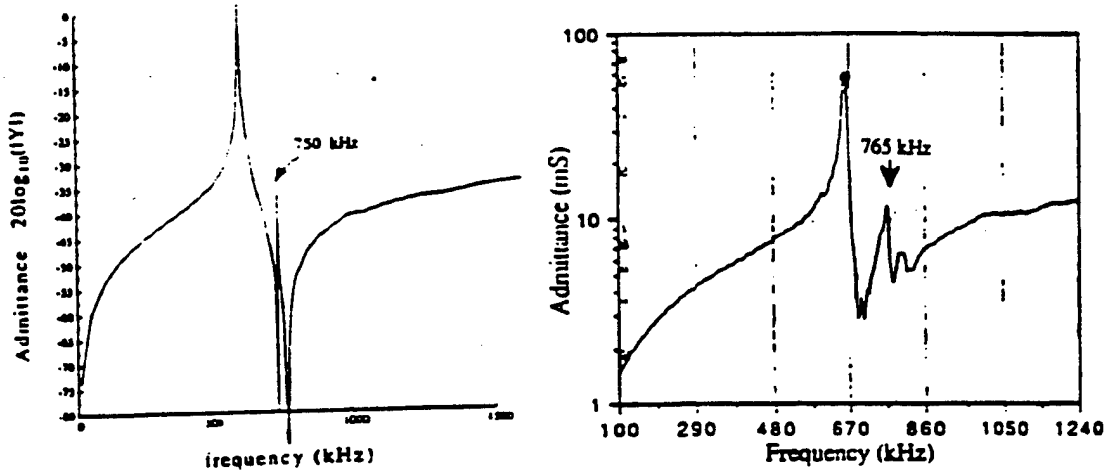

(a) calculated (b) observed

Figure-2. Effect of electrode hole on the admittance spectra of a radially poled hollow sphere

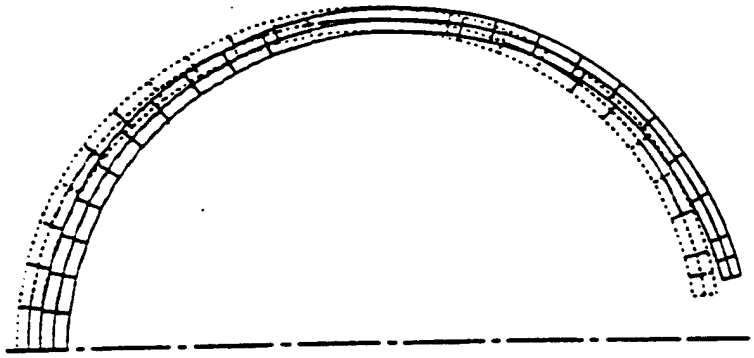

Figure-3. Displacement field of the radially poled hollow sphere with hole at 750 kHz (with an arbitrary amplitude)

4.3. Modes of vibration of tangentially poled spheres

Finite element studies on the spheres with top-to-bottom electrode configuration concluded that only the unelectroded region between the electrode caps is tangentially polarized, and the material under the electrodes is unpoled and inactive [10]. Therefore, the size of the electrode gap is expected to control the dielectric and piezoelectric properties.

Finite element analysis of the tangentially poled spheres indicates the main modes of vibrations as an ellipsoidal, a higher order circumferential and a breathing mode near 230 kHz, 350 kHz and 700 kHz, respectively. Higher frequency modes, which consist of coupling

between ellipsoidal and thickness modes, or between circumferential and thickness modes were also determined for this poling configuration. The admittance vs. frequency spectrum of a type-4 sphere obtained from analytic calculations and experimental measurements are compared in figure-4 as an example. Comparison of the results indicate that there is a close match between the calculated and measured values for the resonance-antiresonance frequencies of the three main modes of vibration. However, this is not the case for the coupled modes. Since these higher frequency modes are formed as a result of a coupling between the eilipsoidal and the thickness, or the circumferential and the thickness modes, the non-uniform wall thickness is expected to disrupt and broaden these coupled modes. The displacement fields and the resonance frequencies of these modes were discussed in details elsewhere [10].

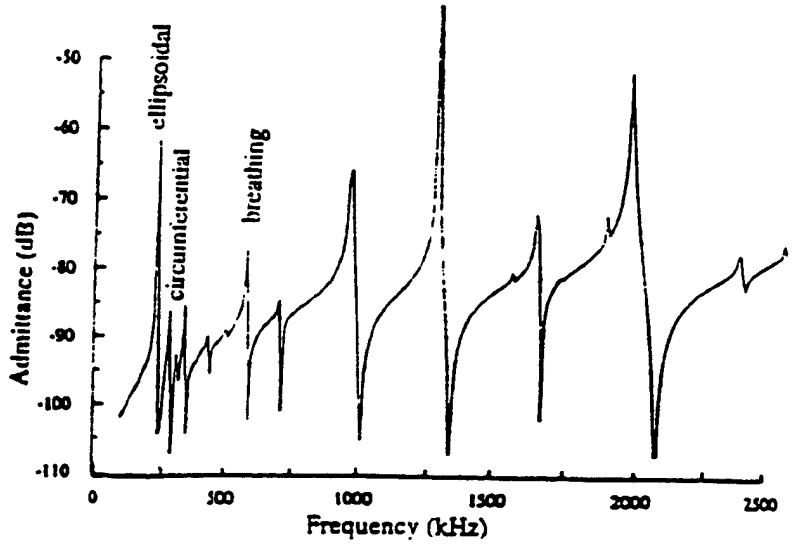

(a) calculated

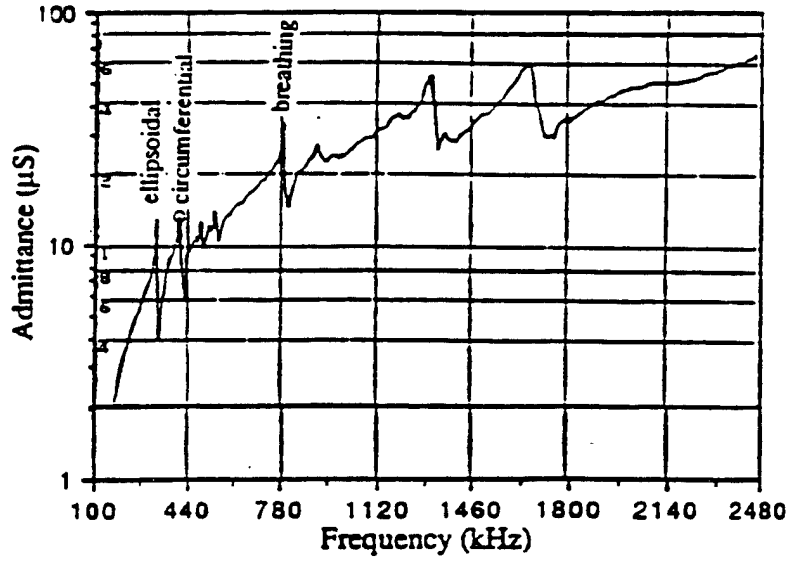

(b) observed

Figure-4. Admittance spectra of a tangentially poled PZT hollow sphere (Type-4)

4.4. Hydrostatic sensitivity of the spheres

Partial evaluation of the performance of hollow sphere piezoelectric transducers as underwater hydrophones were achieved through the hydrostatic piezoelectric charge coefficient, d_h measurements. These measurements are carried out under hydrostatic pressures from 100 to 1,000 psi with a 30 Hz stimulus. A PZT-5 disc was also used in the measurements to compare the spheres with the bulk material. From the results of these measurements, hydrostatic piezoelectric voltage coefficient (g_h) and hydrophone figure of merit are calculated using the following equations. The results are given in table-1 and plotted in figure-5

$$g_h = \frac{d_h}{\varepsilon_{33}} \tag{3}$$

$$figure\ of\ merit\ =\ d_h * g_h \tag{4}$$

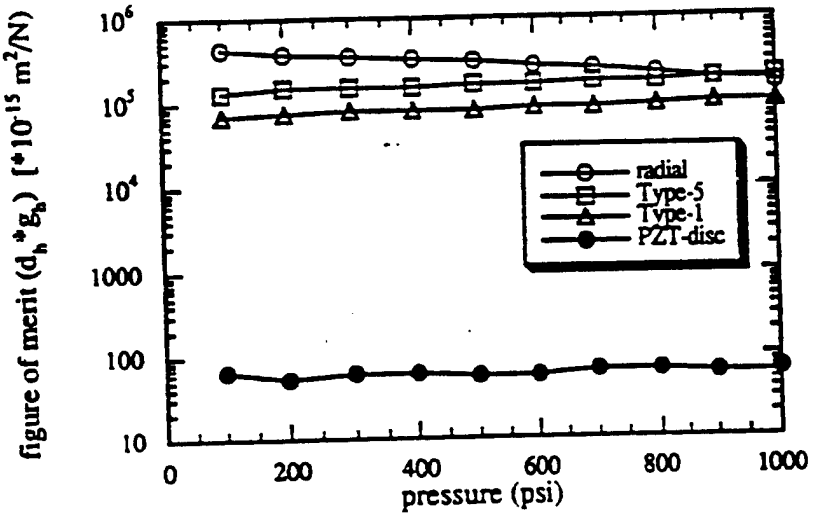

Figure-5. Comparison of the hydrophone figure of merit of the hollow spheres

In figure-5 only two types of tangentially poled spheres, namely type-1 with the lowest values measured and type-5 with the highest values measured, were plotted. The other three types were found to fall within this range. The results indicate that hollow sphere piezoelectric transducers posses three orders of magnitude higher hydrophone figure of merits. The amplification of the sensitivity results from the transformation of a hydrostatic pressure into tangential and radial stresses on a spherical geometry. In this geometry, radius to thickness ratio (r/t) can be taken as the stress amplification factor. A detailed discussion along with a simplified model for this amplification is given by Alkoy et al. [10]. The results of these hydrostatic measurements also shows that increasing the active surface area, i.e. unelectroded and tangentially polarized region, leads to an increase in the hydrostatic sensitivity. The change of hydrophone figure of merit with increasing active area is shown in figure-6.

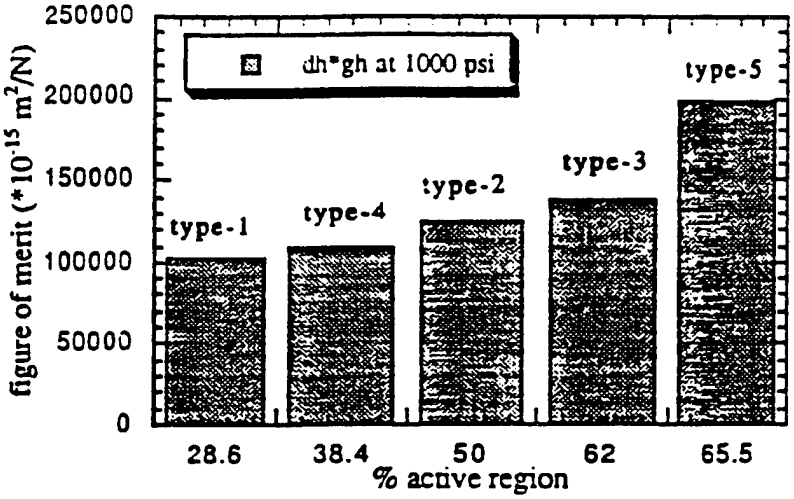

Figure-6. Change of hydrophone figure of merit with the area of the active region

5. Conclusion

Piezoelectric transducers were prepared from PZT based millimeter size ceramic hollow spheres. Dielectric, piezoelectric and hydrostatic characterization and a modeling study was carried out on radially and tangentially poled spheres. The principal modes of vibration were found to be breathing and thickness modes for radial poling, and ellipsoidal, higher order circumferential and breathing mode for tangentially poled spheres. Higher frequency coupled modes were also observed in the tangentially poled spheres. Compared to the bulk PZT orders of magnitude higher d_h and hydrophone figure of merits were obtained from the PZT hollow spheres.

Acknowledgments

This study is partly funded by ONR through contract # N00014921J1510, and by Gebze Insutute for Advanced Technology - Turkey. We thank Prof. Joe K. Cochran at Georgia Institute of Technology - USA for the fabrication of green spheres and IEMN, Department ISEN - France for letting us use their facilities.

References

1) K.A. Klicker, J.V. Biggers & R.E. Newnham, " Composites of PZT and epoxy for hydrostatic transducer applications", *J. Amer. Ceram. Soc.*, 64, pp.5-9, 1981
2) A. Dogan, "Flextensional moonie and cymbal actuators", *Ph.D. Thesis*, The Pennsylvania State University, University Park, 1994
3) D. Vilkomerson, B. Gardineer, and H. Hojeibane, "Quasi-Omnidirectional Transducers for Ultrasonic Electro-Beacon Guidance of Invasive Devices," *SPIE*, 1733, pp 154-165, 1992

4) L. E. Ivey, "NRL-USRD Series F42 Omnidirectional Standard Transducers, "*Underwater Sound Reference Detachment*, 1979, Naval Research Laboratory, Orlando, Florida
5) S. Fujishima, T. Nakamura and T. Okada, "Characteristics of spherical piezoelectric ceramic speakers", *Proc. Acous. Soc. Jap.*, March 26-28, 1996
6) R. Meyer, Jr., H. Weitzing, Q. Xu, Q. Zhang & R.E. Newnham, " Lead Zirconate Titanate hollow sphere transducers," *J. Amer. Ceram. Soc.*, 77, (6), pp. 1669-1672, 1994
7) L.B. Torobin, " Methods of making hollow, porous microspheres", *U.S. Patent* No. 4,671,909 , 1987
8) J.T. Fielding, Jr., D. Smith, R. Meyer, Jr., S. Trolier-McKinstry & R.E. Newnham, "Characterization of PZT hollow sphere transducers", *IEEE Int. Symp. Appl. Ferroelec.*, 1994, pp.202-205
9) A.C. Hladky-Hennion and J.N. Decarpigny, "Finite element modeling of active periodic structures: application to 1-3 piezocomposites", *J. Acous. Soc. Am.* , 94, pp.621-635, 1993
10) S. Alkoy, A.Dogan, A.C. Hladky, P. Langlet, J.K. Cochran and R.E. Newnham, "Miniature piezoelectric hollow sphere transducers", *Proc. IEEE Int. Freq. Cont. Symp.*, June 1996, in press

APPENDIX 47

Accelerometer Application of the Modified Moonie (Cymbal) Transducer

Burhanettin KOC, Aydin DOGAN, Jose F. FERNANDEZ, Robert E. NEWNHAM and Kenji UCHINO
International Center for Actuators and Transducers, Materials Research Laboratory, The Pennsylvania State University, University Park, PA 16802, USA

(Received November 8, 1995; accepted for publication May 23, 1996)

The modified Moonie (Cymbal) transducer has been investigated for an accelerometer application. High effective piezoelectric charge coefficients (d_{33}) of the Cymbal transducer was observed around 15000 pC/N, which is much higher than that of the piezoelectric ceramic itself (~ 550 pC/N). With this feature the Cymbal trasducer is a good candidate for high sensitive accelerometer applications. The sensitivity of the Cymbal accelerometer was measured as a function of driving frequency and compared with the single plate ceramic disk which was used as driving component in the transducer. Besides, the geometry of the transducer such as endcap thickness, the effect of different Lead Zirconate Titanate (PZT) compositions and metal endcaps on sensitivity was investigated. The sensitivity 50 times higher than the PZT disk was obtained.

KEYWORDS: accelerometer, piezoelectric effect, modified Moonie (Cymbal) transducer, sensitivity

1. Introduction

Accelerometers are used widely throughout engineering, both as research and development tools and as control-system components. However, the most popular application area is using of accelerometer for vehicle dynamics.[1] Since the market especially for vehicle dynamics is very large, various types of acceleromeeter design have been reported.[2-7]

One of the most popular techniques to measure acceleration is using the piezoelectric effect of materials. In the piezoelectric effect, no matter which mode is used, such as compression (longitudinal), bending or shear, the sensitivity of acceleration sensor depends on piezoelectric charge coefficients of the material. When a longitudinal mode is used, the sensitivity is directly proportional to d_{33} of the material. Lead zirconate titanate (PZT) based ceramics exhibit a large d_{33} constant, but still it is not high enough to measure acceleration efficiently. Therefore, PZT-polymer composites have been used by Ohara and Miyayama and the sensitivity has been tripled in comparison with the single PZT plate.[2] The other way of improving sensitivity taken by Ohtsuki *et al.* was using multilayer piezoelectric ceramics,[4] with sacrificing the cost. Since piezoelectric sensors have various advantages such as fast response, which is very important for shock measurement, and simple detecting circuits, they are preferred for some applications such as safety and suspension systems in the automobile. A metal-piezoceramic composite structure with very high effective d_{33} constant may be a good alternative for acceleration sensors.

A metal-ceramic composite design, Moonie, was first used for hydrophones which sense weak pressure wave in fluid.[8] The metal endcaps of the Moonie were recently modified, and as an actuator higher displacements were obtained than multilayer actuators (see Fig. 1).[9,10] The new transducer, "Cymbal", named after the endcap shape like cymbals, has also higher piezoelectric charge coefficients and an easy production method than the Moonie trasducer.

In this study, the cymbal transducer has been used to detect acceleration, with metal endcaps transfering a longitudinal stress into a radial stress. When the metal endcaps move radially due to the compressive stress, the bonded PZT disk is stretched. Therefore, the ineffective d_{31} of a single PZT disk becomes effective, and that causes higher effective piezoelectric charge coefficient (d_{33}^{eff}) and thus much higher sensitivity.

2. Acceleration Sensitivity of the Cymbal

The force from a mass (m) due to acceleration ($F = ma$) is transferred through the two metal endcaps on to the PZT thin disk, and it causes a stress toward the circumference of the ceramic disk, most of which is in the radial direction and some part of which acts as a compressive stress in the thickness direction (Fig. 1(b)).

The polarization vector due to the stress acting on the polycrystalline piezoelectric disk is defined as:

$$\begin{bmatrix} P_x \\ P_y \\ P_z \end{bmatrix} = \begin{bmatrix} 0 & 0 & 0 & 0 & d_{15} & 0 \\ 0 & 0 & 0 & d_{15} & 0 & 0 \\ d_{31} & d_{31} & d_{33} & 0 & 0 & 0 \end{bmatrix} \begin{bmatrix} X_1 \\ X_2 \\ X_3 \\ X_4 \\ X_5 \\ X_6 \end{bmatrix}, \quad (1)$$

where, P_x, P_y and P_z are the polarization vectors in a cartesian coordinate, d_{31}, d_{33} and d_{15} are the piezoelectric charge coefficients of radial, longitudinal and shear mode and X_i's ($i = 1, \cdots, 6$) are the stress components. In a cylindrical coordinate system, which is more suitable for the geometry of the piezoelectric thin disk, the stress components are:

$$X_1 = X_2 = -K_r F$$
$$X_3 = K_z F \quad \text{and} \quad X_4 = X_5 = X_6 = 0. \quad (2)$$

Then the polarization vector can be obtained as

$$P_z = (d_{33} K_z - 2 d_{31} K_r) F. \quad (3)$$

Here, the proportional constants, K_r and K_z, depend on geometry of the metal endcaps and the piezoelectric ceramic disk such as cavity angle of the metal endcap θ, thicknesses, diameter and elastic constant of the metal endcaps and the piezoelectric disk (A paper that has a detail expression for K_r and K_z will be reported in the

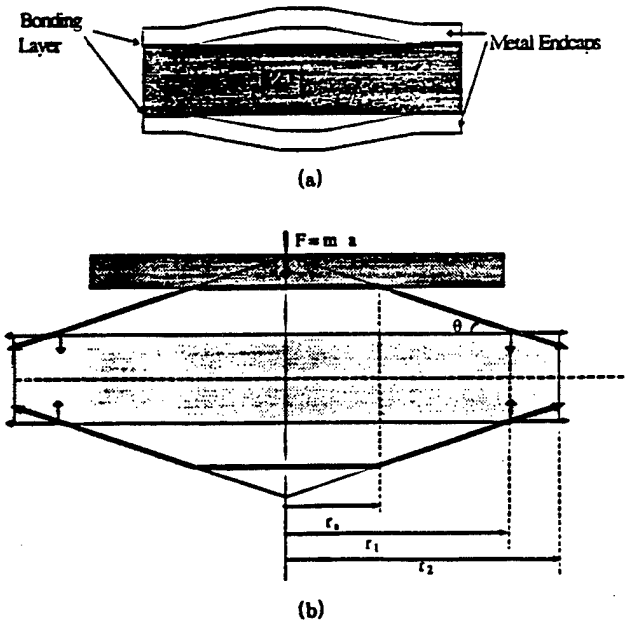

Fig. 1. (a) Structure of the modified Moonie (Cymbal). (b) Schematic compressive force transformation to the radial direction on a ideal metal endcap.

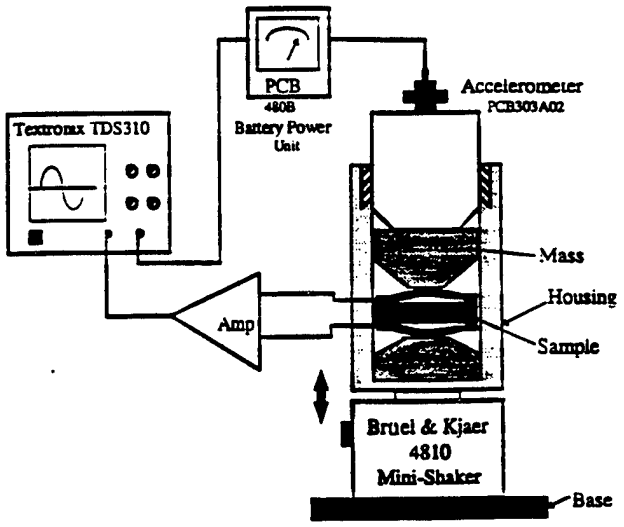

Fig. 2. Experimental setup for the sensitivity measurement.

near future). Note that the negative value of d_{31} acts positively because of the negative sign of the summation. Then. charge generation for the whole disk can be defined as:

$$Q = \pi r_2^2 (d_{33} K_z - 2 d_{31} K_r) m a \qquad (4)$$

and finally the charge sensitivity of this transducer defined by the charge generation by unit acceleration becomes:

$$S_q = \pi r_2^2 (d_{33} K_z - 2 d_{31} K_r) m \quad [\mathrm{pC/(m/s^2)}]. \qquad (5)$$

3. Experimental Procedure

The composite transducers were made of electroded ceramic disks (12.7 mm in diameter and 1.0 mm in thickness) and metal endcaps (12.7 mm in diameter with thickness ranging from 0.18 to 0.30 mm). Piezoelectric properties of the PZT disks and elastic characteristics of the metal endcaps are given in Table I and Table II. respectively. Truncated-cone shape endcap was fabricated first by punching and then pressing the metal sheet up to 100 MPa to give 250 μm cavity depth. The ceramic disk and metal endcaps were bonded together around the circumference with two component epoxy (Eccobond). The epoxy was distributed by taking care neither to fill the cavity nor to make open circuit between the endcaps and the electroded face of the PZT. After 24 h epoxy curing process under a small pressure. the samples became ready for the measurements.

Figure 2 shows the experimental setup of the sensitivity measurement of the metal-ceramic composite transducer. The transducer was fixed with added mass (8.4 g) inside a housing unit. A commercialized accelerometer (PCB 302A02) was mounted on the top of the housing unit to produce a reference signal. A mini-shaker (Bruel & Kjaer 4810) was used to produce vibration. A charge amplifier circuitry has been used during the Cymbal and the single PZT disk measurement. The output signals (mV/G) of the purposed transducer and the commercial accelerometer were measured simultaneously with a digital oscilloscope (Tektronix TDS 310).

Table I. Piezoelectric properties of PZT disks used in the Cymbal transducer.

CERAMIC	ε'	$tg\delta$	d_{31} (pC/N)	d_{33} (pC/N)
PZT 8D	1104	0.003	−107	289
PZT 5A	1802	0.016	−208	429
PZT 5H	3500	0.016	−285	581

Table II. Elastic characteristics of metal endcaps used in the Cymbal transducer.

Metal endcap	Density (g/cm^3)	Young's modulus (E) (GPa)
Zirconium	6.49	77
Brass	8.53	110
Tungsten	19.30	405
PZT 5H	7.5	71

4. Result and Discussion

The metal endcaps of the Cymbal transducer transfer some part of the acceleration stress in the normal direction into the radial direction. Therefore. the sensitivity of the transducer depends not only on d_{33} but also on d31 of the piezo-ceramic. The Cymbal transducers with different piezoelectric ceramics whose piezoelectric charge coefficients are different, are compared in Fig. 3. The ceramic with the larger d_{33} and d_{31} in magnitude provides the higher sensitivity. As shown in Table I, PZT-5H shows the highest d_{31} constant. and also shows the highest sensitivity to the acceleration. The identical zirconium endcaps were used for all transducers.

Figure 4 shows the sensitivity versus frequency of the PZT-5H singie disk and of the Cymbal transducers with

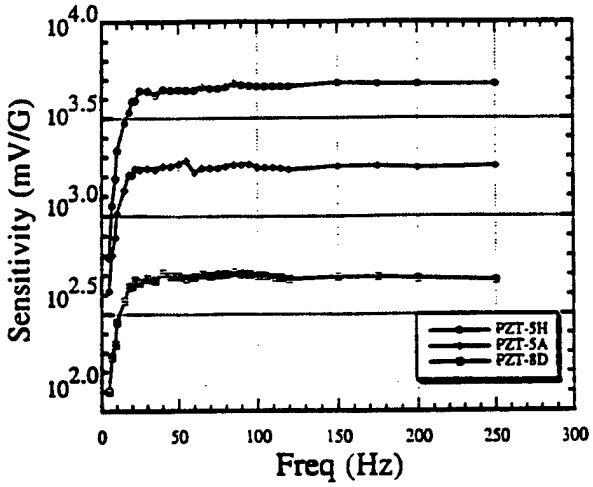

Fig. 3. Dependence of the acceleration sensitivity on the PZT composition.

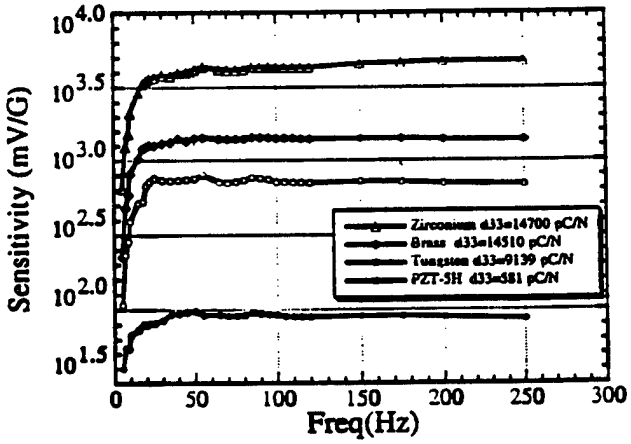

Fig. 4. Sensitivity for various metal endcaps.

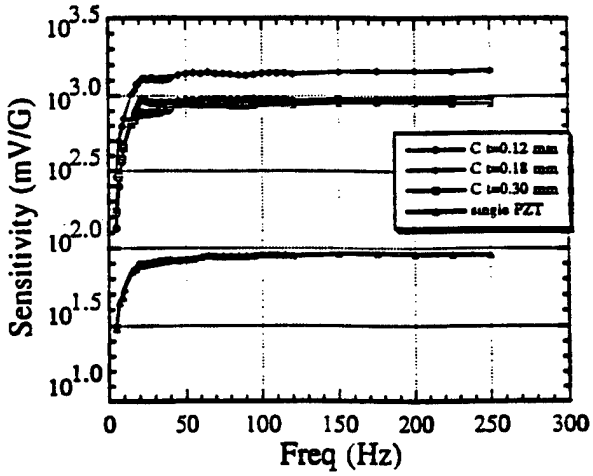

Fig. 5. Dependence of the sensitivity on the endcap thickness.

various metal endcaps. The output of the Cymbal transducer with Zirconium end caps was found to be about 50 times as large as that in PZT-5H itself. Considering the Young's modulus and the density of the PZT 5H ceramic ($E = 71\,\mathrm{GPa}$, $\rho = 7.5\,\mathrm{g/cm^3}$), it may be concluded that the elastic properties similar to the PZT are required to transfer the acceleratin force effectively. It is also possible to compensate thermal dilatation effect on the piezoelectric material by choosing a suitable endcap metal. For example, when tungsten endcaps have been used temperature insensitive displacement actuators have been obtained.[11]

The transferred stress from the metal endcaps, which act as springs, to the ceramic material depends also on the endcap geometry. Then. the sensitivity of the transducer is strongly affected by the thickness of the endcaps. When the endcaps are too thin. they deform without stretching the ceramic causing energy loss. On the contrary when they are too thick. they can not produce enough momentum in the radial direction, but the longitudinal stress on the edge of the ceramic disk. Figure 5 shows the endcap thickness dependence of the sensitivity. The thickness 0.18 mm provided the highest sensitivity for the brass endcaps.

5. Conclusion

A metal-ceramic composite structure (Cymbal transducer) has been investigated for accelerometer applications. The Cymbal transducer has provided 50 times higher sensitivity than the single PZT disk. which was used to make the Cymbal transducer. This 50 times higher sensitivity of the Cymbal transducer compare to single PZT disk corresponds to a voltage sensitivity of 4.5 V/G and a resolution of less than 25 μG, while voltage sensitivity of single PZT disk was 90 mV/G.

The most significant result was that the sensitivity of the purposed acceleration transducer depended on the geometry and the structure such as the cavity depth, thickness, Young's modules of the metal endcaps as well as elastic and piezoelectric properties of the PZT disk.

1) G. A. Macdonald: Sens. & Actuat. A 21–23 (1990) 303.
2) Y. Ohara and M. Miyayama: Sens. & Actuat. A 36 (1993) 121.
3) R. P. Sion. J. K. Atkinson and J. D. Turner: Sens. & Actuat. A 37–38 (1993) 348.
4) Y. Ohtsuki. Y. Fuda and T. Yoshida: Jpn. J. Appl. Phys. 32 (1993) 4209.
5) K. Sato. K. Okamoto. Y. Fuda and T. Yoshida: Jpn. J. Appl. Phys. 33 (1994) 5378.
6) E. Abbaspour-Sani. R-H. Huang and C. Y. Kwok: Sens. & Actuat. A 44 (1994) 103.
7) R. Hiratsuka. D. C. van Duyn. T. Otaredian and P. De Vries: Sens. & Actuat. A 32 (1992) 380.
8) Q. C. Xu, S. Yoshikawa. J. R. Belsick and R. E. Newnham: IEEE Trans. Ultrason. Ferroelect. Freq. Control. 38 (1991) 634.
9) A. Dogan: Ph. D. Dissertation. University Park, Pennsylvania, USA (1994).
10) A. Dogan: USA Patent Application. PSU Invention Disclosure no. 94–1375 (1994).
11) J. F. Fernandez, A. Dogan. J. T. Fielding, K. Uchino and R. E. Newnham: submitted to IEEE Trans. Ultrason. Ferroelect. Freq. Control.

APPENDIX 48

Ferroelectric Letters, 1996, Vol. 21, pp. 11–16
Reprints available directly from the publisher
Photocopying permitted by license only

UNDERWATER ACOUSTIC ABSORPTION BY COLLOCATED SMART MATERIALS

S. KUMAR, A. S. BHALLA and L. E. CROSS
Materials Research Laboratory, The Pennsylvania State University
University Park, PA, USA

(Received for Publication December 20, 1995)

Abstract: Collocated smart structures provide the most effective technique of influencing the stimuli. Such systems can also be used for absorbing underwater acoustic waves. A collocated system is designed by mounting piezoelectric sensor on a multilayer PZT discs stack. Using PZT sensor for narrowband response and modified lead titanate sensor for broadband response, the effectiveness of these smart structures in absorbing acoustic waves is experimentally determined by using an acoustic tube.

INTRODUCTION

It has been shown that collocated smart structures can be used in active vibration control and removal of energy from the vibration field [1,2]. These collocated systems for vibration control are designed by directly mounting a piezoelectric sensor on multilayer stack of piezoelectric (generally PZT) thin discs. The piezoelectric thin discs in the actuator are mechanically in series and electrically in parallel so that displacements of each disc adds up. If the sensor voltage, which develops due to pressure change on the sensor surface, is amplified, inverted in phase and applied to the actuator, the dynamic compliance of the sensor-actuator composite can be controlled and used in active vibration control. The material properties play a crucial role in the designing of the systems. For example to obtain a narrowband response from a simple collocated system, a PZT sensor can be used. But for broadband response, there are restrictions on choice of sensor material. A modified lead titanate sensor is required to obtain broadband response from a simple collocated system. In these systems there is a very strong field coupling between the sensor and the actuator and therefore they are quite difficult to design because of stability considerations. However, they provide the most effective technique of controlling the field since sensing and actuating takes place at the same point. It should also be pointed out that

Communicated by Dr. George W. Taylor

by moving the sensor surface by electronic feedback to the actuator, the acoustic impedance of the smart material (sensor-actuator composite) can be controlled. This presents the opportunity of using these smart systems for underwater acoustic absorption and therefore making them useful in many applications. In this work we investigate the underwater acoustic absorption by collocated smart materials.

Experimental

Figure 1 shows the collocated smart system which has been used to absorb energy from underwater acoustic waves. For this investigation, an acoustic tube experiment was set up as shown in fig. 2. A 3 feet long aluminum tube with 3 inch internal diameter and 0.5 inch wall thickness was used as an acoustic tube.

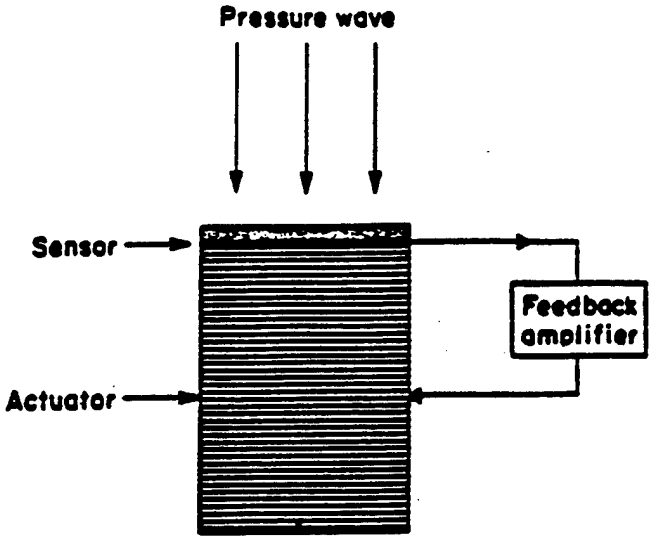

FIGURE 1. Collocated Smart Material.

Standard navy transducer J9, which operates at low frequencies, was placed on one side of the acoustic tube and a cell as shown in fig. 3, was designed to house sensor-actuator combination. The cell was placed on the other side of the acoustic tube. A solid aluminum cone was joined to the sensor in the cell to increase the effective area of the sensor. The cell was filled with castor oil so that the gap between the rubber diaphragm and the aluminum cone contain castor oil which would provide acoustic coupling between the diaphragm and the cone. Because of air bubble problems the cell design was changed to remove castor oil. The rubber diaphragm was glued directly to the aluminum cone.

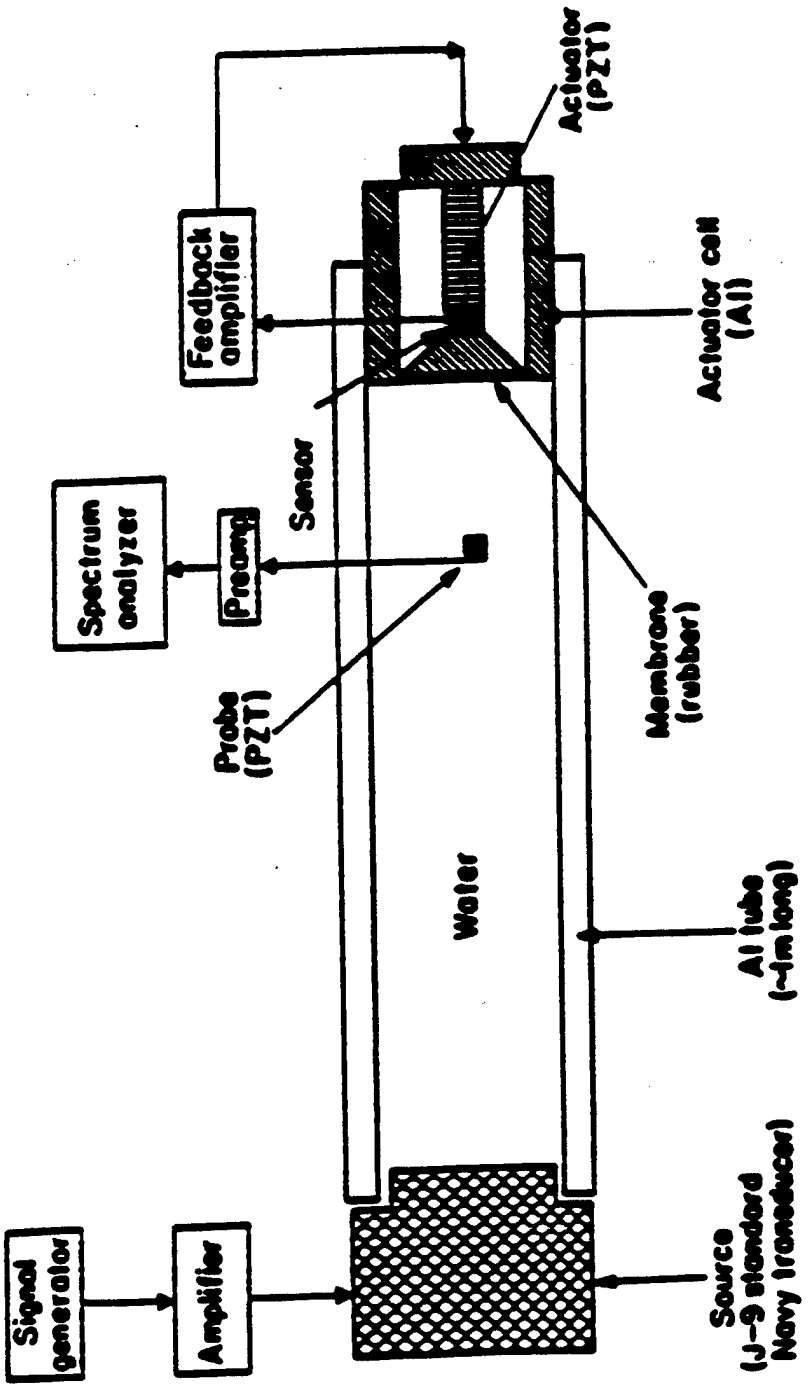

FIGURE 2. Acoustic tube set up for underwater acoustic wave absorption measurement.

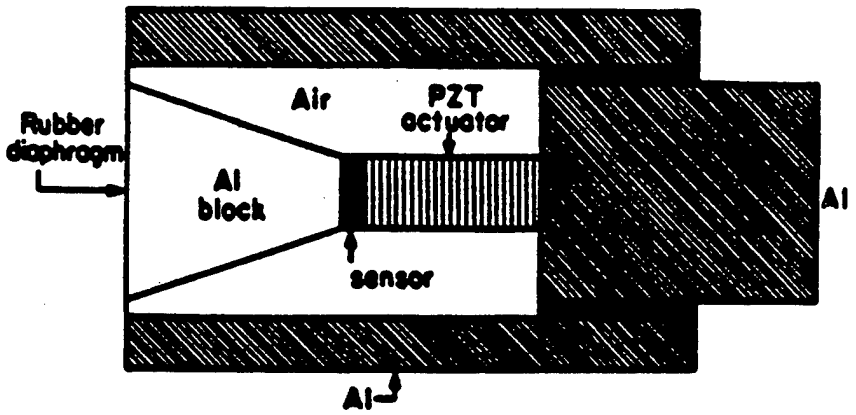

FIGURE 3. Cell containing collocated sensor actuator combination. A low noise preamplifier is housed in a cavity in the aluminium block behind the actuator.

Narrowband Response

In this case a PZT disc was used as a sensor in sensor-actuator smart composite and a high Q bandpass filter was placed in the feedback circuit. Assuming that diameter of the tube is small compared to the wavelength so that plane wave propagates in the tube, the pressure as a function of length in the acoustic tube can be calculated by solving the well known Helmholtz equation and applying the appropriate boundary conditions. This assumption is clearly valid for the low frequencies used in the experiment. In the experimental set up, provision was made to monitor the pressure along the axis of the tube by placing very small pressure sensors through very small holes in the wall of the tube. The acoustic tube was lowered in the water tank and filled with water so that whole acoustic tube with J9 and cell on its sides was submerged in the water. Care was taken to remove all air bubbles from the acoustic tube. The signal from the sensor was amplified, passed through the bandpass filter which was tuned to the J9 frequency, inverted in phase and applied to the actuator. The effect of the sensor-actuator combination on the pressure along the axis of the tube could not be seen due to small applied voltages to the actuator. Alternatively, the sensor voltage was monitored with and without feedback applied to the actuator. The frequency of the standard transducer J9 was changed and the bandpass filter in the feedback circuit was tuned to the same frequency. Figure 4 shows the effect of feedback on the sensor voltage. The reduction in sensor voltage when feedback was applied implies that the smart material partially absorbed the incident acoustic wave.

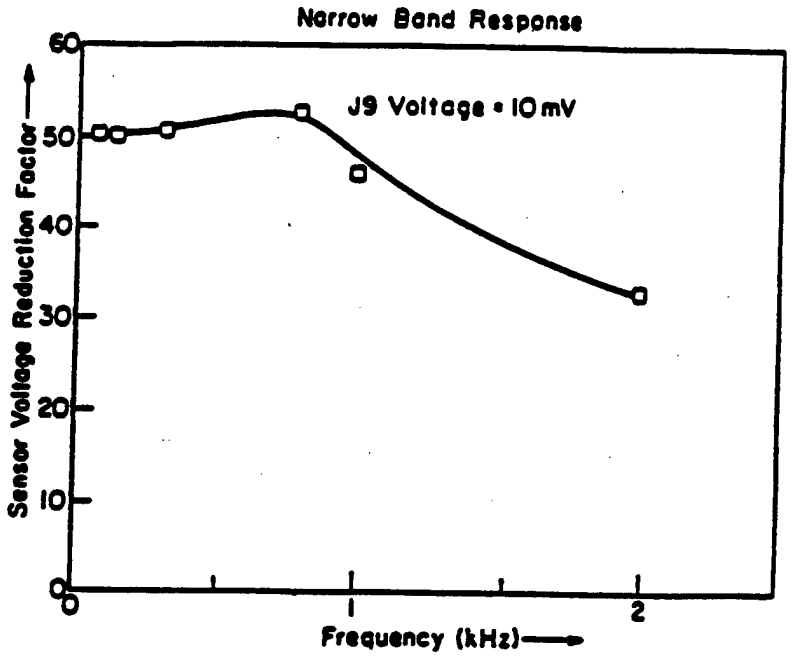

FIGURE 4. Narrowband response of the collocated sensor-actuator combination for the under water acoustic absorption.

Broadband Response

The PZT sensor was replaced with modified lead titanate sensor in the cell and the high Q bandpass filter was removed from the feedback circuit. The feedback circuit used in this system is described elsewhere [2]. The sensor voltage was monitored with and without feedback to the actuator. The frequency of transducer J9 was changed and sensor voltage again monitored. Figure 5 shows the broadband response of the smart system.

RESULTS AND DISCUSSION

Figure 4 shows the narrowband response in which the ratio of sensor voltage without and with feedback applied to the actuator as function of frequency is plotted. Higher reduction factor implies higher effectiveness of the smart system since the sensor voltage is a measure of acoustic impedance of the smart system. The reduction factor obtained is about 50 at low frequencies dropping to about 35 around 2 kHz. The drop in sensor voltage reduction factor is expected since response time of the actuator comes into picture.

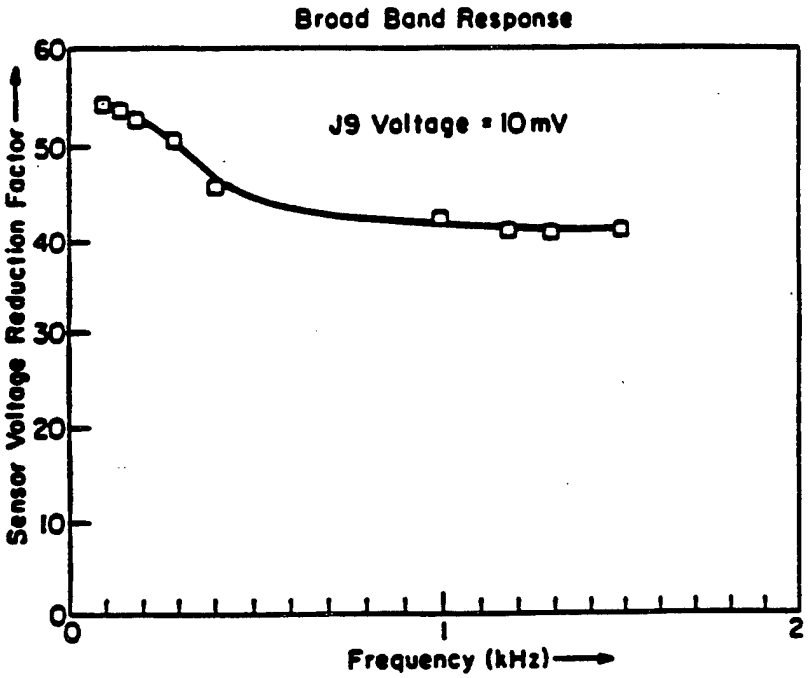

FIGURE 5. Broadband response of the collocated sensor-actuator combination for the underwater acoustic absorption.

The broadband response of the smart system is obtained without using a higher order filter in the feedback circuit. This design is possible because of low planar coupling coefficient of modified lead titanate. Again the sensor voltage reduction factor is seen to be 55 at low frequencies dropping to 40 at 1.5 kHz. This is a broadband response of the smart system since there is no bandpass filter in the feedback circuit and only J9 frequencies are changed keeping the J9 voltage same at each frequency. These results for narrowband and broadband response show that it is possible to control the acoustic impedance of the smart structures and remove energy from the incident acoustic waves.

REFERENCES

1. S. Kumar, A. S. Bhalla, L. E. Cross. " Smart Ceramics for Acoustic and Vibration Control." *J. Intelligent Material Systems and Structures*, Vol. 5, No. 5, 678-682 (1994).
2. S. Kumar, A. S. Bhalla, L. E. Cross. " Broadband Vibration Control Using Smart Ceramics." *J. Intelligent Material Systems and Structures*, Vol. 5, No. 5, 673-677 (1994).